University of California
Santa Barbara

Distributed Control of Inverter-Based Power Grids

A dissertation submitted in partial satisfaction
of the requirements for the degree

Doctor of Philosophy
in
Mechanical Engineering

by

John William Simpson-Porco

Committee in charge:

Professor Francesco Bullo, Chair
Professor Igor Mezić
Professor Jeff Moehlis
Professor João Hespanha

December 2015

The Dissertation of John William Simpson-Porco is approved.

Professor Igor Mezić

Professor Jeff Moehlis

Professor João Hespanha

Professor Francesco Bullo, Committee Chair

May 2015

Distributed Control of Inverter-Based Power Grids

by

John William Simpson-Porco

To my family, friends, and mentors.

Acknowledgements

I have had the privilege of having two mentors guide and support me throughout my time in Santa Barbara. Firstly, my advisor Francesco. Francesco was the graduate chair when I was accepted, and his enthusiasm was a major factor in my decision to accept the offer of admission and move to California. It is hard to count all the work and life lessons I have learned from Francesco, and I am extremely grateful for the trust he placed in me to pursue my own ideas freely.

While Francesco was my formal advisor and mentor, an equally important role was played by my colleague Florian, especially during my formative first and second years in graduate school. Sitting only a few seats apart in the lab, each day Florian and I would discuss controls, attempt (sometimes with little success) to teach ourselves power systems on the whiteboard, and poke fun at whatever we saw fit. Florian was and continues to be a great role model.

A number of senior researchers have helped shape my attitudes, and to them I am also indebted. From my days at Queen's, thank you to Martin Guay and Abdol-Reza Mansouri for sparking my interest in controls, and to David McKay for being an even-tempered role model during my summer at University of Toronto. On my committee, thank you to João for your thoughtful questions, Igor for your infectious enthusiasm and big thinking, and Jeff for your dedicated teaching and dry humor; likewise on teaching for Andy Teel, and thank you to Bassam Bamieh for his invaluable career advice. Special thanks to Brad Paden for the hours in his office discussing the practical side of control engineering, Sandro Zampieri for his lighthearted approach and perspective, and to Ian Hiskens and Ian Dobson for their encouragement and support.

Thanks to all my colleagues in Motion Lab, especially Anahita for keeping the lab fun, Fabio for his acerbic wit, and Vaibhav for "keeping me human". Thank you to Basilio,

Hedi, Qobad, and Marco for their hard work on our joint projects, to my colleagues Michael Gaultois and Alan Derk dozens of stimulating discussions over lunch, and to everyone else who has made my time in Santa Barbara unforgettable.

Finally, thank you to Jamie for her patience, for all the late night drives back from concerts in LA, and all the fun trips around California and beyond.

Curriculum Vitæ

John William Simpson-Porco

Education

2015	Ph.D. Mechanical Engineering University of California, Santa Barbara
2010	B.Sc Engineering Physics Queen's University

Research Interests

1. Control of inverter-based microgrids
2. Power system voltage stability
3. Dynamic phenomena in complex networks
4. Incremental stability & contraction theory

Honors and Awards

2014	Peter J. Frenkel Foundation Fellowship Institute for Energy Efficiency
2014	Automatica Prize International Federation of Automatic Control
2015	CCDC Outstanding Scholar Fellowship Center for Control, Dynamical Systems, and Computation
2011	NSERC Doctoral Fellowship Natural Sciences and Engineering Research Council of Canada
2011	CCDC Outstanding Scholar Fellowship Center for Control, Dynamical Systems, and Computation
2010	NSERC Masters Fellowship Natural Sciences and Engineering Research Council of Canada
2010	Engineering Physics Design Award Department of Physics, Queen's University
2010	CAP Prize Examination Award Department of Physics, Queen's University
2010	NSERC Summer Fellowship Natural Sciences and Engineering Research Council of Canada
2009	Kern Partners Ltd. Scholarship Faculty of Applied Science, Queen's University
2009	NSERC Summer Fellowship Natural Sciences and Engineering Research Council of Canada

2008	James H. Rattray Scholarship Faculty of Applied Science, Queen's University
2006	Queen's University Excellence Scholarship Faculty of Applied Science, Queen's University

Technical Reviewer

Journals	IEEE Transactions on Automatic Control ∘ IEEE Transactions on Control Systems Technology ∘ IEEE Transactions on Circuits and Systems ∘ IEEE Emerging and Selected Topics in Circuits and Systems ∘ Automatica ∘ IEEE Transactions on Power Systems ∘ IEEE Transactions on Smart Grid ∘ IEEE Transactions on Power Electronics
Conferences	IEEE Conference on Decision and Control ∘ American Control Conference ∘ IFAC Symposium on Robust Control Design ∘ IFAC Workshop on Lagrangian and Hamiltonian Methods for Non Linear Control ∘ IEEE Multiconference on Systems and Control

Professional Affiliations

2011-	Institute for Electrical and Electronics Engineers (IEEE) Control Systems Society (CSS) ∘ Power & Energy Society (PES) Student 2011-
2010-	Society for Industrial and Applied Mathematics (SIAM) Student 2011-

Talks, Seminars, and Presentations

Invited Seminars

July '15	University of Waterloo Department of Electrical and Computer Engineering
May '15	University of British Columbia Department of Electrical and Computer Engineering
Mar '15	University of Southern California Department of Electrical Engineering
Mar '15	Pacific Northwest National Laboratory Advanced Power and Energy Systems Division
Dec '13	University of Padova Department of Information Engineering

Conference Presentations, Poster Sessions, etc.

Apr '15	IEE Research Review, Santa Barbara, CA
Jan '15	Grid Science Winter School and Conference, Santa Fe, NM
Dec '14	IEEE Conference on Decision and Control, Los Angeles, CA
Dec '13	IEEE Conference on Decision and Control, Los Angeles, CA
Oct '13	IEEE SmartGridComm, Vancouver, BC
Nov '12	Southern California Control Workshop, San Diego, CA
Sep '12	IFAC Workshop on Control in Networked Systems, Santa Barbara
May '12	Optimization and Control for Smart Grids, Santa Fe, NM

Journal Articles

[1] J. W. Simpson-Porco and F. Bullo. "Distributed Monitoring of Voltage Collapse Sensitivity Indices". In: *IEEE Transactions on Smart Grid* (Aug. 2015). Submitted.

[2] J. W. Simpson-Porco, F. Dörfler, and F. Bullo. "On Resistive Networks of Constant Power Devices". In: *IEEE Transactions on Circuits and Systems II: Express Briefs* 62.8 (2015), pp. 811–815.

[3] J. W. Simpson-Porco, F. Dörfler, and F. Bullo. "Voltage Collapse in Complex Power Grids". In: *Nature Communications* (2015). Submitted.

[4] J. W. Simpson-Porco, F. Dörfler, and F. Bullo. "Voltage Stabilization in Microgrids via Quadratic Droop Control". In: *IEEE Transactions on Automatic Control* (July 2015). Submitted.

[5] J. W. Simpson-Porco et al. "Secondary Frequency and Voltage Control of Islanded Microgrids via Distributed Averaging". In: *IEEE Transactions on Industrial Electronics* (2015). To appear.

[6] F. Dörfler, J. W. Simpson-Porco, and F. Bullo. "Breaking the Hierarchy: Distributed Control & Economic Optimality in Microgrids". In: *IEEE Transactions on Control of Network Systems* (Jan. 2014). Accepted.

[7] J. W. Simpson-Porco and F. Bullo. "Contraction Theory on Riemannian Manifolds". In: *Systems & Control Letters* 65 (2014), pp. 74–80.

[8] J. W. Simpson-Porco, F. Dörfler, and F. Bullo. "Synchronization and Power Sharing for Droop-Controlled Inverters in Islanded Microgrids". In: *Automatica* 49.9 (2013), pp. 2603–2611.

[9] D. C. McKay et al. "Low-temperature high-density magneto-optical trapping of potassium using the open $4S \to 5P$ transition at 405 nm". In: *Phys. Rev. A* 84.6 (2011), p. 063420.

Conference Articles

[10] J. W. Simpson-Porco, F. Dorfler, and F. Bullo. "Avoiding Collapse: Reactive Loading Margins in Power Networks". In: *IEEE Conf. on Decision and Control*. To appear. Osaka, Japan, Dec. 2015.

[11] M. Todescato et al. "Optimal Voltage Support and Stress Minimization in Power Networks". In: *IEEE Conf. on Decision and Control*. To appear. Osaka, Japan, Dec. 2015.

[12] F. Dörfler, J. W. Simpson-Porco, and F. Bullo. "Plug-and-play control and optimization in microgrids". In: *IEEE Conf. on Decision and Control*. Los Angeles, CA, USA, Dec. 2014, pp. 211–216.

[13] B. Gentile et al. "On reactive power flow and voltage stability in microgrids". In: *American Control Conference*. Portland, OR, USA, June 2014, pp. 759–764.

[14] H. Bouattour et al. "Further results on distributed secondary control in microgrids". In: *IEEE Conf. on Decision and Control*. Florence, Italy, Dec. 2013, pp. 1514–1519.

[15] J. W. Simpson-Porco, F. Dörfler, and F. Bullo. "Voltage stabilization in microgrids via quadratic droop control". In: *IEEE Conf. on Decision and Control*. Florence, Italy, Dec. 2013, pp. 7582–7589.

[16] J. W. Simpson-Porco et al. "Stability, power sharing, & distributed secondary control in droop-controlled microgrids". In: *IEEE Int. Conf. on Smart Grid Communications*. Vancouver, BC, Canada, Oct. 2013, pp. 672–677.

[17] J. W. Simpson-Porco, F. Dörfler, and F. Bullo. "Droop-controlled inverters are Kuramoto oscillators". In: *IFAC Workshop on Distributed Estimation and Control in Networked Systems*. Santa Barbara, CA, USA, Sept. 2012, pp. 264–269.

Abstract

Distributed Control of Inverter-Based Power Grids

by

John William Simpson-Porco

Electrical power is the bedrock of modern civilization, and the large-scale hierarchical structure of bulk generation, transmission, and distribution has served us well for more than one hundred years. Currently however, the landscape of energy production is shifting, as economic, environmental, and technological factors are pushing power generation towards a future dominated by distributed generation from renewable energy sources. While grid-wide control strategies and architectures in bulk power systems were designed for slow time-scales and large synchronous generators, renewable energy interfaced through power electronic inverters allows for rapid response and greater flexibility in both local controller design and grid-wide control architectures.

This thesis focuses on exploring the limitations of both local controller design and control architectures for inverter-based power grids. Our contributions can be broadly divided into two categories. First, we study the classic primary droop controllers proposed for inverter-based power grids, and provide the first nonlinear analysis of the closed-loop frequency and voltage dynamics resulting from the controllers. We present tight analytic conditions for the existence and uniqueness of stable equilibrium points, thereby quantifying the fundamental limits of these controllers. In the second portion of the thesis, we propose and analyze a distributed control architecture which takes the place of the classical centralized secondary control layer. The distributed controllers combine classic droop ideas from power systems with agreement algorithms studied in cooperative control and multi-agent systems, leading to a scalable control architecture which achieves

centralized performance. The algorithms require only sparse communication between nearby inverters in the power grid, and require no a priori knowledge of the grid topology or load demands. We present extensive analysis results, along with experimental results validating our designs, and outline directions for future research.

Contents

List of Figures

List of Tables

Chapter 1

Introduction

This introductory chapter will be quite brief. We first state some permissions and attributions associated with the work presented herein. We then provide a sparse, big-picture outline of microgrids and hierarchical control architectures, leaving detailed descriptions of problem setups and technical details to later chapters of this dissertation.

1.1 Permissions and Attributions

1. Some of the content of Chapter 2 is the result of collaboration with Basilio Gentile, Florian Dörfler, and Sando Zampieri, and has previously appeared in [9]. Relevant material is Copyright © IEEE 2013.

2. Chapter 3 is the result of collaboration with Florian Dörfler, with some content previously appearing in [28, 29]. Reference [29] is Copyright © IEEE 2013, while [28] is Copyright © Elsevier 2013.

3. Chapter 4 is the result of collaboration with Florian Dörfler, Qobad Shafiee, Josep M. Guerrero, Juan C. Vasquez, with some content previously appearing in [30, 4]. References are Copyright © IEEE 2013 and 2015, respectively.

4. Some of the tangential contributions in Chapter 5 are the result of collaborations with Florian Dörfler and Hedi Bouattour, and have previously appeared in [16, 21, 2, 8, 3]. Reference [16] is Copyright © Elsevier 2014 while the remaining references are Copyright © IEEE 2013, 2014, and 2015.

1.2 Microgrids and Hierarchical Control

Economic factors, environmental concerns, and the rapidly expanding integration of small-scale renewable energy sources are all pushing the incumbent centralized power generation paradigm towards a more distributed future. As a bridge between high-voltage transmission and low-voltage distributed generation (DG), the concept of a *microgrid* continues to gain popularity [67, 40, 35, 25, 26]. Microgrids are low-voltage electrical distribution networks, heterogeneously composed of distributed generation, storage, load, and managed autonomously from the larger primary network. An example microgrid is shown in Figure 1.1. Microgrids can connect to a larger power system through a

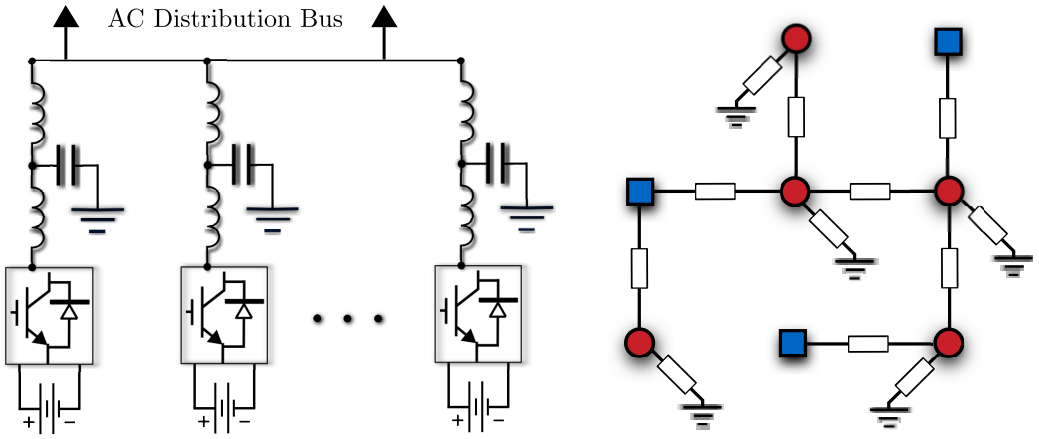

Figure 1.1: (a) Schematic of a "parallel" microgrid, in which several inverters supply power to a distribution bus (effectively a single load) (b) A simple non-parallel microgrid consisting of five loads ● and three inverters ■.

Point of Common Coupling (PCC), but are also able to "island" themselves and operate

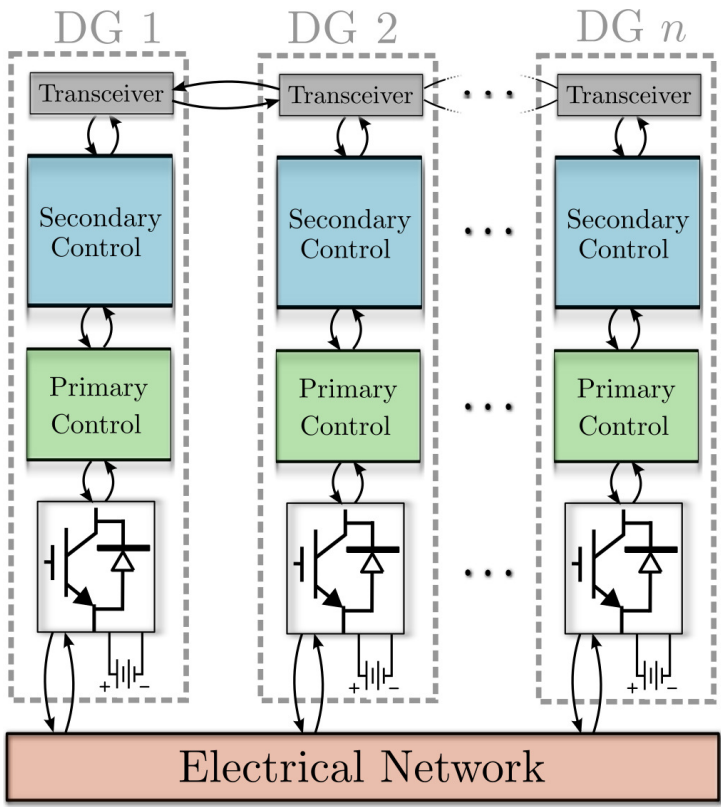

Figure 1.2: Low-detail schematic of microgrid control architecture.

independently [40]. Islanded operation of a microgrid could be planned, or could occur spontaneously if a fault triggers the disconnection of the microgrid from the primary grid.

Energy generation within a microgrid can be quite heterogeneous, including photovoltaic, wind, micro-turbines, etc. Such sources generate either DC power or variable frequency AC power, and are interfaced with a synchronous AC grid via power electronic *inverters*. It is through these inverters that cooperative actions must be taken to ensure synchronization, voltage regulation, power balance and load sharing in the network [59]. Control strategies ranging from centralized to completely decentralized have been proposed to address these challenges [45], and have subsequently been aggregated into a hierarchical control architecture [40] (Figure 1.2).

The control hierarchy consists of three levels. The first and most basic level is *primary*

control, which stabilizes the microgrid and establishes power sharing. Although centralized architectures have been used for primary control [45], in order to enhance redundancy and enable plug-and-play functionality, the current standard is to employ proportional control loops locally at each inverter. In Chapter 3 we provide additional introductory detail on these controllers. Our main contribution is the first detailed analyses of these controllers, giving necessary and sufficient conditions under which the network possess stable equilibrium points in closed-loop operation.

While successful for stabilization, these decentralized "droop" controllers force the bus voltages and the steady-state network frequency to deviate from their nominal values [85, 59, 49]. This leads naturally to the next level in the hierarchy, termed *secondary* control. Broadly speaking, the goal of secondary control is to remove the aforementioned deviations in both global frequency and local voltage [59]. Centralized techniques for secondary control have been well studied in high-voltage transmission and distribution networks [53]. These centralized strategies have also been applied in the context of microgrids, and the term "secondary" has been broadened to include additional control goals such as reactive power sharing [12, 14], harmonic compensation, and voltage unbalance [40, 59, 85, 36].

Several recent works (see Chapter 4) have proposed secondary control strategies for microgrids. However, to date no single control strategy has been able to offer a flexible, plug-and-play architecture guaranteeing frequency and voltage regulation while maintaining precise active and reactive power sharing among non-identical DGs. Currently, this combination of goals appears infeasible with decentralized control using only local information (voltage, power, ect.) at each DG [5]. As such, *communication between DGs* has been identified as a key ingredient in achieving these goals while avoiding a centralized control architecture [28, 30, 27, 5, 34, 21, 14]. In Chapter 4 we provide additional introductory information on secondary control. Our main contribution is our

development of a distributed secondary control architecture for frequency and voltage regulation in microgrids. This distributed architecture uses communication among inverters along with local control actions to achieve centralized control performance in a scalable, redundant way.

The final level of *tertiary* control is concerned with global economic dispatch over the network, and depends on current energy markets and prices. The focus of this thesis is not on tertiary control, and we comment only briefly on it in Chapter 5.2.

Chapter 2

Preliminaries and Models

This chapter recalls some preliminaries, introduces relevant models of power network components, algorithms for distributed averaging, and states a few basic results which will prove useful as foundational knowledge later on.

2.1 Mathematical Foundations: Graphs, Matrices, and Graph Matrices

In this section we introduce the basic mathematical tools and models used in this thesis. Our notation in this section is mostly standard, and we introduce only the essential concepts necessary to develop our subsequent results. We refer the interested reader to [47], for further details on matrix theory, [82, 69] for algebraic graph theory, and to [48, 44] for control applications of graphs and/or algebraic graph theory.

Sets, Numbers, and Functions: Given a finite set $\mathcal{V}$, let $|\mathcal{V}|$ denote its cardinality. The set $\mathbb{R}$ (resp. $\mathbb{R}_{\geq 0}$, $\mathbb{R}_{>0}$) is the field of real (resp. nonnegative real, strictly positive real) numbers, and $\mathbb{C}$ is the field of complex numbers. Throughout, $\mathbf{j}$ is the imaginary unit. For any $z \in \mathbb{C}$, $\mathrm{conj}(z)$ is its complex conjugate. For $x = (x_1, \ldots, x_n)^T \in \mathbb{R}^n$, $\mathbf{sin}(x) = (\sin(x_1), \ldots, \sin(x_n))^T \in \mathbb{R}^n$.

Vectors and matrices: Given a real n-tuple $(x_1, \ldots, x_n)$, we let $x \in \mathbb{R}^n$ be the associated vector. We let $\mathbb{1}_n$ and $\mathbb{0}_n$ be the n-dimensional vectors of unit and zero entries, while $\mathbb{0}$ denotes a zero matrix of appropriate dimension, determined by the context in which it is used. The $n \times n$ identity matrix is I_n. For $x \in \mathbb{R}^n$, $\text{span}(x) = \{v \in \mathbb{R}^n \ : \ v = \alpha x, \alpha \in \mathbb{R}\}$. The set $\mathbb{1}_n^\perp \triangleq \{x \in \mathbb{R}^n \ : \ \mathbb{1}_n^T x = 0\}$ is the subspace of all vectors in $\mathbb{R}^n$ orthogonal to $\text{span}(\mathbb{1}_n)$. Given $x \in \mathbb{R}^n$ or an equivalent n-tuple, $\text{diag}(x)$ or $\text{diag}(x_1, \ldots, x_n)$ denote the associated diagonal matrices with x on the diagonal. We will also find the equivalent compact notation $[x]$ useful for the same diagonal matrix. Given $x, y \in \mathbb{R}^n$, we write $x \gg y$ if $x_i > y_i$ for each $i \in \{1, \ldots, n\}$. For a vector $x \in \mathbb{R}^n$, $\|x\|_1 = \sum_{k=1}^n |x_k|$, $\|x\|_2 = (\sum_{i=k}^n x_k^2)^{1/2}$ and $\|x\|_\infty = \max_k |x_k|$.

For $A \in \mathbb{R}^{n \times m}$, $\ker(A)$ and $\text{Image}(A)$ denote the kernel and image of A, respectively. The *inertia* of $A \in \mathbb{R}^{n \times n}$ is the triple $\{\nu_s, \nu_c, \nu_u\}$, where ν_s (resp. ν_u) denotes the number of stable (resp. unstable) eigenvalues of A in the open left (resp. right) half complex plane, and ν_c denotes the number of "center" eigenvalues, which have zero real part. For $A = A^T \in \mathbb{R}^{n \times n}$, we implicitly will assume its eigenvalues are arranged in increasing order $\lambda_1(A) \leq \lambda_2(A) \leq \cdots \leq \lambda_n(A)$. For $A \in \mathbb{R}^{n \times n}$, $\|A\|_2 = |\lambda_{\max}(A)|$ (the largest absolute eigenvalue), while $\|A\|_\infty = \max_i \sum_{k=1}^n |A_{ik}|$.

A matrix $A \in \mathbb{R}^{n \times n}$ is a *Z-matrix* if $A_{ij} \leq 0$ for all $i \neq j$. The *spectral radius* $\rho(A)$ of a real-valued matrix $A \in \mathbb{R}^{n \times n}$ is $\rho(A) = \max\{|\lambda|_{\mathbb{C}} \ : \ \det(\lambda I_n - A) = 0\}$, where $|x|_{\mathbb{C}}$ is the magnitude of $x \in \mathbb{C}$. A Z-matrix $A \in \mathbb{R}^{n \times n}$ is an *M-matrix* if it can be expressed as $A = sI_n - B$, where $B \in \mathbb{R}^{n \times n}$ has nonnegative elements and $s \geq \rho(B)$. In this case A is positive definite, and the elements of A^{-1} are nonnegative [101]. Moreover, if the graph induced by the sparsity pattern of A is strongly connected, then A is irreducible and the elements of A^{-1} are all strictly positive [81, 101].

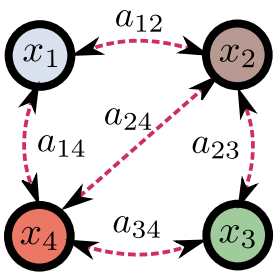

$$A = \begin{pmatrix} 0 & a_{12} & 0 & a_{14} \\ a_{12} & 0 & a_{23} & a_{24} \\ 0 & a_{23} & 0 & a_{34} \\ a_{14} & a_{24} & a_{34} & 0 \end{pmatrix}$$

Figure 2.1: Example of weighted graph and adjacency matrix for four nodes, with $\mathcal{V} = \{1, 2, 3, 4\}$ and $\mathcal{E} = \{(1, 2), (2, 1), (2, 3), (3, 2), (3, 4), \ldots\}$.

Digraphs and graph matrices: A *digraph* with n nodes is a triple $G = (\mathcal{V}, \mathcal{E}, A)$ where $\mathcal{V} = \{1, \ldots, n\}$ is the set of vertices (or nodes, or buses), $\mathcal{E} \subseteq \mathcal{V} \times \mathcal{V}$ is the set of directed edges (or branches, or lines), and $A \in \mathbb{R}^{n \times n}$ is the *adjacency matrix*. The entries of A satisfy $a_{ij} \geq 0$ for each edge $(i, j) \in \mathcal{E}$ and are zero otherwise. Note that any nonnegative matrix A induces a weighted directed graph G, where diagonal elements correspond to self-connections or *self-loops*. We typically restrict ourselves to digraphs without self-loops: all diagonal elements of A are zero. A directed path of length K on G from node i_0 to node i_ℓ is an ordered set of distinct nodes $\{i_0, i_1, \ldots, i_K\} \subset \mathcal{V}$ such that $(i_{k-1}, i_k) \in \mathcal{E}$ for each $j \in \{1, \ldots, K\}$. A *directed cycle of length* K is a non-trivial directed path $\{v_{i_0}, v_{i_1}, \ldots, v_{i_K}\}$ such that $v_{i_0} = v_{i_K}$. The *cycle space* of G is the subspace of $\mathbb{R}^{|\mathcal{E}|}$ spanned by the cycles of G. That is, by assigning a number $\ell \in \{1, \ldots, |\mathcal{E}|\}$ to each edge $(i, j) \in \mathcal{E}$, $\xi = (\ell_1, \ldots, \ell_{|\mathcal{E}|}$ is an element of the cycle space if the directed path induced by ξ is a directed cycle. The digraph is *acyclic* if the cycle space is empty. If there is a directed path in G from one node $i \in \mathcal{V}$ to another node $j \in \mathcal{V}$, then j is reachable from i. If node $i \in \mathcal{V}$ is reachable from every node $j \in \mathcal{V} \setminus \{i\}$ in the digraph, then i is *globally reachable*.

For each node $i \in \mathcal{V}$, the weighted out degree is $\deg_i = \sum_{j \neq i} a_{ij}$, corresponding to the sum of the weights of all outgoing edges from node i. The associated out-degree matrix is $\mathrm{diag}(\{\deg_i\}_{i=1}^n)$. The *Laplacian matrix* is defined as $L = \mathrm{diag}(\{\deg_i\}_{i=1}^n) - A$. Note that

by construction $\sum_{j=1}^{n} L_{ij} = 0$ for each $i \in \mathcal{V}$, and hence $\mathbb{1}_n \in \ker(L)$. It follows from the Geršgorin disk theorem [94, Theorem 6.1.1] that all eigenvalues of L have nonnegative real parts, and the zero eigenvalue is simple if and only if the digraph features a globally reachable node [61].

Undirected graphs and graph matrices: In this work we will be particularly interested in the special case of undirected graphs: a digraph $G = (\mathcal{V}, \mathcal{E}, A)$ is undirected if $(i,j) \in \mathcal{E}$ and $a_{ij} > 0$ implies that $(j,i) \in \mathcal{E}$ and $a_{ji} = a_{ij}$. Since the edges are bidirectional and of identical weight, we will simply write $\{i,j\} \in \mathcal{E}$ to refer to the single undirected edge. In this case, the adjacency and Laplacian matrices are symmetric: $A = A^T$ and $L = L^T$.

If a unique number $\ell \in \{1, \ldots, |\mathcal{E}|\}$ and an arbitrary direction are assigned to each edge $\{i,j\} \in \mathcal{E}$, the (oriented) *node-edge incidence matrix* $H \in \mathbb{R}^{n \times |\mathcal{E}|}$ is defined component-wise by $H_{k\ell} = 1$ if node k is the sink node of edge ℓ and $H_{k\ell} = -1$ if node k is the source node of edge ℓ; all other elements are zero. Note that for $x \in \mathbb{R}^n$, $H^T x \in \mathbb{R}^{|\mathcal{E}|}$ is the vector of edge-wise differences $x_i - x_j$. If $\mathcal{A} = \operatorname{diag}(\{a_{ij}\}_{\{i,j\} \in \mathcal{E}}$ is the diagonal matrix of edge weights, then one may show that

$$L = H \mathcal{A} H^T .$$

If the graph is connected, then $\operatorname{Ker}(H^T) = \operatorname{Ker}(L) = \operatorname{span}(\mathbb{1}_n)$, and all $n-1$ non-zero eigenvalues of L are strictly positive. The second smallest eigenvalue $\lambda_2(L)$ is termed the *algebraic connectivity*, and quantifies the convergence speed of the distributed averaging algorithms we will employ in the sequel. It can be shown that $\lambda_2(L) > 0$ if and only if G is connected.

It can be shown that the cycle space of G is given by $\ker(H)$. In particular, G is

acyclic if and only if $\ker(H) = \emptyset$. This implies that for every $x \in \mathbb{1}_n^\perp$, there exists a unique $\xi \in \mathbb{R}^{|\mathcal{E}|}$ such that $H\xi = x$. The vector x can be interpreted as a vector of injections of some quantity (for example, electrical current); $x \in \mathbb{1}_n^\perp$ means that inflows must balance outflows, and ξ is then interpreted as the resulting branch-wise flows of this quantity within the graph.

Differential-Algebraic Systems: Consider the differential-algebraic system

$$\mathbb{0}_n = g(x, y)\,, \quad \dot{x} = f(x, y)\,, \tag{2.1}$$

where $x \in \mathbb{R}^m$, $y \in \mathbb{R}^n$, and $f : \mathbb{R}^{n+m} \to \mathbb{R}^m$, $g : \mathbb{R}^{n+m} \to \mathbb{R}^n$ are sufficiently smooth. Let $\mathcal{M} = \{(x, y) \in \mathbb{R}^{n+m} \ : \ \mathbb{0}_n = g(x, y)\}$ be the constraint set of (2.1), and define the *singular set* $\mathcal{S}$ of $g(x, y)$ by

$$\mathcal{S} \triangleq \left\{ (x, y) \in \mathcal{M} \;\middle|\; \det \frac{\partial g}{\partial y} = 0 \right\}. \tag{2.2}$$

The singular set $\mathcal{S}$ decomposes $\mathcal{M}$ into open sets $\mathcal{M}_i$ where $\det \frac{\partial g}{\partial y}$ is sign-definite and such that $\mathcal{M} = \mathcal{S} \cup (\cup_i \mathcal{M}_i)$. Components $\mathcal{M}_i$ with $\det \frac{\partial g}{\partial y} < 0$ (resp. $\det \frac{\partial g}{\partial y} > 0$) are called *stable* (resp. *unstable*)[100].

2.2 Electric Power Grids

For our purposes, an AC electric power grid is most conveniently modeled using circuit theoretic tools. For stable and reliable operation, the frequencies of all AC signals in power grids must remain very close to the nominal network frequency of $\omega^*/2\pi$ =50/60Hz; a frequency deviation of only a few percent is enough to cause protection equipment to trip devices out of the network, potentially resulting in a large-scale blackout. For practical

operation, we may therefore assume quasi-synchronous operation, and represent time varying signals $f(t)$ within the grid as harmonic signals $f(t) = \mathrm{Re}(Fe^{\mathbf{j}\omega^* t})$, where $F \in \mathbb{C}$ is the amplitude of the harmonic signal, containing both magnitude and phase-shift information. This phasor modeling allows for the convenient representation of voltages and currents in terms of magnitude and phase, and for the modeling of transmission lines as static impedances as opposed to partial or ordinary differential equations.

2.2.1 Phasor Modeling and AC Power Flow

We may model a power grid in quasi-synchronous steady-state as a undirected, connected, and complex-weighted graph $G = (\mathcal{V}, \mathcal{E}, A)$, where $\mathcal{V}$ is the set of buses and $\mathcal{E}$ is the set of transmission lines. We partition the set of buses as $\mathcal{V} = \mathcal{L} \cup \mathcal{I}$; buses $\mathcal{L}$ will correspond to *load* buses, while buses $\mathcal{I}$ will be associated with *inverters*. The modeling distinctions between these two sets of buses will be covered shortly. For notational convenience, we set $n \triangleq |\mathcal{L}|$ and $m \triangleq |\mathcal{I}|$, for a total of $n + m$ buses. An edge $\{i, j\} \in \mathcal{E}$ corresponds to a transmission line, with which we associate a complex-valued *admittance* $y_{ij} = g_{ij} + \mathbf{j}b_{ij} \in \mathbb{C}$. The *conductance* of the transmission line is g_{ij}, while the *susceptance* of the line is b_{ij}. It is always the case that $g_{ij} = 0$, while for typical lines with inductive characteristics $b_{ij} \leq 0$.

The large-scale structure of a power grid is most conveniently described by the *bus admittance matrix* $Y \in \mathbb{C}^{(n+m)\times(n+m)}$, a Laplacian-like matrix which encodes the topology and branch-weights of the network. In the absence of phase-shifting transformers, the

admittance matrix is symmetric $Y = Y^T$ and may be defined element-wise as

$$Y_{ij} = \begin{cases} -y_{ij} & \text{if } i \neq j \text{ and } \{i,j\} \in \mathcal{E} \\ 0 & \text{if } i \neq j \text{ and } \{i,j\} \notin \mathcal{E} \\ \sum_{j \neq i} y_{ij} + y_{\text{shunt},i} & \text{if } i = j\,, \end{cases} \tag{2.3}$$

where $y_{\text{shunt},i} \in \mathbb{C}$ is the shunt admittance (direct connection to ground) at bus $i \in \mathcal{V}$.

To each node $i \in \mathcal{V}$, we associate a voltage phasor $V_i \in \mathbb{C}$ and a phasor current injection $I_i \in \mathbb{C}$. Similarly, along each edge $\{j,k\}$ we associate a complex voltage difference $v_{jk} \in \mathbb{C}$[1] and a current flow $i_{jk} \in \mathbb{C}$. With this notation, Kirchoff's voltage law, current law, and Ohm's law may be written as

$$v_{jk} = V_j - V_k\,, \tag{2.4a}$$

$$I_j = \sum\nolimits_{k \in \mathcal{V}} i_{jk} + i_{\text{shunt},j}\,, \tag{2.4b}$$

$$i_{jk} = y_{jk} v_{jk}\,, \tag{2.4c}$$

$$i_{\text{shunt},j} = y_{\text{shunt},j} V_j \tag{2.4d}$$

where $i_{\text{shunt},j}$ is the shunt current to ground at node j. In vector notation this reads as

$$v = H^T V\,, \tag{2.5a}$$

$$I = Hi + i_{\text{shunt}}\,, \tag{2.5b}$$

$$i = \text{diag}(\{y_{ij}\}_{\{i,j\} \in \mathcal{E}}) v\,, \tag{2.5c}$$

$$i_{\text{shunt}} = \text{diag}(y_{\text{shunt}}) V\,. \tag{2.5d}$$

[1]Reference directions for this difference are taken as the same as those used in the definition of the incidence matrix, although this choice is not necessary.

where B is the node-edge incidence matrix of the graph and all variables have been vectorized in the obvious manner. Eliminating v, i and i_{shunt} from (2.5), we obtain

$$I = \left(H\text{diag}(\{y_{ij}\}_{\{i,j\}\in\mathcal{E}})H^T + \text{diag}(y_{\text{shunt}})\right)V\,.$$

A little thought shows that the matrix in brackets is exactly the bus admittance matrix Y, and we have therefore derived the nodal relationship

$$I = YV\,.$$

and the vectorized formula for Y as

$$Y = H\text{diag}(\{y_{ij}\}_{\{i,j\}\in\mathcal{E}})H^T + \text{diag}(y_{\text{shunt}})\,.$$

Unlike a standard Laplacian matrix, the row sums of the bus admittance matrix Y are not necessarily zero.

The complex electrical power $S_{\text{e},i} = P_{\text{e},i} + \mathbf{j}Q_{\text{e},i}$ injected into node $i \in \mathcal{V}$ is defined as $S_i = V_i \cdot \text{conj}(I_i)$. In vector notation, this reads as $S_{\text{e}} = V \circ \text{conj}(YV)$, where $\circ$ is the Hadamard (element-wise) product. We now represent the phasor voltage in polar form as $V_i = E_i e^{\mathbf{j}\theta_i} \in \mathbb{C}$ corresponding to the magnitude $E_i > 0$ and the phase angle $\theta_i \in \mathbb{S}^1$ of the harmonic voltage signal at bus $i \in \mathcal{V}$. Similarly, we decompose the admittance matrix in rectangular form as $Y = G + jB$, where $G \in \mathbb{R}^{(n+m)\times(n+m)}$ is the *conductance matrix* and $B \in \mathbb{R}^{(n+m)\times(n+m)}$ is the susceptance matrix. With some effort, one may

expand out the nodal power relations to obtain the *power flow equations*

$$P_{\mathrm{e},i} = \sum\nolimits_{j\in\mathcal{V}} B_{ij}E_iE_j \sin(\theta_i-\theta_j) + \sum\nolimits_{j\in\mathcal{V}} G_{ij}E_iE_j\cos(\theta_i-\theta_j)\,, \quad i\in\mathcal{V}\,, \tag{2.6a}$$

$$Q_{\mathrm{e},i} = -\sum\nolimits_{j\in\mathcal{V}} B_{ij}E_iE_j \cos(\theta_i-\theta_j) + \sum\nolimits_{j\in\mathcal{V}} G_{ij}E_iE_j\sin(\theta_i-\theta_j)\,, \quad i\in\mathcal{V}\,. \tag{2.6b}$$

The quantity $P_{\mathrm{e},i}$ is called the *active* (or *real*) power, and represents the average over one AC cycle of the power which can be used to do work. Active power results from current draw which is in phase with the nodal voltage, and is the type of power we often speak of informally. Conversely, $Q_{\mathrm{e},i}$ is termed the *reactive power*, and is associated with current injection I_i which is $\pi/2$ out of phase with the nodal voltage V_i. If $Q_{\mathrm{e},i}<0$, bus $i\in\mathcal{V}$ is consuming reactive power, an inductive-type behavior. Conversely, $Q_{\mathrm{e},i}>0$, corresponds to an injection of reactive power, associated with capacitive behavior of the device connected at bus i.

Unlike active power which represents an average, reactive power represents the peak power needed to energize the electromagnetic fields of the device connected at bus i during each AC cycle. This electromagnetic energy is stored and released during each AC cycle, and thus averages to zero. While active power takes economic effort to produce, reactive power can be produced with zero marginal cost by appropriate equipment. However, like active power, the transmission of reactive power contributes to total transmission losses, and it is therefore desirable to either generate reactive power as close as possible to its point of consumption, or to compensate loads such that they consume less reactive power (for example, shunt compensation).

Since we will use it extensively in this thesis, we collect here some properties of the susceptance matrix B.

Lemma 2.2.1. (Properties of Susceptance Matrix). *Consider a connected linear electrical network describable by an admittance matrix $Y = G + \mathbf{j}B$. Assume that*

the network is connected, that all lines have inductive characteristics (i.e., no line is overcompensated by series capacitors), and that the network contains no phase shifting transformers. Then the susceptance matrix B satisfies

(i) **Symmetry:** $B = B^T$;

(ii) **Inductive Lines:** $B_{ij} \geq 0$ *for* $i \neq j$, *with strict inequality if and only if* $\{i, j\} \in \mathcal{E}$, *and* $B_{ii} < 0$ *for all* $i \in \mathcal{V}$;

(iii) **Definiteness:** *If the network contains no reactive shunt elements (including line charging capacitors), then B is negative semidefinite with a simple eigenvalue at zero corresponding to the eigenvector $\mathbb{1}_{n+m}$. If the network contains no shunt capacitors but contains at least one shunt reactor, then B is negative definite.*

Lemma 2.2.1 (iii) follows from diagonal dominance arguments.

2.2.2 Decoupled AC Power Flow

For the analysis and design purposes of this work the lossy coupled AC power equations (2.6) must be simplified to a more tractable form. The first simplification we perform is to neglect the conductance matrix G, and assume that lines are dominantly inductive, resulting in the lossless coupled AC power flow equations

$$P_{\mathrm{e},i} = \sum\nolimits_{j\in\mathcal{V}} B_{ij} E_i E_j \sin(\theta_i - \theta_j)\,, \quad i \in \mathcal{V}\,, \tag{2.7a}$$

$$Q_{\mathrm{e},i} = -\sum\nolimits_{j\in\mathcal{V}} B_{ij} E_i E_j \cos(\theta_i - \theta_j)\,, \quad i \in \mathcal{V}\,. \tag{2.7b}$$

The second and final key simplification we make is the classic *active/reactive power decoupling assumption* [84, 76], where

(i) voltage magnitudes E_i, E_j are held constant at nominal values in (2.7a), leaving the active power injection as a function of only the phase angles, and

(ii) phase angle difference $\theta_i - \theta_j$ are held constant at nominal values (typically approximated as zero) in (2.7b), leaving the reactive power injection as a function of only the voltage magnitudes E_i and E_j.

This assumption is based on the linearized behavior of (2.7) around practical power grid operating points, which typically satisfy $|\theta_i - \theta_j| < 1$ for all $\{i, j\} \in \mathcal{E}$. It follows by examining the system Jacobian that $\partial P_{\mathrm{e}}/\partial E \simeq \mathbb{0}$ and $\partial Q_{\mathrm{e}}/\partial \theta \simeq \mathbb{0}$, leading to the decoupling assumption. Under the decoupling assumption, we obtain the *decoupled power flow equations*

$$P_{\mathrm{e},i}(\theta) = \sum\nolimits_{j\in\mathcal{V}} B_{ij} E_i E_j \sin(\theta_i - \theta_j)\,, \quad i \in \mathcal{V}\,, \tag{2.8a}$$

$$Q_{\mathrm{e},i}(E) = -\sum\nolimits_{j\in\mathcal{V}} B_{ij} E_i E_j\,, \quad i \in \mathcal{V}\,. \tag{2.8b}$$

In particular, the decoupling assumption allows us to treat frequency and voltage control problems as decoupled from one another, significantly simplifying analysis and design. Additional information and results regarding decoupled load flow are available in [96, 92, 93].

Observations regarding decoupled active power flow: The decoupled active power flow (2.8a) displays a clear diffusive behavior, with branch-wise power flows $B_{ij}E_iE_j \sin(\theta_i - \theta_j)$ from bus i to bus j ($\{i, j\} \in \mathcal{E}$) depending only on the odd coupling function $\sin(\theta_i - \theta_j)$. It follows that $\sum_{i\in\mathcal{V}} P_{\mathrm{e},i}(\theta) = 0$, since each term $B_{ij}E_iE_j \sin(\theta_i - \theta_j)$ matches with an equal and opposite term $B_{ij}E_iE_j \sin(\theta_j - \theta_i)$ in the sum. This is simply the statement that the network lines are lossless, and dissipate no active power. It follows that active power satisfies a KCL conservation law of the form $P_{\mathrm{e},i}(\theta) = H \cdot \xi(\theta)$, where $\xi_{ij}(\theta) = B_{ij}E_iE_j \sin(\theta_i - \theta_j)$. In vector notation, the decoupled active power flow therefore

reads as

$$P_{\mathrm{e}}(\theta) = H \cdot \mathrm{diag}(\{B_{ij}E_iE_j\}_{\{i,j\}\in\mathcal{E}}) \cdot \mathbf{sin}(H^T\theta)\,.$$

Observations regarding decoupled reactive power flow: While the active power flow is diffusive and sinusoidal, the decoupled reactive power flow (2.8b) appears to be quadratic, and when written in the form (2.8b), the diffusive character of the reactive power flow is less apparent. However, using the definition of the admittance matrix from (2.3), one may equivalently write (2.8b) as

$$Q_{\mathrm{e},i}(E) = -b_{\mathrm{shunt},i}E_i^2 + E_i \sum\nolimits_{j\in\mathcal{V}} B_{ij}(E_i - E_j)\,.$$

While the presence of terms $E_i - E_j$ suggests a diffusive behavior, there are two notable wrinkles. First, the presence of shunt capacitors or reactors generates reactive power injections which scale as the square of the local voltage E_i, independent of neighboring buses. Second, the coupling function in the second term is no longer odd, since the sum is scaled by E_i. A consequence of this is that, unlike active power, reactive power satisfies no clean conservation law, as one may verify by noting that

$$\sum\nolimits_{j\in\mathcal{V}} Q_{\mathrm{e},i} = -\sum\nolimits_{j\in\mathcal{V}} b_{\mathrm{shunt},i}E_i^2 + \sum\nolimits_{i,j\in\mathcal{V}} B_{ij}(E_i - E_j)^2\,.$$

That is, reactive power is dissipated by inductive lines and shunts. In vector notation, the decoupled active power flow (2.8b) reads simply as

$$Q_{\mathrm{e}}(E) = -[E]BE\,, \tag{2.9}$$

where $[E] = \mathrm{diag}(E)$.

Remark 2.2.1. (State Space of Reactive Power Flow). *Within the phasor modeling*

framework, E_i represents a voltage magnitude*, and we therefore restrict our attention to voltage magnitude vectors $E \in \mathbb{R}^{n+m}_{\geq 0}$. Additionally, it is convenient to further exclude the case where any voltage magnitude is identically zero, and we therefore assume that $E \in \mathbb{R}^{n+m}_{>0}$. If the voltage magnitude at any bus was identically zero, the corresponding power injection must be identically zero, and the node can be eliminated from the network via Kron reduction. This choice of state space will simplify our analysis by excluding non-physical and short-circuit equilibria which would not occur in practice.* □

Remark 2.2.2 (Lossless and Decoupling Assumptions)**.** *. The approximation of lossless power flow is usually valid in high-voltage transmission networks, where the inductive characteristics of lines dominate any resistive losses; typical transmission losses are on the order of 8%, which for control design purposes may be neglected. Low-voltage grids typically do not enjoy such favorable line characteristics, with conductance/susceptance ratios in distribution grids on the order of unity. Nonetheless, the lossless assumption is typically justified in the setting of microgrids, which are highly engineered. In particular, inverter output impedances can be controlled to dominate over network impedances [60],[35, Chapter 7]. Moreover, under the less restrictive assumption of uniform reactance/resistance ratios $\varphi = \operatorname{atan2}(-b_{ij}, g_{ij}) = const.$, the change of coordinates*[2]

$$\begin{bmatrix} \tilde{P}_{\mathrm{e},i} \\ \tilde{Q}_{\mathrm{e},i} \end{bmatrix} = \begin{bmatrix} \sin(\varphi) & -\cos(\varphi) \\ \cos(\varphi) & \sin(\varphi) \end{bmatrix} \begin{bmatrix} P_{\mathrm{e},i} \\ Q_{\mathrm{e},i} \end{bmatrix}$$

transforms the lossy equations (2.6) *into a form identical to the lossless equations* (2.7)*, with the susceptance matrix entries being modified as $\widetilde{B}_{ij} = B_{ij}\sqrt{1+\tan^2\varphi}$. For example, the constant R/X assumption holds if all transmission lines are made from the same material. While this coordinate transformation robs active and reactive power of their*

[2]Strictly speaking, all shunt admittances must also share this common reactance/resistance ratio.

physical meanings, for control purposes it allows for techniques from decoupled power flow to be applied rigorously in lossy grids for frequency and voltage stabilization.

The decoupling assumption is extremely accurate in practical power networks, and has been shown to yield accurate even far from the normal operating regime [9]. Extremely close to the bifurcation points of the system, the decoupling assumption must be taken with caution; voltage magnitudes can no longer be considered as constant in the active power flow, and phase angles can no longer be considered as small in the reactive power flow. From the perspective of control design though we are interested in a regime around nominal operating conditions, and in the sequel, we may without much loss of detail restrict our attention to the decoupled power flow equations (2.8). □

2.2.3 Linear Approximations for Reactive Power Flow

We review here the approximation techniques developed in [9] for the decoupled reactive power flow equation (2.9). This approximation technique will be used in Section (3.3.1) to investigate the stability properties of equilibria for voltage dynamics under our proposed quadratic droop controller. We assume that all loads are constant power loads $Q_{\mathrm{load},i}(E_i) = Q_i^*$, and assume that the voltage magnitudes E_i at inverter buses $i \in \mathcal{I}$ are fixed. As we will see in Section 3.3.1, these assumptions are not restrictive, and the resulting formulae can be adapted to study system behavior under different load models and for inverters implementing droop control rather than regulating their voltages. We partition the bus susceptance matrix B, the vector of voltage magnitudes E, and the vector of power injections Q_{e} according to loads and inverters as

$$B = \begin{pmatrix} B_{LL} & B_{LI} \\ B_{IL} & B_{II} \end{pmatrix}, \qquad E = \begin{pmatrix} E_L \\ E_I \end{pmatrix}, \qquad Q_{\mathrm{e}} = \begin{pmatrix} Q_L \\ Q_I \end{pmatrix}.$$

With this notation, the reactive power balance equation at the load buses $i \in \mathcal{L}$ can be written in vector notation as

$$Q_L = -[E_L](B_{LL}E_L + B_{II}E_I)\,. \tag{2.10}$$

Define the *open-circuit load voltages* $E_L^{\mathrm{oc}} \in \mathbb{R}^n_{>0}$ and the *short-circuit load matrix* $Q_{\mathrm{crit}} \in \mathbb{R}^{n\times n}$ by

$$\begin{aligned} E_L^{\mathrm{oc}} &= -B_{LL}^{-1}B_{LI}E_I\,,\\ Q_{\mathrm{sc}} &= [E_L^{\mathrm{oc}}]B_{LL}[E_L^{\mathrm{oc}}]\,. \end{aligned}$$

In particular, note that E_L^{oc} is the unique high-voltage solution of (2.10) when $Q_L = \mathbb{0}_n$. In [9] it was shown that then the high-voltage solution of (2.8b) is given to first order by

$$E_L = [E_L^{\mathrm{oc}}]\left(\mathbb{1}_n + Q_{\mathrm{sc}}^{-1}Q_L\right) + \text{h.o.t.}\,. \tag{2.12}$$

See [9, 24] for a quantification of the error term. The basic formula can be derived by linearizating the system (2.9) around the open-circuit solution E_L^{oc}. The "short-circuit ratio" $Q_{\mathrm{sc}}^{-1}Q_L$ quantifies the percentage deviation $(E_i - E_i^{\mathrm{oc}})/E_i^{\mathrm{oc}}$ of how far the load voltages E_L deviate from their open-circuit values E_L^{oc}.

2.2.4 Microgrids and DC/AC Inverters

radial topology

$$\omega_i = u_i\,, \qquad i \in \mathcal{I}\,, \tag{2.13a}$$

$$\tau_i\dot{E}_i = v_i\,, \qquad i \in \mathcal{I}\,. \tag{2.13b}$$

Comment on actuation delay for frequency change as well.

2.2.5 Load Modeling

A *load model* is a static or dynamic model which specifies how the power consumption at a load bus $i \in \mathcal{L}$ evolves over time as a function internal states and external network conditions. Load modeling is one of the most complex and controversial aspects of power systems analysis. Despite decades of research, no consensus has been achieved regarding the most appropriate load models for different types of stability studies, and it seems likely that this will remain the case. Not surprisingly, a large spectrum of possible load models exists with varying levels of complexity. The simplest class of models are *static* load models, which specify the active $P_{\text{load},i}$ and reactive $Q_{\text{load},i}$ power injections (negative demands) of loads as algebraic functions of local frequency deviations and local voltage levels, resulting in the nodal power balance requirements

$$0 = P_{\text{load},i} - P_{\text{e},i}\,, \qquad i \in \mathcal{L}\,, \tag{2.14a}$$

$$0 = Q_{\text{load},i} - Q_{\text{e},i}\,, \qquad i \in \mathcal{L}\,. \tag{2.14b}$$

In this thesis we will focus on the network-theoretic aspects of power grid stability, it behooves us to minimize the complexity of nodal dynamics, and we therefore consider the following static models for load buses $i \in \mathcal{L}$.

Constant active power loads: These load models will be used in Section 3.2 for our analysis of primary frequency control. All load buses $i \in \mathcal{L}$ are assumed to be *PV buses* with fixed voltage magnitudes E_i and fixed active power injections $P_i^* \in \mathbb{R}$, yielding the model

$$P_{\text{load},i} = P_i^*\,, \qquad i \in \mathcal{L}\,. \tag{2.15}$$

With our sign conventions, $P_i^* < 0$ corresponds to power consumption, while $P_i^* > 0$ corresponds to power production. This model is standard in load flow analyses where the goal is to characterize the steady-state operating point of the network after transients have died out. Note that the model results in a static algebraic equation, and thus when paired with dynamic models of inverters, the resulting closed-loop system is differential-algebraic.

Frequency-dependent active power loads: These load models will also be used in Section 3.2 for our analysis of primary frequency control. All load buses $i \in \mathcal{L}$ are assumed to be *PV buses* with fixed voltage magnitudes E_i and fixed active power injections $P_i^* \in \mathbb{R}$, yielding the model

$$P_{\text{load},i} = P_i^* - D_i \dot{\theta}_i \,, \qquad i \in \mathcal{L} \,. \tag{2.16}$$

With our sign conventions, $P_i^* < 0$ corresponds to power consumption, while $P_i^* > 0$ corresponds to power production. The gain D_i is always positive. This model was proposed in [98] for bulk power systems, and a derivation from first principles can be found in [75, Chapter 7]. While the presence of $\dot{\theta}_i$ in fact results in a differential equation for the load, the model is still termed "static" as it lacks internal state variables.

General reactive power loads: We assume a static load model for reactive power of the form

$$Q_{\text{load},i} = Q_{\text{load},i}(E_i) \,, \tag{2.17}$$

that is, a smooth function of a local supplied voltage E_i. To state more detailed results, we will at times find it useful to specialize this model to the so-called *ZIP* model, where reactive power demand is modeled as a second-order polynomial in the local voltage E_i.

The model takes the form

$$Q^{\text{ZIP}}_{\text{load},i} = b_{\text{shunt},i}E_i^2 + I_{\text{shunt},i}E_i + Q_i^* \,, \quad i \in \mathcal{L} \,, \tag{2.18}$$

where $b_{\text{shunt},i}$ represents a shunt admittance, $I_{\text{shunt},i}$ represents a constant shunt current, and Q_i^* represents a constant power consumption. For inductive loads which consume reactive power, these parameters are negative, while for capacitive loads they are positive. At times for analytical or notational reasons we will find it convenient to specialize more by removing terms to arrive at the ZI model

$$Q^{\text{ZI}}_{\text{load},i} = b_{\text{shunt},i}E_i^2 + I_{\text{shunt},i}E_i \,, \quad i \in \mathcal{L} \,, \tag{2.19}$$

and the P model

$$Q^{\text{P}}_{\text{load},i} = Q_i^* \,, \quad i \in \mathcal{L} \,. \tag{2.20}$$

2.3 The Generalized Kuramoto Model of Oscillator Networks

Another set of literature relevant to our investigation is that pertaining to synchronization of phase-coupled oscillators, in particular the classic and celebrated *Kuramoto model*. A generalization of this model considers $n \geq 2$ coupled oscillators, each represented by a phase $\theta_i \in \mathbb{S}^1$ (the unit circle) and a natural frequency $\Omega_i \in \mathbb{R}$. The system of coupled oscillators obeys the dynamics

$$D_i\dot{\theta}_i = \Omega_i - \sum\nolimits_{j=1}^{n} a_{ij}\sin(\theta_i - \theta_j) \,, \; i \in \{1, \ldots, n\} \,, \tag{2.21}$$

where $a_{ij} \geq 0$ is the coupling strength between the oscillators i and j and D_i is the time constant of the i^{th} oscillator. Figure 2.2 shows a mechanical analog of (2.21), in

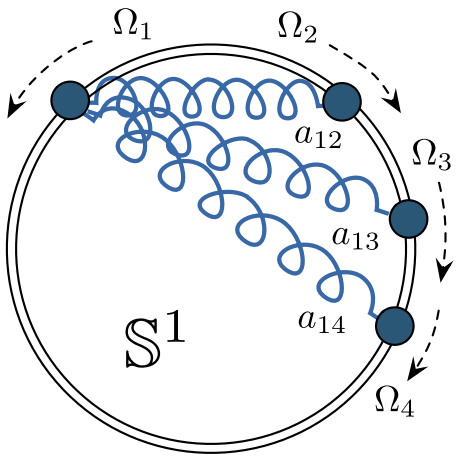

Figure 2.2: Mechanical analog of a Kuramoto oscillator network. The particles have no inertia and do not collide with another.

which the oscillators can be visualized as a group of n kinematic particles, constrained to rotate around the unit circle. The particles rotate with preferred directions and speeds specified by the natural frequencies Ω_i, and are connected together by elastic springs of stiffness a_{ij}. The rich dynamic behavior of the system (2.21) arises from the competition between the tendency of each oscillator to align with its natural frequency Ω_i, and the synchronization enforcing coupling $a_{ij}\sin(\theta_i - \theta_j)$ with its neighbors. We refer to the recent surveys [51, 73, 39] for applications and theoretic results.

Torus Geometry and Synchronization: The set $\mathbb{S}^1$ denotes the *unit circle*, an *angle* is a point $\theta \in \mathbb{S}^1$, and an *arc* is a connected subset of $\mathbb{S}^1$. The *geodesic distance* between two angles $\theta_1, \theta_2 \in \mathcal{S}^1$, denoted by $|\theta_1 - \theta_2|$, is the minimum length of the counter-clockwise and clockwise arcs connecting θ_1 and θ_2. The *n-torus* $\mathbb{T}^n = \mathbb{S}^1 \times \cdots \times \mathbb{S}^1$ is the Cartesian product of n unit circles. For $\gamma \in [0, \pi/2[$ and a given graph $G(\mathcal{V}, \mathcal{E}, \cdot)$, let $\Delta_G(\gamma) = \{\theta \in \mathbb{T}^{|\mathcal{V}|} : \max_{\{i,j\}\in\mathcal{E}} |\theta_i - \theta_j| \leq \gamma\}$ be the closed set of angle arrays $\theta = (\theta_1, \ldots, \theta_n)$ with neighboring angles θ_i and θ_j, $\{i, j\} \in \mathcal{E}$ no further than γ apart.

Consider the first order phase-coupled oscillator model (2.21) defined on a graph

$G(\mathcal{V}, \mathcal{E}, \cdot)$. A solution $\theta : \mathbb{R}_{\geq 0} \to \mathbb{T}^{|\mathcal{V}|}$ of (2.21) is said to be *synchronized* if (a) there exists a constant $\omega_{\text{sync}} \in \mathbb{R}$ such that for each $t \geq 0$, $\dot{\theta}(t) = \omega_{\text{sync}} \mathbb{1}_{|\mathcal{V}|}$ and (b) there exists a $\gamma \in [0, \pi/2[$ such that $\theta(t) \in \Delta_G(\gamma)$ for each $t \geq 0$.

2.4 Distributed Averaging Algorithms

This section overviews distributed averaging (or more simply, consensus) protocols from multi-agent systems. We review the basic ideas, properties, and convergence results. Our treatment focuses on protocols written as continuous-time dynamical systems; analogous statements can be made in discrete-time.

2.4.1 Continuous-Time Agreement Protocols (Consensus)

Consider a system consisting of n autonomous agents, each characterized by a scalar state variable $x_i \in \mathbb{R}^n$. A rudimentary task for the agents to perform is to achieve agreement on a common state value. For example, if the agents represent autonomous vehicles, it may be desirable to agree on a rendezvous location, or to agree on a common alignment and speed for group locomotion. The agents can not communicate with each other in an arbitrary fashion, but can interact only through a digraph $G = (\mathcal{V}, \mathcal{E}, A)$ with the adjacency matrix $A \in \mathbb{R}^{n \times n}$ describing the interaction between agents. This interaction could consist of communication, or a form of physical coupling through a common infrastructure network (such as a power grid). More formally, consensus is achieved asymptotically if

$$\lim_{t \to +\infty} x_i(t) = x_\infty \,,$$

for each agent $i \in \mathcal{V}$ and some finite $x_\infty \in \mathbb{R}$. To achieve this objective, consider the *consensus protocol* [57, 58, 48, 43, 44]

$$\dot{x}_i = -\sum\nolimits_{j\in\mathcal{V}} a_{ij}(x_i - x_j)\,, \qquad i \in \mathcal{V}\,. \tag{2.22}$$

By rearranging (2.22), we may equivalently write

$$\frac{1}{\deg_i}\dot{x}_i = -x_i + \sum\nolimits_{j\neq i} w_{ij}x_j\,,$$

where the coefficients $w_{ij} = a_{ij}/\deg_i$ are nonnegative and satisfy $\sum_j w_{ij} = 1$ for all $i \in \mathcal{V}$. That is, with time constant $1/\deg_i$, the state of agent $i \in \mathcal{V}$ evolves towards a convex combination (weighted average) of its neighbors states. In vector notation, (2.22) reads as $\dot{x} = -Lx$, where L is the Laplacian matrix of G. As noted in Section 2.1, it holds that $\ker(L) = \operatorname{span}(\mathbb{1}_n)$. It follows that the consensus dynamics (2.22) are *translationally invariant*, meaning that $x(t)$ and $x(t) + c\mathbb{1}_n$ satisfy the same dynamics, for any choice of $c \in \mathbb{R}$. The equilibrium subspace $\operatorname{span}(\mathbb{1}_n)$ is called the agreement subspace. It can be shown that the agreement subspace is exponentially stable if and only if the graph G has a globally reachable node.

While various extensions are possible, in this work we will make use of only the simplest consensus algorithms. In particular, we will assume that the interaction topology described by G is undirected and constant for all time, and that the edge weights a_{ij} are also constant. In this case, the graph has a globally reachable node if and only if it is connected, which we assume throughout. Let $\bar{x} = \frac{1}{n}\mathbb{1}_n^T x$ be the average of the state variables across all agents. Then

$$\dot{\bar{x}}(t) = -\mathbb{1}_n^T L x(t) = \mathbb{0}_n\,.$$

Thus, the average of the states is a conserved quantity for all $t \geq 0$. We conclude that if the consensus protocol is convergent, the asymptotic consensus value x_∞ must be equal to the average of the initial conditions, $x_\infty = \frac{1}{n}\mathbb{1}_n^T x(0)$. Using the disagreement vector $\delta = x - x_\infty \mathbb{1}_n$ and the quadratic Lyapunov function $V(\delta) = \|\delta\|_2^2$, a simple calculation shows that the convergence rate of the consensus protocol (2.22) is no worse than $\lambda_2(L)$, the algebraic connectivity.

Chapter 3

Primary Control of Inverter-Based Power Grids

3.1 Introduction

Primary control is the first layer in the control hierarchy for microgrids, and is concerned with the fast balancing of active and reactive power demands over time-scales on the order of seconds. This balancing of power is required to maintain network stability. A key additional objective of interest within the microgrid community is that of accurately sharing both active and reactive power among a bank of inverters operated *in parallel*. Such a network is depicted in Figure 1.1a, in which each inverter transmits power directly to a common load. Roughly speaking, power sharing occurs when the fraction of total generation supplied by each inverter is proportional to its generation capacity. Said differently, as a percentage of its generation capacity, each unit supplies the same fraction of power. The purpose of this power sharing objective is to prevent any one inverter from becoming overloaded, which can easily occur due to poor distributions of power demands across the network and localized response of generation.

Although several control architectures have been proposed to solve these problems, the so-called *droop controllers* have attracted the most attention, as they are ostensibly decentralized and generally effective [77, 40, 65, 59, 54, 50, 49, 35]. The original reference for this methodology is [85], where Chandorkar *et. al.* introduce what we will refer to as the *conventional droop controller*. For inductive lines, the conventional droop controller attempts to emulate the behavior of a classical synchronous generator by imposing an inverse relation at each inverter between frequency and active power injection, and between terminal voltage and reactive power injections. [83]. Under other network conditions, the controller takes different forms [60, 42, 35]. Some representative references for the basic methodology are [77, 65, 59, 54, 50] and [49]. For networks with inductive lines, the droop controllers specify the inverter frequency ω_i and the inverter output voltage E_i for each inverter $i \in \mathcal{I}$ according to

$$\omega_i = \omega^* - m_i(P_{\mathrm{e},i} - P_i^*)\,, \qquad i \in \mathcal{I}\,, \tag{3.1a}$$

$$E_i = E_i^* - n_i(Q_{\mathrm{e},i} - Q_i^*)\,, \qquad i \in \mathcal{I}\,. \tag{3.1b}$$

In the frequency controller (3.1a), ω^* is the rated network (angular) frequency, $P_{\mathrm{e},i}$ is the active electrical power injection at inverter given by (2.8a), and $P_i^* \in [0, \overline{P}_i]$ is the inverters nominal active power injection. The controller gain $m_i > 0$ is referred to as the *droop coefficient*. The controller balances the active power demand in the network by specifying the frequency ω_i of the voltage signal at the inverters terminals. In the voltage controller (3.1b), E_i^* is the nominal inverter voltage, $Q_{\mathrm{e},i}$ is the reactive electrical power injection at the inverter given by (2.8b), and Q_i^* is the inverters nominal reactive power injection. [1] The gain $n_i > 0$ is again called a droop coefficient. The voltage controller balances reactive power demands by adjusting the terminal voltage of the inverter.

[1] The setpoints Q_i^* and P_i^* are typically designed to satisfy an apparent power constraint $(P_i^*)^2 + (Q_i^*)^2 \leq (S_i^*)^2$.

Small-signal stability analyses for two inverters operating in parallel are presented under various assumptions in [66, 63, 56, 55] and the references therein. The recent work [34] highlights some drawbacks of the conventional droop controller. Distributed controllers based on tools from synchronous generator theory and multi-agent systems have also been proposed for synchronization and power sharing. See [57, 58] for a broad overview, and [35, 20, 41] for various works. Lower voltage levels and uncompensated loads in microgrids can cause voltage magnitudes to fall to dangerously low levels, leading to voltage instability and collapse [86]. At the transmission level, these phenomena have received increasing attention after recent voltage instability induced blackouts in Scandinavia (2003), Canada/USA (2003), and Greece (2004) [53]. Indeed, the U.S. Department of Energy has recently invested significant resources studying strategies for reactive power support and the shaping of network voltage profiles [38].

Limitations of the Literature: Despite forming the foundation for the operation of parallel VSIs, the frequency-droop control law (3.1a) has never been subject to a nonlinear analysis [34]. No conditions have been presented under which the controller (3.1a) leads the network to a synchronous steady state, nor have any statements been made about the convergence rate to such a steady state should one exist. Stability results that are presented rely on linearization for the special case of two inverters, and sometimes come packaged with extraneous assumptions [54, 49]. No guarantees are given in terms of performance. Schemes for power sharing based on ideas from multi-agent systems often deal directly with coordinating the real and reactive power injections of the distributed generators, and assume implicitly that a low level controller is bridging the gap between the true network physics and the desired power injections. Moreover, conventional schemes for frequency restoration typically rely on a combination of local integral action and separation of time scales, and are generally unable to maintain an

appropriate sharing of power among the inverters.

The widespread deployment and practical utility of the E-Q controller has led to several attempts at analysis [34, 31]. However, these attempts have met with remarkably little success. To our knowledge, the only provably correct conditions for stability were presented in [31]. Unfortunately, the conditions in [31] are extremely conservative, and hold only for the all-to-all networks of inverters which appear in network-reduced models. Analyses which *begin* from network-reduced models — models in which the load nodes are eliminated from the network — are inherently unable to address the heart of the problem; the voltage levels seen at the load terminals of the true physical network. Said differently, the literature offers no guidance on the foundational issue of operating point feasibility. That is, the existence and locations of equilibria for the network. This large gap of knowledge regarding E-Q controlled networks means that precise reactive loading limits and security margins are inherently unknown, making system monitoring and non-conservative operation difficult.

3.1.1 Contributions and Organization

The contributions of this chapter are as follows.

Frequency Droop Control (Section 3.2): In Section 3.2.1, we begin with our key observation that the equations governing a microgrid under the frequency-droop controller can be equivalently cast as a generalized Kuramoto model of the form (2.21). In Section 3.2.2 we present a necessary and sufficient condition for the existence of a locally exponentially stable and unique synchronized solution of the closed-loop, and provide a lower bound on the exponential convergence rate to the unique synchronized solution. We state a robustified version of our stability condition which relaxes the assumption of fixed voltage magnitudes and admittances. In Section 3.2.3 we demonstrate rigorously

— and without assumptions on large output impedances or identical voltage magnitudes — that if the droop coefficients are selected proportionally, then power is shared among the units proportionally. We provide explicit bounds on the set of serviceable loads. Finally, in Section 3.2.4 we examine how the droop controller gains can be selected to achieve desired steady-state power injections and/or branch flows within the microgrid. All results presented for active power extend past the classic case of a parallel topology of inverters and hold for generic acyclic interconnections of inverters and loads.

Voltage Droop Control (Section 3.3): In Section 3.3.1 we present a novel alternative to the conventional voltage-droop controller, which we refer to as the *quadratic droop controller*. In contrast with the conventional controller — the design of which is motivated by the local, linear behavior of power flow near a steady-state operating point — our proposed design is inspired by the "control by interconnection" approach from port-Hamiltonian systems [68]. We find that the analysis of the network is greatly simplified by designing a controller which preserves the quadratic structure of the AC power flow equations in closed-loop. In particular, we show that the equilibria of the network when controlled by our quadratic droop controller are in exact correspondence with the solutions of a reduced power flow equation (RPFE). We then examine the solutions of this reduced power flow equation and their stability properties for particular load models. For ZI load models, we solve the reduced power flow equation explicitly for the unique high-voltage operating point. We then use the approximation techniques detailed in Section 2.2.3 to study the stability properties of the high-voltage equilibrium for ZIP loads and for dynamic constant power loads. All results in this subsection hold for general topologies.

In Section 3.3.2 we consider in detail the common and practically relevant case of a parallel microgrid (Figure 1.1a). By explicitly solving our RPFE we provide a necessary

and sufficient condition on the network load for the existence of a locally exponentially stable high-voltage equilibrium point. Confirming classic intuition, our condition establishes the existence of a critical inductive load for the network, which depends only on the network topology, admittances, inverter set point voltages, and controller gains. The condition succinctly states that the network load must be less inductive than this critical value. In addition, we study the (in)stability properties of the complementary low-voltage equilibrium point, and in doing so provide a quite complete picture of the network state space.

Finally, in Section 3.3.3 we use the results we derive for the quadratic droop controller to draw a correspondence between the equilibria of the quadratic droop-controlled network and the equilibria of the same network when controlled by the conventional droop controller. While not a bidirectional correspondence, in doing so we provide the first characterization of the network equilibrium points (and their stability properties) under the conventional voltage-droop controller.

Classic intuition developed in power systems is that loading distorts the spatial voltage profile in a network by dragging down the voltage magnitudes at loaded buses, and forcing larger deviations between phase angles at adjacent buses. The former is associated primarily with reactive power loading, while the latter is due to the branch-wise transfer of active power. Moreover, it is generally accepted that high-voltage, small-phase-difference equilibria of such networks are stable, while low-voltage, large-phase-difference equilibria are unstable [53]. Taken together, these rules of thumb suggest the existence of a *critical active power loading* and a *critical reactive power loading* which depend on the network under consideration. If the respective loads are less than these critical values, the the network voltage profile will be sufficiently homogeneous and a stable equilibrium will exist. The papers [87, 97, 88, 74, 86] give some conservative estimates of these critical loading limits. A fundamental outstanding problem regarding the voltage stability of

droop-controlled microgrids is therefore to relate the existence of stable equilibria to the network topology, line admittances, loads, and controller gains, and to determine the exact locations of the equilibria should any exist. One can interpret the results that follow as partially addressing these problems, in that we consider *decoupled* active and reactive power flow problems.

3.2 Analysis of Frequency Droop Control

3.2.1 Equivalence of Generalized Kuramoto Model and Frequency-Droop Controlled Microgrid

In this section we connect the frequency-droop controller (3.1a) to a network of first-order phase-coupled oscillators of the form (2.21). We restrict our attention to active power flows, and for the moment assume that the voltage magnitudes E_i are fixed at every bus. To begin, note that by defining $D_i \triangleq m_i^{-1}$ and by writing $\omega_i(t) = \omega^* + \dot{\theta}_i(t)$, we can equivalently write the frequency-droop controller (3.1a) as

$$D_i \dot{\theta}_i = P_i^* - P_{\mathrm{e},i}\,, \qquad i \in \mathcal{I}\,. \tag{3.2}$$

Note that $\dot{\theta}_i$ is the *deviation* of the frequency at inverter $i \in \mathcal{I}$ from the nominal frequency ω^*. Inserting the active power flow equations (2.8a), the droop controller (3.2) becomes

$$D_i \dot{\theta}_i = P_i^* - \sum\nolimits_{j=1}^{n+m} E_i E_j B_{ij} \sin(\theta_i - \theta_j)\,, \qquad i \in \mathcal{I}\,. \tag{3.3}$$

In the event of an energy shortage where an inverter $i \in \mathcal{I}$ is unable to implement the droop characteristic (3.3), we formally set $D_i = 0$ and allow P_i^* to track the maximum power output available from the inverter, which reduces (3.3) to a constant power load as in (2.15). Using the frequency-dependent load model (2.16) where $P_{\mathrm{load},i} = P_i^* - D_i \dot{\theta}_i$,

the active power balance equations (2.14a) become

$$D_i\dot{\theta}_i = P_i^* - \sum\nolimits_{j=1}^{n+m} E_i E_j B_{ij} \sin(\theta_i - \theta_j)\,, \qquad i \in \mathcal{L}\,. \tag{3.4}$$

Equations (3.3)–(3.4) constitute our system model. If the droop-controlled system (3.3)–(3.4) achieves synchronization, then we can — without loss of generality — transform our coordinates to a *rotating frame of reference*, where the synchronization frequency is zero and the study of synchronization reduces to the study of equilibria.

We can now identify the droop-controlled system (3.3)–(3.4) with a network of generalized Kuramoto oscillators described by (2.21) and arrive at the following insightful relation.

Lemma 3.2.1. (Equivalence of Perturbed Droop-Controlled System and Kuramoto Model). *The following two models are equivalent:*

(i) The droop-controlled microgrid (3.3)–(3.4)*, with frequency-dependent loads* $P_{\text{load},i} = P_i^* - D_i\dot{\theta}_i$ *(*$i \in \mathcal{L}$*), droop coefficients* $m_i = 1/D_i > 0$*, nominal power injections* $P_i^* \in \mathbb{R}$ *(*$i \in \mathcal{I}$*), nodal voltage phases* $\theta_i \in \mathbb{S}^1$*, nodal voltages magnitudes* $E_i > 0$*, and branch susceptances* $-B_{ij} < 0$*;*

(ii) The generalized Kuramoto model (2.21)*, with time constants* $D_i > 0$*, natural frequencies* $\nu_i \in \mathbb{R}$*, phase angles* $\theta_i \in \mathbb{S}^1$ *and coupling weights* $a_{ij} > 0$*.*

The parametric quantities of the two models are related via $P_i^* = \nu_i$ *and* $E_i E_j B_{ij} = a_{ij}$*.*

In light of Lemma 3.2.1 and for notational simplicity, we define the vector of constant power loads and nominal power injections $P^* \triangleq (P_1^*, \dots, P_{n+m}^*)^T$, the matrix of time constants (frequency-dependent load gains and inverse droop coefficients) $D \triangleq \operatorname{diag}(D_1, \dots, D_{n+m})$, and for $\{i,j\} \in \mathcal{E}$ we use the shorthand $a_{ij} \triangleq E_i E_j B_{ij}$ and set

$\mathcal{A} \triangleq \mathcal{A}$. The droop-controlled system (3.3)–(3.4) then reads in vector notation as

$$D\dot{\theta} = P^* - B\mathcal{A}\mathbf{sin}(B^T\theta)\,, \tag{3.5}$$

where $\theta \triangleq (\theta_1, \ldots, \theta_{n+m})^T$ and $B \in \mathbb{R}^{(n+m)\times|\mathcal{E}|}$ is the node-edge incidence matrix of the underlying graph $G = (\mathcal{V}, \mathcal{E}, A)$.

3.2.2 Necessary and Sufficient Condition for Existence of a Stable, Synchronous Steady-State

While Lemma 3.2.1 was convenient to state using the frequency-dependent load model (2.16), from this point onward we instead use the constant power load model (2.15), or equivalently set $D_i = 0$ for all $i \in \mathcal{L}$. Explicitly, the model we consider now is

$$D_i\dot{\theta}_i = P_i^* - \sum\nolimits_{j=1}^{n+m} E_iE_jB_{ij}\sin(\theta_i - \theta_j)\,, \qquad i \in \mathcal{I} \tag{3.6a}$$

$$0 = P_i^* - \sum\nolimits_{j=1}^{n+m} E_iE_jB_{ij}\sin(\theta_i - \theta_j)\,, \qquad i \in \mathcal{L}\,. \tag{3.6b}$$

In terms of the vectorized model (3.5), the matrix D is now block diagonal, with the first block being all zeros. This choice of load model makes the stability analysis more interesting, and avoids introducing any unneeded or unrealistic frequency dependence in the loads. A natural question now arises: under what conditions on the power injections, network topology, susceptances, and droop coefficients does the differential-algebraic closed-loop system (3.3)–(3.4) possess a stable, synchronous solution?

Theorem 3.2.1. (Existence and Stability of Sync'd Solution). *Consider the frequency droop-controlled microgrid* (3.3)–(3.4) *defined on an acyclic network with node-*

edge incidence matrix B. Define the scaled power imbalance ω_{avg} by

$$\omega_{\text{avg}} \triangleq \frac{\sum_{i\in\mathcal{L}\cup\mathcal{I}} P_i^*}{\sum_{i\in\mathcal{I}} D_i}\,,$$

and let $\xi \in \mathbb{R}^{|\mathcal{E}|}$ be the unique vector of edge power flows satisfying KCL, given implicitly by $P^* - \omega_{\text{avg}} D\mathbb{1}_n = B\xi$. The following two statements are equivalent:

(i) **Synchronization:** *There exists an arc length $\gamma \in [0, \pi/2[$ such that the closed-loop system (3.3)–(3.4) possess a locally exponentially stable and unique synchronized solution $t \mapsto \theta^*(t) \in \Delta_G(\gamma)$ for all $t \geq 0$;*

(ii) **Flow Feasibility:** *The power flow is feasible, i.e.,*

$$\Gamma \triangleq \|\mathcal{A}^{-1}\xi\|_\infty < 1\,. \tag{3.7}$$

If the equivalent statements (i) and (ii) hold true, then the quantities $\Gamma \in [0, 1[$ and $\gamma \in [0, \pi/2[$ are related uniquely via $\Gamma = \sin(\gamma)$, and the following statements hold:

a) **Explicit Synchronized Solution:** *The synchronized solution satisfies $\theta^*(t) = \theta_0 + (\omega_{\text{sync}} t\mathbb{1}_n) \pmod{2\pi}$ for some $\theta_0 \in \Delta_G(\gamma)$, where $\omega_{\text{sync}} = \omega_{\text{avg}}$, and the synchronized angular differences satisfy $\mathbf{sin}(B^T\theta^*) = \mathcal{A}^{-1}\xi$;*

b) **Explicit Synchronization Rate:** *The local exponential synchronization rate is no worse than*

$$\lambda \triangleq \frac{\lambda_2(L)}{\max_{i\in\mathcal{I}} D_i}\sqrt{1-\Gamma^2}\,, \tag{3.8}$$

where $L = B\mathcal{A}B^T$ is the Laplacian matrix of the network with weights a_{ij}.

Remark 3.2.2. (Physical Interpretation). *From the droop controller (3.2), it holds that $P^* - \omega_{\text{sync}} D\mathbf{1}_n \in \mathbb{1}_n^\perp$ is the vector of steady state power injections. The power*

injections therefore satisfy the Kirchoff Current Law, and $\xi \in \mathbb{R}^{|\mathcal{E}|}$ *is the associated vector of power flows along edges [91]. Physically, the parametric condition* (3.7) *therefore states that the active power flow along each edge be feasible, i.e., less than the physical maximum* $a_{ij} = E_i E_j B_{ij}$*. While the necessity of this condition seems plausible, its sufficiency is perhaps surprising. Theorem 3.2.1 shows that equilibrium power flows are invariant under constant scaling of all droop coefficients, as overall scaling of* D *appears inversely in* ω_{avg}*. Although grid stress varies with specific application and loading, the condition* (3.7) *is typically satisfied with a large margin of safety – a practical upper bound for* γ *would be* 10°*, corresponding to* $\Gamma \simeq 0.2$*. See [23] for a detailed discussion of synchronization results for networks with cycles.*

Proof. To begin, note that if a solution $t \mapsto \theta(t)$ to the system (3.5) is frequency synchronized, then by definition there exists an $\omega_{\text{sync}} \in \mathbb{R}$ such that $\dot{\theta}(t) = \omega_{\text{sync}} \mathbf{1}_n$ for all $t \geq 0$. Summing over all equations (3.3)–(3.4) gives $\omega_{\text{sync}} = \omega_{\text{avg}}$. Without loss of generality, we can consider the *auxiliary system* associated with (3.5) defined by

$$D\dot{\theta} = \widetilde{P} - B\mathcal{A}\mathbf{sin}(B^T\theta)\,, \tag{3.9}$$

where $\widetilde{P}_i = P_i^*$ for $i \in \mathcal{L}$ and $\widetilde{P}_i = P_i^* - \omega_{\text{avg}} D_i$ for $i \in \mathcal{I}$. Since $\widetilde{P} \in \mathbb{1}_n^\perp$, system (3.9) has the property that $\widetilde{\omega}_{\text{avg}} = 0$ and represents the dynamics (3.5) in a reference frame rotating at an angular frequency ω_{avg}. Thus, frequency synchronized solutions of (3.5) correspond one-to-one with *equilibrium* points of the system (3.9). Given the Laplacian matrix $L = B\mathcal{A}B^T$, (3.9) can be equivalently rewritten in the insightful form

$$D\dot{\theta} = B\mathcal{A} \cdot \left(B^T L^\dagger \widetilde{P} - \mathbf{sin}(B^T\theta)\right). \tag{3.10}$$

Here, we have made use of the facts that $LL^\dagger = L^\dagger L = I_n - \frac{1}{n}\mathbb{1}_n\mathbb{1}_n^T$ and $\widetilde{P} \in \mathbb{1}_n^\perp$.

Since $\ker(B) = \emptyset$, equilibria of (3.10) must satisfy $B^T L^\dagger \widetilde{P} = B^T L^\dagger B \xi = \mathbf{sin}(B^T \theta)$. We claim that $B^T L^\dagger B = \mathcal{A}^{-1}$. To see this, define $X \triangleq B^T L^\dagger B$ and notice that $X\mathcal{A}B^T = B^T L^\dagger (B\mathcal{A}B^T) = B^T L^\dagger L = B^T$. Since $\ker(B) = \emptyset$, it therefore holds that $X\mathcal{A} = I_{|\mathcal{E}|}$ and the result follows. Hence, equilibria of (3.10) satisfy

$$\mathcal{A}^{-1}\xi = \mathbf{sin}(B^T\theta)\,. \tag{3.11}$$

Equation (3.11) is uniquely solvable for $\theta^* \in \Delta(\gamma)$, $\gamma \in [0, \pi/2[$, if and only if $\Gamma \triangleq \max_{\{i,j\}\in\mathcal{E}}(\xi_{ij}/a_{ij}) \leq \sin(\gamma)$. Since the right-hand side of the condition $\Gamma \leq \sin(\gamma)$ is a concave and monotonically increasing function of $\gamma \in [0, \pi/2[$, there exists an equilibrium $\theta^* \in \Delta_G(\gamma)$ for some $\gamma \in [0, \pi/2[$ if and only if the condition $\Gamma \leq \sin(\gamma)$ is true with the strict inequality sign for $\gamma = \pi/2$. This leads immediately to the claimed condition $\Gamma < 1$. In this case, the explicit equilibrium angles are then obtained from the n decoupled equations (3.11). See [23, Theorems 1, 2(G1)] for additional information. Local exponential stability of the equilibrium $\theta^* \in \Delta(\gamma)$ is established by recalling the equivalence between the index-1 differential-algebraic system (3.10) and an associated reduced set of pure differential equations (see also the proof of (b)). In summary, the above discussion shows the equivalence of (i) and (ii) and statement (a). To show statement (b), consider the linearization of the dynamics (3.9) about the equilibrium $\theta^* \in \Delta(\gamma)$ given by

$$\frac{\mathrm{d}}{\mathrm{d}t}\begin{bmatrix}\mathbb{0}_n\\ \Delta\theta_I\end{bmatrix} = -\begin{bmatrix}I_{|\mathcal{L}|} & \mathbb{0}\\ \mathbb{0} & D_I^{-1}\end{bmatrix}\begin{bmatrix}L_{LL} & L_{LI}\\ L_{IL} & L_{II}\end{bmatrix}\begin{bmatrix}\Delta\theta_L\\ \Delta\theta_I\end{bmatrix},$$

where we have partitioned the matrix $L(\theta^*) = B\mathrm{diag}(\{a_{ij}\cos(\theta_i^* - \theta_j^*)\}_{\{i,j\}\in\mathcal{E}})B^T$ according to load nodes $\mathcal{L}$ and inverter nodes $\mathcal{I}$, and defined $D_I \triangleq \mathrm{diag}(\{D_i\}_{i\in\mathcal{I}})$. Since $\theta^* \in \Delta_G(\gamma)$, the matrix $L(\theta^*)$ is a Laplacian and thus positive semidefinite with a simple eigenvalue at zero corresponding to rotational invariance of the dynamics under a uniform

shift of all angles. It can be easily verified that the upper left block L_{LL} of $L(\theta^*)$ is non-singular [22], or equivalently that θ^* is a *regular* equilibrium point. Solving the set of $|\mathcal{L}|$ algebraic equations and substituting into the dynamics for $\Delta\theta_I$, we obtain $\mathrm{d}(\Delta\theta_I)/\mathrm{d}t = -D_I^{-1}L_{\mathrm{red}}(\theta^*)\Delta\theta_I$, where $L_{\mathrm{red}} \triangleq L_{II} - L_{IL}L_{LL}^{-1}L_{LI}$. The matrix $L_{\mathrm{red}}(\theta^*) \in \mathbb{R}^{|\mathcal{I}|\times|\mathcal{I}|}$ is also a Laplacian matrix, and therefore shares the same properties as $L(\theta^*)$ [22]. Thus, it is the *second* smallest eigenvalue of $D_I^{-1}L_{\mathrm{red}}(\theta^*)$ which bounds the convergence rate of the linearization, and hence the local convergence rate of the dynamics (3.9). A simple bound on $\lambda_2(D_I^{-1}L_{\mathrm{red}}(\theta^*))$ can be obtained via the Courant-Fischer Theorem [70]. For $x \in \mathbb{1}_m^\perp$, let $y = D_I^{1/2}x$, and note that $x^TL_{\mathrm{red}}(\theta^*)x/(x^TD_Ix) = y^TD_I^{-1/2}L_{\mathrm{red}}(\theta^*)D_I^{-1/2}y/(y^Ty)$. Thus, $y \in (D_I^{-1/2}\mathbb{1}_m)^\perp$ is an eigenvector of $D_I^{-1/2}L_{\mathrm{red}}(\theta^*)D_I^{-1/2}$ with eigenvalue $\mu \in \mathbb{R}$ if and only if $x = D_I^{-1/2}y$ is an eigenvector of $D_I^{-1}L_{\mathrm{red}}(\theta^*)$ with eigenvalue μ. For $y \neq \mathbb{0}_m$, we obtain

$$\begin{aligned}
&\lambda_2(D_I^{-1}L_{\mathrm{red}}(\theta^*)) = \min_{y\in(D_I^{-1/2}\mathbf{1}_{|\mathcal{I}|})^\perp} \frac{y^TD_I^{-\frac{1}{2}}L_{\mathrm{red}}(\theta^*)D_I^{-\frac{1}{2}}y}{y^Ty} \\
&= \min_{x\in\mathbf{1}_{|\mathcal{I}|}^\perp} \frac{x^TL_{\mathrm{red}}(\theta^*)x}{x^TD_Ix} \geq \frac{1}{\max_{i\in\mathcal{I}} D_i} \min_{x\in\mathbf{1}_{|\mathcal{I}|}^\perp} \frac{x^TL_{\mathrm{red}}(\theta^*)x}{x^Tx} \\
&\geq \frac{\lambda_2(L_{\mathrm{red}}(\theta^*))}{\max_{i\in\mathcal{I}} D_i} \geq \frac{\lambda_2(L(\theta^*))}{\max_{i\in\mathcal{I}} D_i},
\end{aligned}$$

where we have made use of the *spectral interlacing* property of Schur complements [22] in the final inequality. Since $\theta^* \in \Delta_G(\gamma)$, the eigenvalue $\lambda_2(L(\theta^*))$ can be further bounded as $\lambda_2(L(\theta^*)) \geq \lambda_2(L)\cos(\gamma)$, where $L = B\mathcal{A}B^T$ is the Laplacian with weights $\{a_{ij}\}_{\{i,j\}\in\mathcal{E}}$. This fact and the identity $\cos(\gamma) = \cos(\sin^{-1}(\Gamma)) = \sqrt{1-\Gamma^2}$ complete the proof. □

An analogous stability result for inverters operating in parallel now follows as a corollary.

Corollary 3.2.3. (Existence and Stability of Sync'd Solution for Parallel In-

verters). *Consider a parallel interconnection of inverters, as depicted in Figure 1.1a. The following two statements are equivalent:*

(i) **Synchronization:** *There exists an arc length $\gamma \in [0, \pi/2[$ such that the closed-loop system (3.5) possess a locally exponentially stable and unique synchronized solution $t \mapsto \theta^*(t) \in \Delta_G(\gamma)$ for all $t \geq 0$;*

(ii) **Power Injection Feasibility:**

$$\Gamma \triangleq \max_{i \in \mathcal{I}} |(P_i^* - \omega_{\text{avg}} D_i)/a_{i0}| < 1 \,. \tag{3.12}$$

Proof. For the parallel topology of Figure 1.1a there is one load fed by m inverters, and the incidence matrix of the graph $G(\mathcal{V}, \mathcal{E}, A)$ takes the form $B = [-\mathbb{1}_m \; I_m]^T$. Letting $\widetilde{P}$ be as in the previous proof, we note that ξ is given uniquely as $\xi = (B^T B)^{-1} B^T \widetilde{P}$. In this case, a set of straightforward but tedious matrix calculations reduce condition (3.7) to condition (3.12). □

Our analysis so far has been based on the assumption that each term $a_{ij} \triangleq E_i E_j B_{ij}$ is a *constant and known* parameter for all $\{i, j\} \in \mathcal{E}$. In a realistic power system, both effective line susceptances and voltage magnitudes are dynamically adjusted by additional controllers. The following result states that as long as these controllers can regulate the effective admittances and nodal voltages above prespecified lower bounds $\underline{B_{ij}}$ and $\underline{E_j}$, the stability results of Theorem 3.2.1 go through with little modification.

Corollary 3.2.4. (Robustified Stability Condition). *Consider the frequency-droop controlled system (3.3)–(3.4). Assume that the nodal voltage magnitudes satisfy $E_i \geq \underline{E_i} > 0$ for all $i \in \mathcal{L} \cup \mathcal{I}$, and that the line susceptance magnitudes satisfy $B_{ij} \geq \underline{B_{ij}} > 0$ for all $\{i, j\} \in \mathcal{E}$. For $\{i, j\} \in \mathcal{E}$, define $\underline{a_{ij}} \triangleq \underline{E_i}\,\underline{E_j} B_{ij}$, and let $\underline{\mathcal{A}} = \text{diag}(\{\underline{a_{ij}}\}_{\{i,j\} \in \mathcal{E}})$. The following two statements are equivalent:*

(i) **Robust Synchronization:** *For all possible voltage magnitudes $E_i \geq \underline{E_i}$ and line susceptances $B_{ij} \geq \underline{B_{ij}}$, there exists an arc length $\gamma \in [0, \pi/2[$ such that the closed-loop system (3.3)–(3.4) possess a locally exponentially stable and unique synchronized solution $t \mapsto \theta^*(t) \in \Delta_G(\gamma)$ for all $t \geq 0$;*

(ii) **Worst Case Flow Feasibility:** *The active power flow is feasible for the worst case voltage and line admittance magnitudes, that is,*

$$\|\underline{\mathcal{A}}^{-1}\xi\|_\infty < 1\,. \tag{3.13}$$

Proof. The result follows by noting that a_{ij} (resp. $\underline{a_{ij}}$) appears exclusively in the *denominator* of (3.7) (resp. (3.13)), and that the vector $\xi \in \mathbb{R}^{|\mathcal{E}|}$ defined in Theorem 3.2.1 does not depend on the voltages or line admittances. □

Finally, regarding the assumption of purely inductive lines, we note that since the eigenvalues of a matrix are continuous functions of its entries, the exponential stability property established in Theorem 3.2.1 is robust, and the stable synchronous solution persists in the presence of sufficiently small line conductances [79]. See also Remark 2.2.2.

3.2.3 Power Sharing and Actuation Limits

While Theorem 3.2.1 gives the necessary and sufficient condition for the existence of a synchronized solution to the closed-loop system (3.3)–(3.4), it offers no immediate guidance on how to select the control parameters P_i^* and D_i to satisfy the actuation constraint $P_{\mathrm{e},i} \in [0, \overline{P}_i]$. The following definition gives the proper criteria for selection.

Definition 3.2.5. (Proportional Droop Coefficients). *The droop coefficients are selected proportionally if $P_i^*/D_i = P_j^*/D_j$ and $P_i^*/\overline{P}_i = P_j^*/\overline{P}_j$ for all $i, j \in \mathcal{I}$.*

Theorem 3.2.6. (Power Flow Constraints and Power Sharing). *Consider a synchronized solution of the frequency-droop controlled system* (3.3)–(3.4)*, and let the droop coefficients be selected proportionally. Define the total load* $P_{\mathrm{TL}} \triangleq \sum_{i\in\mathcal{L}} P_i^*$*. The following two statements are equivalent:*

(i) **Injection Constraints:** $0 \le P_{\mathrm{e},i} \le \overline{P}_i\,, \qquad \forall i \in \mathcal{I};$

(ii) **Load Constraint:** $-\sum_{j\in\mathcal{I}} \overline{P}_j \le P_{\mathrm{TL}} \le 0\,.$

Moreover, the inverters share the total load P_{TL} *proportionally according to their power ratings, that is,* $P_{\mathrm{e},i}/\overline{P}_i = P_{\mathrm{e},j}/\overline{P}_j$*, for each* $i, j \in \mathcal{I}$*.*

Proof. From (3.2), the steady state active power injection at each inverter is given by $P_{\mathrm{e},i} = P_i^* - \omega_{\mathrm{sync}} D_i$. By imposing $P_{\mathrm{e},i} \ge 0$ for each $i \in \mathcal{I}$, substituting the expression for ω_{sync} from Theorem 3.2.1, and rearranging terms, we obtain, for each $i \in \mathcal{I}$,

$$\begin{aligned} P_{\mathrm{e},i} = P_i^* - \left(\frac{P_{\mathrm{TL}} + \sum_{j\in\mathcal{I}} P_j^*}{\sum_{j\in\mathcal{I}} D_j}\right) D_i \ge 0 \\ \iff P_{\mathrm{TL}} \le -\sum_{j\in\mathcal{I}} \left(P_j^* - \frac{P_i^*}{D_i} D_j\right) = 0\,, \end{aligned}$$

where in the final equality we have used Definition 3.2.5. Along with the observation that $P_{\mathrm{e},i} \ge 0$ if and only if $P_{e,j} \ge 0$ $(i, j \in \mathcal{I})$, this suffices to show that $0 \le P_{\mathrm{e},i}$ for each $i \in \mathcal{I}$ if and only if $P_{\mathrm{TL}} \le 0$. If we now impose for $i \in \mathcal{I}$ that $P_{\mathrm{e},i} \le \overline{P}_i$ and again use the expression for ω_{sync} along with Definition 3.2.5, a similar calculation yields

$$P_{\mathrm{e},i} \le \overline{P}_i \iff P_{\mathrm{TL}} \ge -\frac{\overline{P}_i}{P_i^*} \sum\nolimits_{j\in\mathcal{I}} P_j^* = -\sum\nolimits_{j\in\mathcal{I}} \overline{P}_j.$$

Along with the observation that $P_{\mathrm{e},i} \le \overline{P}_i$ if and only if $P_{\mathrm{e},j} \le \overline{P}_j$ $(i, j \in \mathcal{I})$, this shows that $P_{\mathrm{e},i} \le \overline{P}_i$ for each $i \in \mathcal{I}$ if and only if the total load P_{TL} satisfies the above

inequality. In summary, we have demonstrated two if and only if inequalities, which when taken together show the equivalence of (i) and (ii). To show the final statement, note that the fraction of the rated power capacity injected by the i^{th} inverter is given by

$$\frac{P_{\mathrm{e},i}}{\overline{P}_i} = \frac{P_i^* - \omega_{\mathrm{sync}} D_i}{\overline{P}_i} = \frac{P_j^* - \omega_{\mathrm{sync}} D_j}{\overline{P}_j} = \frac{P_{\mathrm{e},j}}{\overline{P}_j}\,,$$

for each $j \in \mathcal{I}$. This completes the proof. □

Power sharing results for parallel inverters supplying a single load follow as a corollary of Theorem 3.2.6, with $P_{\mathrm{TL}} = P_0^*$. Note that the coefficients D_i must be selected with global knowledge. The frequency-droop controller therefore requires a centralized design for power sharing despite its decentralized implementation. We remark that Theorem 3.2.6 holds independently of the network voltage magnitudes and line susceptances, as long as the condition of (3.2.2) is satisfied for the existence of a synchronized solution.

3.2.4 Power Flow Shaping

The coefficient selection (3.2.5) results in proportional power sharing among the inverter units and eliminates all remaining degrees of freedom in the controller, as all droop coefficients are determined up to a positive constant. We now address the following "reachability" question: given a set of desired power injections for the inverters, can one select the droop coefficients to generate these injections?

We define a *power injection setpoint* as a point of power balance, at fixed load demands and subject to the basic feasibility condition (3.7) given in Theorem 3.2.1.

Definition 3.2.7. (Feasible Power Injection Setpoint). *Let $\gamma \in [0, \pi/2[$. A vector $P^{\mathrm{set}} \in \mathbb{R}^{n+m}$ is a* γ-feasible power injection setpoint *if it satisfies the following three properties:*

1. **Power balance:** $P^{\mathrm{set}} \in \mathbb{1}_n^{\perp}$;

2. **Load invariance:** $P_i^{\mathrm{set}} = P_i^*$ *for all loads* $i \in \mathcal{L}$;

3. **γ-feasibility:** *the associated branch power flows defined through KCL as* $\xi^{\mathrm{set}} = B^{\dagger} P^{\mathrm{set}}$ *are feasible with phase cohesiveness* γ, *that is,* $\|\mathcal{A}^{-1}\xi^{\mathrm{set}}\|_{\infty} \leq \sin(\gamma)$.

The next result characterizes the relationship between droop controller designs and γ-feasible injection setpoints. In particular, any γ-feasible power injection setpoint can be achieved by an appropriate choice of droop coefficients. The converse statement holds as well: *only* the set of γ-feasible power injections can be reached via droop control.

For simplicity, we omit the singular case where $\sum_{j=i}^{n+m} P_i^* = 0$. In this case, $\omega_{\mathrm{sync}} = 0$, and the droop coefficients offer no control over the steady-state inverter injections $P_{\mathrm{e},i}(\theta^*) = P_i^* - D_i\omega_{\mathrm{sync}}$.

Theorem 3.2.8. (Power Flow Shaping). *Consider the droop-controlled system* (3.6). *Assume* $\omega_{\mathrm{sync}} \neq 0$, *let* $P^{\mathrm{set}} \in \mathbb{1}_n^{\perp}$, *and let* $\gamma \in [0, \pi/2[$. *The following statements are equivalent:*

(i) **Coefficient selection:** *there exists a selection of droop coefficients* D_i, $i \in \mathcal{I}$, *such that the steady-state injections satisfy* $P_{\mathrm{e}}(\theta^*) = P^{\mathrm{set}}$, *with* $[\theta^*] \subset \overline{\Delta}_G(\gamma)$;

(ii) **Feasibility:** P^{set} *is a* γ*-feasible power injection setpoint.*

If the equivalent statements (i) and (ii) hold true, then the quantities D_i *and* P_i^{set} *are related with arbitrary* $\beta \neq 0$ *as*

$$D_i = \beta(P_i^* - P_i^{\mathrm{set}}), \quad i \in \mathcal{I}. \tag{3.14}$$

Moreover, $[\theta^*]$ *is locally exponentially stable if and only if* $\beta(P_i^* - P_i^{\mathrm{set}})$ *is nonnegative for all* $i \in \mathcal{I}$.

Proof. **(i) $\Longrightarrow$ (ii):** Since by assumption $\theta^* \in \overline{\Delta}_G(\gamma)$, and since by definition $P_{\mathrm{e}}(\theta^*) \in \mathbb{1}_n^{\perp}$, Theorem 3.2.1 shows that P^{set} is a γ-feasible injection setpoint.

(ii) $\Longrightarrow$ (i): Let P^{set} be a γ-feasible injection setpoint. Consider the droop coefficients $D_i = \beta(P_i^* - P_i^{\mathrm{set}})$. Since $\omega_{\mathrm{sync}} \neq 0$, for each $i \in \mathcal{I}$ we obtain the steady-state injection

$$\begin{aligned} P_{\mathrm{e},i}(\theta^*) = \widetilde{P}_i &= P_i^* - D_i\omega_{\mathrm{sync}} \\ &= P_i^* - \beta(P_i^* - P_i^{\mathrm{set}})\frac{1}{\beta}\underbrace{\frac{\sum_{i\in\mathcal{V}} P_i^*}{\sum_{i\in\mathcal{I}}(P_i^* - P_i^{\mathrm{set}})}}_{=1} = P_i^{\mathrm{set}}\,, \end{aligned}$$

where we used $\sum_{i\in\mathcal{I}} P_i^{\mathrm{set}} = -\sum_{i\in\mathcal{L}} P_i^*$. Since $P_{\mathrm{e},i}(\theta^*) = P_i^* = P_i^{\mathrm{set}}$ for each $i \in \mathcal{L}$, we have $P_{\mathrm{e}}(\theta) = P^{\mathrm{set}}$. Since P^{set} is γ-feasible, θ^* is well defined in $\overline{\Delta}_G(\gamma)$. This completes the converse. From the reasoning in the proof of Theorem 3.2.1, one may conclude that θ^* is locally exponentially stable if and only if all D_i are nonnegative. □

Note that since the mapping between nodal injections and branch flows is one-to-one for acyclic graphs, the set of feasible setpoint branch flows is *exactly* the image under $B^{\dagger}$ of the set of γ-feasible power injection setpoints.

Remark 3.2.9. (Generation Constraints). *The definition of a γ-feasible injection set point makes no reference to the inverter generation constraint $P_{\mathrm{e},i} \in [0, \overline{P}_i]$, and these constraints are therefore not guaranteed to hold. However, in the case where $P_i^* = 0$ (a common parameter choice for islanded microgrids), if the problem parameters satisfy*

$$-\sum\nolimits_{j\in\mathcal{L}} P_j^* \leq \left(\overline{P}_i/D_i\right)\sum\nolimits_{j\in\mathcal{I}} D_j\,, \quad i \in \mathcal{I}\,, \tag{3.15}$$

then the inverters will all satisfy their actuation constraints. The inequalities (3.15) *limit the heterogeneity of the inverter power injections, and are sufficient for the load*

serviceability condition

$$-\sum\nolimits_{i\in\mathcal{L}} P_i^* \leq \sum\nolimits_{i\in\mathcal{I}} \overline{P}_i\,, \tag{3.16}$$

as one can see by rearranging and summing over all $i \in \mathcal{I}$*. Similarly, under the controller gain selection* $P_i^* = \overline{P}_i$ *for each* $i \in \mathcal{I}$*, if the load serviceability condition* (3.16) *holds, then* $\omega_{\text{sync}} > 0$ *and the inverter actuation constraints are always satisfied.*

3.3 Analysis of Voltage Droop Control

The *voltage droop controller* is the second half of the droop control strategy and the counterpart to the frequency controller (3.1a). For the case of inductive lines, the controller specifies the inverter output voltage E_i by [35, Chapter 19]

$$E_i = E_i^* - n_i(Q_{\text{e},i} - Q_i^*)\,, \qquad i \in \mathcal{I}\,, \tag{3.17}$$

where $E_i^* > 0$ is the nominal voltage for inverter unit $i \in \mathcal{I}$ inverter, $Q_i^* \in \mathbb{R}$ is the unit's nominal reactive power injection, and $Q_{\text{e},i}$ is the *measured* reactive power injection[2]. As in the primary frequency controller (3.1a), the gain $n_i > 0$ is called the droop coefficient. From (3.17), it is clear that if an inverter injects a non-zero amount of reactive power $Q_{\text{e},i}$, its voltage will deviate from E_i^*.

The equation (3.18) is algebraic, and is to be thought of as a *target* which we would like to implement. To model actuation delay in adjusting the voltage magnitude and to simplify the subsequent analysis problems, it will be convenient to add an integral channel to the controller (3.17) yielding the first-order system

$$\tau_i \dot{E}_i = -C_i(E_i - E_i^*) - Q_{\text{e},i}\,, \tag{3.18}$$

[2]See [52, 35] for details regarding estimation of active/reactive powers.

where $\tau_i > 0$ is the actuation time constant and $C_i \triangleq n_i^{-1}$. Note that solutions of the algebraic equations (3.17) correspond to steady states of (3.18). In terms of the first order inverter model (2.13b), the conventional droop controller specifies a feedback $v_i = -C_i(E_i - E_i^*) - Q_{\mathrm{e},i}$, consisting of a local proportional control $C_i(E_i - E_i^*)$ and a nonlinear diffusive feedback $Q_{\mathrm{e},i}$.

Despite its extensive history, the voltage droop controller (3.17) has so far resisted any rigorous stability analysis. In our opinion, the key obstacle has been — and remains — the difficulty in determining the equilibria of the closed-loop system. We remove this obstacle in the next section by proposing a controller based on the nonlinear physics of AC power flow.

3.3.1 Quadratic Voltage Droop Control

While the droop controller (3.17) is simple and intuitive, it is based on the linear behavior of AC power flow around the system's open-circuit operating point, and does not respect the inherently quadratic nature of reactive power flow. We instead propose a physically-motivated modification of the conventional voltage-droop controller (3.17). In place of (3.17), consider instead the *quadratic droop controller*

$$\boxed{v_i = K_i E_i (E_i - E_i^*) - Q_{\mathrm{e},i}(E)\,, \quad i \in \mathcal{I}\,,} \tag{3.19}$$

where $K_i < 0$ is a controller gain. Note that compared to the conventional controller (3.17), the gain on the local feedback term is no longer constant, but scales with the local inverter voltage. Combining the decoupled reactive power flow (2.8b) with an algebraic load model (2.17) of the form $Q_{\mathrm{load},i}(E_i)$ at each load bus $i \in \mathcal{L}$, we must also satisfy the

power balance equations

$$0 = Q_{\text{load},i}(E_i) - Q_{\text{e},i}(E)\,, \qquad i \in \mathcal{L}\,. \tag{3.20}$$

Combining now the inverter model (2.13), the quadratic droop controller (3.19), the load power balance (3.20), and the power flow equation (2.9), the closed-loop dynamical system is differential-algebraic, and can be written compactly as

$$\begin{pmatrix} \mathbb{0}_n \\ \tau_I \dot{E}_I \end{pmatrix} = \begin{pmatrix} Q_L(E_L) \\ [E_I] K_I (E_I - E_I^*) \end{pmatrix} + [E] B E\,, \tag{3.21}$$

where $\tau_I = \text{diag}(\tau_{n+1}, \dots, \tau_{n+m})$, $K_I = \text{diag}(K_{n+1}, \dots, K_{n+m})$, $E_I = (E_{n+1}, \dots, E_{n+m})$, and $Q_L(E_L) = (Q_{\text{load},1}(E_1), \dots, Q_{\text{load},n}(E_n))$. The closed-loop dynamics (3.21) highlight the competition in the network between the driving terms in parentheses, which attempt to distort the network voltage profile, and the homogenizing effect of the network $[E]BE$ which attempts to drive the voltages towards the subspace spanned by $\mathbb{1}_{n+m}$. (Lemma 2.2.1 (ii)). Since the variables E_i represent voltage magnitudes referenced to ground, they are intrinsically positive, and for physical consistency we restrict our attention to positive voltage magnitudes. In particular, let $\mathcal{M} \triangleq \{E \in \mathbb{R}^{n+m} \,:\, (3.20) \text{ holds } \forall i \in \mathcal{L}\}$ denote the m-dimensional manifold in $\mathbb{R}^{n+m}$ where all algebraic equations (3.20) hold. We consider (3.21) to be defined only on the intersection $\mathcal{M}_{>0} \triangleq \mathcal{M} \cap \mathbb{R}^{n+m}_{>0}$.

We offer two interpretations of the controller (3.19), one theoretical and one pragmatic.

Circuit-theoretic interpretation: In analogy with feedback strategies used in the study of port-Hamiltonian systems [68], the design (3.19) can be interpreted as *control by interconnection*, where we interconnect the physical electrical network with fictitious

"controller circuits" at the inverter nodes $i \in \mathcal{I}$ [46]. Indeed, consider the two-node

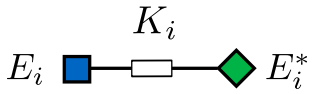

Figure 3.1: Linear circuit representation of the quadratic droop controller (3.19).

circuit of Figure 3.1, where the blue node has variable voltage E_i and is connected via a susceptance $K_i < 0$ to the green node of fixed voltage E_i^*. The current-voltage relations for this fictitious circuit are

$$\begin{pmatrix} I_i \\ I_i^* \end{pmatrix} = \mathbf{j} \begin{pmatrix} K_i & -K_i \\ -K_i & K_i \end{pmatrix} \begin{pmatrix} E_i \\ E_i^* \end{pmatrix} , \tag{3.22}$$

where I_i (resp. I_i^*) is the current injection at the node with voltage E_i (resp. E_i^*). Now, let there be m of the two-node circuits in Figure 3.1; one for each inverter. If we identify the variable-voltage blue nodes of these circuits with the inverter nodes of our original network (Figure 3.2a), and impose that the current injected into the first must exit from the second, we obtain an augmented network with $n + 2m$ nodes, and in vector notation the current-voltage relations in the new network are

$$\begin{pmatrix} I_L \\ \mathbb{0}_m \\ I_I^* \end{pmatrix} = \mathbf{j} \begin{pmatrix} B_{LL} & B_{LI} & \mathbb{0} \\ B_{IL} & B_{II} + K_I & -K_I \\ \mathbb{0} & -K_I & K_I \end{pmatrix} \begin{pmatrix} E_L \\ E_I \\ E_I^* \end{pmatrix} . \tag{3.23}$$

where we have partitioned all variables accordingly. In this augmented network, the inverters behave as interior nodes joining the fictitious controller nodes to the loads, and do not sink or source power themselves. Left multiplying the first two blocks of equations in (3.23) by $[E]$ and noting that by definition $\mathbf{j}[E_L]I_L = Q_L(E_L)$, we immediately obtain the right hand side of (3.21). Thus, unlike the conventional droop controller (3.17), the

quadratic droop controller *preserves the structure of the circuit equations* in closed-loop operation.

Practical interpretation: Far from being linear, voltage/reactive power capability characteristics of synchronous generators display significant nonlinearities. In the absence of saturation constraints, the characteristics are in fact quadratic [53, Equation 3.105], and thus the quadratic droop controller (3.19) more accurately mimics the behavior of a true synchronous generator compared to the classical controller (3.17). Intuitively, this quadratic dependence can be interpreted as follows: the marginal voltage drop (voltage deviation per unit increase in reactive power) increases with reactive power provided.

Remark 3.3.1. (Generalizations of Quadratic Droop). *The quadratic droop controller* (3.19) *is a special case of the more general feedback controller*

$$u_i = E_i \sum\nolimits_{j\in\mathcal{I}} \left(\alpha_{ij}E_j + \beta_{ij}E_j^*\right) , \tag{3.24}$$

where α_{ij}, β_{ij} *are gains. One recovers* (3.19) *by setting* $\alpha_{ii} = K_i$, $\beta_{ii} = -K_i$, *and all other parameters to zero. While the decentralized control* (3.19) *can be interpreted as control-by-interconnection with the simple circuit of Figure 3.1, the controller* (3.24) *represents a more general, densely interconnected circuit with* m *variable-voltage nodes and* m *fixed voltage nodes. While interesting in and of itself, decentralized control strategies are generally preferable in microgrids for redundancy, so for this reason and simplicity of presentation we restrict our attention to the decentralized controller* (3.19)*, with the understanding that all results extend to the more general feedback controller* (3.24). □

For mathematical convenience and simplicity of presentation, we make the following assumption in our subsequent calculations, which can be eliminated at the cost of a less elegant development.

Assumption 3.3.2. (No Shunts). *There are no shunt elements at inverter buses $i \in \mathcal{I}$, and shunts at load buses $i \in \mathcal{L}$ are included in the load model $Q_{\mathrm{load},i}$ and not in the susceptance matrix B.*

It follows that B is negative semidefinite with a simple eigenvalue at zero corresponding to eigenvector $\mathbb{1}_{n+m}$ (Lemma 2.2.1 (iii)).

A basic question regarding the closed-loop system (3.21) is the following: under what conditions on load, network topology, admittances, and controller gains does the differential-algebraic system (3.21) possess a locally exponentially stable equilibrium? Our first result exploits the structure of the control law (3.19) to establish a correspondence between the equilibria of (3.21) and the solutions of a power flow equation for a reduced network.

Theorem 3.3.3. (Reduced Power Flow Equation for Quadratic Droop Network). *Consider the closed-loop system* (3.21) *resulting from the quadratic droop controller* (3.19)*. Partition the susceptance matrix and nodal voltage variables according to loads and inverters as*

$$B = \begin{pmatrix} B_{LL} & B_{LI} \\ B_{IL} & B_{II} \end{pmatrix}, \qquad E = (E_L, E_I)^T,$$

and define

$$B_{\mathrm{red}} \triangleq B_{LL} - B_{LI}\left(B_{II} + K_I\right)^{-1} B_{IL} \in \mathbb{R}^{n\times n}, \tag{3.25}$$

$$W_1 \triangleq -B_{\mathrm{red}}^{-1} B_{LI}\left(B_{II} + K_I\right)^{-1} K_I \in \mathbb{R}^{n\times m}, \tag{3.26}$$

$$E_L^* \triangleq W_1 E_I^* \in \mathbb{R}^n_{>0}, \tag{3.27}$$

$$W_2 \triangleq \left(B_{II} + K_I\right)^{-1} \begin{pmatrix} -B_{IL} & K_I \end{pmatrix} \in \mathbb{R}^{m\times n}. \tag{3.28}$$

The following two statements are equivalent:

(i) **Original Network:** *The voltage vector* $E = (E_L, E_I) \in \mathcal{M}_{>0}$ *is an equilibrium point of* (3.21)*;*

(ii) **Reduced Network:** *The load voltage vector* $E_L \in \mathbb{R}^n_{>0}$ *is a solution of the reduced power flow equation*

$$\mathbb{0}_n = Q_L(E_L) + [E_L]B_{\mathrm{red}}(E_L - E_L^*)\,, \tag{3.29}$$

and the inverter voltage vector is recovered via

$$E_I = W_2 \begin{pmatrix} E_L \\ E_I^* \end{pmatrix} \in \mathbb{R}^m_{>0}\,. \tag{3.30}$$

Moreover, if the Jacobian of (3.29)*, given by*

$$J_{\mathrm{red}} = \frac{\partial Q_L}{\partial E_L} + [E_L]B_{\mathrm{red}} + [B_{\mathrm{red}}(E_L - E_L^*)]\,, \tag{3.31}$$

is a Hurwitz matrix when evaluated at a solution $E_L \in \mathbb{R}^m_{>0}$ *of* (3.29)*, then the equilibrium point* (E_L, E_I) *of the differential-algebraic system* (3.21) *is locally exponentially stable.*

Proof. That the quantities (3.25)–(3.28) are in fact well-defined follows from Proposition A.2.1, the statement and proof of which can be found in Appendix A.

(i)⇒(ii): Since $E = (E_L, E_I)^T \in \mathcal{M}_{>0}$, it follows by definition that that $E_L \in \mathbb{R}^n_{>0}$ and $E_I \in \mathbb{R}^m_{>0}$. By setting the left-hand side of (3.21) to zero, equilibrium points satisfy

$$\mathbb{0}_{n+m} = \begin{pmatrix} Q_L(E_L) \\ [E_I]K_I(E_I - E_I^*) \end{pmatrix} + \begin{pmatrix} [E_L] & \mathbb{0} \\ \mathbb{0} & [E_I] \end{pmatrix} \begin{pmatrix} B_{LL} & B_{LI} \\ B_{IL} & B_{II} \end{pmatrix} \begin{pmatrix} E_L \\ E_I \end{pmatrix}. \tag{3.32}$$

Since $E \in \mathcal{M}_{>0}$ solves (3.32), we can left-multiply the lower block of equations in (3.32) by $[E_I]^{-1}$ to obtain

$$\mathbb{0}_m = K_I(E_I - E_I^*) + B_{II}E_I + B_{IL}E_L\,, \tag{3.33}$$

and solve for E_I to recover (3.30). Substituting (3.30) into the first block of equations in (3.32), we calculate

$$\begin{aligned} -Q_L(E_L) &= [E_L]B_{LL}E_L - [E_L]B_{LI}(B_{II}+K_I)^{-1}\left(B_{IL}E_L - K_IE_I^*\right) \\ &= [E_L]\underbrace{\left(B_{LL} - B_{LI}(B_{II}+K_I)^{-1}B_{IL}\right)}_{B_{\mathrm{red}}}E_L - [E_L]\underbrace{B_{LI}(B_{II}+K_I)^{-1}K_IE_I^*}_{B_{\mathrm{red}}E_L^*} \\ &= [E_L]B_{\mathrm{red}}(E_L - E_L^*)\,, \end{aligned}$$

which is the reduced power flow equation (3.29).

(ii)⇒(i): Due to (3.30) and Proposition A.2.1 (iii), we have that $E_L \in \mathbb{R}^n_{>0}$ implies that $E_I \in \mathbb{R}^m_{>0}$ and hence $E \in \mathbb{R}^n_{>0}$. An easy computation shows that (3.29) and (3.30) together imply that (E_L, E_I) satisfy the fixed point equations (3.32), and thus $E \in \mathcal{M}_{>0}$.

To show the final statement, we study the local stability of the differential-algebraic system (3.21) at the equilibrium $E \in \mathcal{M}_{>0}$ by appealing to [64, Theorem 1]. Consider the generalized eigenvalue problem (GEP) $Jv = \lambda\tau v$ where $v \in \mathbb{R}^n$, $\tau = \mathrm{blkdiag}(\mathbb{0}, \tau_I)$ and Jacobian matrix J is given by

$$J = [E]B + [BE] + D\,. \tag{3.34}$$

The diagonal matrix $D \in \mathbb{R}^{(n+m)\times(n+m)}$ has elements $D_{ii} = \mathrm{d}Q_{\mathrm{load},i}(E_i)/\mathrm{d}E_i$ for $i \in \mathcal{L}$ and $D_{ii} = K_i(E_i - E_i^*) + K_iE_i$ for $i \in \mathcal{I}$. Since $E \in \mathcal{M}_{>0}$, we can left-multiply through

by $[E]^{-1}$ and formulate the GEP as the symmetric problem

$$Mv = \lambda[E]^{-1}\tau v\,, \tag{3.35}$$

where

$$M = M^T \triangleq B + [E]^{-1}([BE] + D)\,. \tag{3.36}$$

Partitioning the eigenvector v as $v = (v_L, v_I)$, block partitioning M, and eliminating the top set of algebraic equations, we arrive at a reduced GEP $M_{\text{red}}v_I = \lambda[E_I]^{-1}\tau_I v_I$ where $M_{\text{red}} = M_{\text{red}}^T \triangleq M_{II} - M_{IL}M_{LL}^{-1}M_{LI}$. By [64, Lemma 1], $E \in \mathcal{M}_{>0}$ is locally exponentially stable if and only if the eigenvalues of this reduced GEP are all in the open left-half complex plane. The matrices on both sides are symmetric, and in particular the matrix $[E_I]^{-1}\tau_I$ on the right is diagonal. The eigenvalues $\{\lambda_i\}_{i\in\mathcal{I}}$ of this reduced GEP are therefore real, and it holds that $\lambda_i < 0$ for each $i \in \mathcal{I}$ if and only if M_{red} is negative definite [71, Chapter 6]. Hence, to show exponential stability of $E \in \mathcal{M}_{>0}$, we need only show that $-M_{\text{red}}$ is positive definite, which we will do indirectly by combining two standard results on Schur complements. A straightforward computation using (3.25), (3.27), (3.30) and (3.33) yields

$$M = \begin{pmatrix} M_{11} & B_{LI} \\ B_{IL} & B_{II} + K_I \end{pmatrix}.$$

where $M_{11} = [E_L]^{-1}(\partial Q_L/\partial E_L) + B_{LL} + [E_L]^{-1}[B_{\text{red}}(E_L - E_L^*)]$. Since the bottom-right block $-(B_{II} + K_I)$ of $-M$ is positive definite, $-M$ will be positive definite if and only if the Schur complement with respect to this bottom-right block is also positive definite.

This Schur complement is equal to

$$-[E_L]^{-1}\frac{\partial Q_L}{\partial E_L} - B_{\text{red}} - [E_L]^{-1}[B_{\text{red}}(E_L - E_L^*)]\,, \tag{3.37}$$

which is exactly $-[E_L]^{-1}$ times the Jacobian (3.31) of (3.29). Since J_{red} is Hurwitz with nonnegative off-diagonal elements, $-J$ is an M-matrix and is therefore D-stable. It follows that the Schur complement (3.37) is positive definite, and hence that M_{red} is positive definite, which completes the proof. □

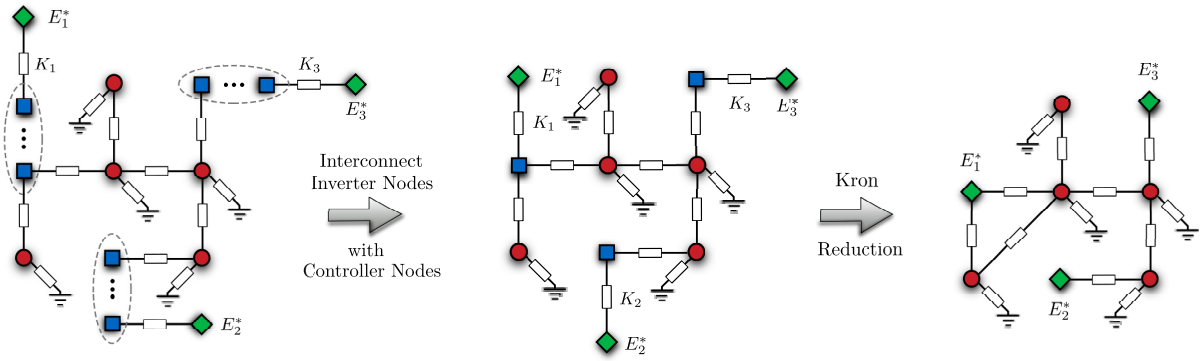

Figure 3.2: Diagram showing network augmentation and reduction for quadratic droop control. First, each inverter node ■ of the network in Figure 1.1b is interconnected with a two-node controller circuit, consisting of an inverter node ■ and fictitious node ◆ at constant voltage E_i^*. In Theorem 3.3.3, the inverter nodes are eliminated via Kron reduction, leaving a reduced network with only fixed voltage nodes ◆ and load nodes ●.

Theorem 3.3.3 states that to study the existence and uniqueness of stable equilibria for the closed-loop system (3.21), we need only study the reduced power flow equation (3.29) and its Jacobian matrix. Voltages at inverters may then be recovered uniquely from (3.30). In fact, since W_2 is row-stochastic (Proposition A.2.1), the inverter voltages (3.30) are weighted averages of load voltages E_L^* and inverter set point voltages E_I^*. Similarly, W_1 is row-stochastic, and hence the open-circuit load voltages E_L^* in (3.27) are weighted averages of inverter set points.

The reduced power flow equation (3.29) is straightforward to interpret in terms of the circuit-reduction of Figure 3.2. Eliminating the inverter voltages E_I from the augmented network current balance (3.23) through Kron reduction [22], one obtains the input/output equivalent reduced circuit

$$\begin{pmatrix} I_L \\ I_I^* \end{pmatrix} = \begin{pmatrix} B_{\mathrm{red}} & -B_{\mathrm{red}} W_1 \\ -W_1^T B_{\mathrm{red}} & K_I (B_{II} + K_I)^{-1} B_{II} \end{pmatrix} \begin{pmatrix} E_L \\ E_I^* \end{pmatrix} . \tag{3.38}$$

This reduction process is shown pictorially in Figure 3.2. Left-multiplying the first block in (3.38) by $[E_L]$ immediately yields the reduced power flow (3.29). Hence (3.29) is exactly the reactive power balance equation $Q_L = [E_L] I_L$ in the reduced network (c.f. [76, Equation 2.10b]). The bottom block of equations in (3.38) can be thought of as determining the fictitious controller current injections once the top block is solved for E_L.

The reduced power flow equation (3.29) can be solved exactly for the specific case we now outline.

Corollary 3.3.4. (Stability for "ZI" Loads). *Consider the reduced power flow equation* (3.29) *for constant-impedance/constant-current loads*

$$Q_L^{\mathrm{ZI}}(V_L) = [E_L][b_{\mathrm{shunt}}] E_L + [E_L] I_{\mathrm{shunt}} , \tag{3.39}$$

where $b_{\mathrm{shunt}} \in \mathbb{R}^n$ *(resp.* $I_{\mathrm{shunt}} \in \mathbb{R}^n$*) is the vector of constant-impedance loads (resp. constant current loads). Assume that*

(i) $-([b_{\mathrm{shunt}}] + B_{\mathrm{red}})$ *is an* M*-matrix, and*

(ii) $I_{\mathrm{shunt}} > B_{\mathrm{red}} E_L^*$ *component-wise.*

Then the unique solution $E_L^{\mathrm{ZI}} \in \mathbb{R}^n_{>0}$ *to* (3.29) *is given by*

$$E_L^{\mathrm{ZI}} = (B_{\mathrm{red}} + [b_{\mathrm{shunt}}])^{-1}(B_{\mathrm{red}}E_L^* - I_{\mathrm{shunt}})\,, \tag{3.40}$$

and the associated equilibrium point (E_L^{ZI}, E_I^{ZI}) *of* (3.21) *is locally exponentially stable.*

The first technical condition in Corollary 3.3.4 restricts the impedance loads from being overly capacitive, while the second restricts the current loads from being overly inductive (since $B_{\mathrm{red}}E_L^* < 0$ component-wise). Note in the case of open-circuit operation (no loading) when $I_{\mathrm{shunt}} = b_{\mathrm{shunt}} = 0$, (3.40) reduces to $E_L^{\mathrm{ZI}} = E_L^*$.

Proof. Corollary 3.3.4 Substituting the ZI load model (3.39) into the reduced power flow equation (3.29), we obtain

$$\begin{aligned} \mathbb{0}_n &= [E_L]\left\{(B_{\mathrm{red}} + [b_{\mathrm{shunt}}])E_L - (B_{\mathrm{red}}E_L^* - I_{\mathrm{shunt}})\right\}\,, \\ &= [E_L](B_{\mathrm{red}} + [b_{\mathrm{shunt}}])(E_L - E_L^{\mathrm{ZI}}) \end{aligned} \tag{3.41}$$

where in the second line we have factored out $(B_{\mathrm{red}} + [b_{\mathrm{shunt}}])$ and identified the second term in parentheses with (3.40). We observe that $E_L = E_L^{\mathrm{ZI}}$ is a solution. Since $(B_{\mathrm{red}} + [b_{\mathrm{shunt}}])$ is nonsingular and we require that $E_L \in \mathbb{R}^n_{>0}$, E_L^{ZI} is the unique solution if $E_L^{\mathrm{ZI}} \in \mathbb{R}^n_{>0}$. Since $-(B_{\mathrm{red}} + [b_{\mathrm{shunt}}])$ is an M-matrix, the inverse $(B_{\mathrm{red}} + b_{[\mathrm{shunt}]})^{-1}$ inverse has nonpositive elements [62], and hence multiplication by the strictly negative vector $B_{\mathrm{red}}E_L^* - I_{\mathrm{shunt}}$ yields a strictly positive vector $E_L^{\mathrm{ZI}} \in \mathbb{R}^n_{>0}$. To show stability, we apply Theorem 3.3.3 and check that the Jacobian of (3.41) evaluated at (3.40) is Hurwitz. Differentiating (3.41), we calculate that

$$J_{\mathrm{red}} = [E_L](B_{\mathrm{red}} + [b_{\mathrm{shunt}}]) + [(B_{\mathrm{red}} + [b_{\mathrm{shunt}}])(E_L - E_L^{\mathrm{ZI}})]\,,$$

and therefore that

$$J_{\text{red}}|_{E_L=E_L^{\text{ZI}}} = [E_L^{\text{ZI}}](B_{\text{red}} + [b_{\text{shunt}}])\,,$$

which is Hurwitz since $-(B_{\text{red}} + [b_{\text{shunt}}])$ is by assumption an M-matrix and M-matrices are D-stable. □

A more general static load model still is the ZIP model $Q_i(E_i) = b_{\text{load},i}E_i^2 + I_{\text{load},i}E_i + Q_i$, $i \in \mathcal{L}$, which augments the ZI model (3.39) with an additional constant power demand $Q_i \in \mathbb{R}$ [83, 76]. In vector notation, this generalizes (3.39) as

$$Q_L^{\text{ZIP}}(E_L) = [E_L][b_{\text{shunt}}]E_L + [E_L]I_{\text{shunt}} + Q_L\,. \tag{3.42}$$

Unlike the ZI model (3.39), the reduced power flow equation (3.29) cannot be solved analytically for ZIP loads, except for the special case of a parallel microgrid which we detailed in [29]. Indeed, even this special case demonstrates that the network can have multiple equilibrium points with non-trivial stability properties. The following result builds on [9, 1] and provides an approximate characterization of the high-voltage reduced power flow solution when "Q_L is small".

Theorem 3.3.5. (Stability with "ZIP" Loads). *Consider the reduced power flow equation* (3.29) *with the ZIP load model* (3.42)*, let the conditions of Corollary 3.3.4 hold, and let* E_L^{ZI} *be the high-voltage solution of* (3.29) *for ZI loads as given in Corollary 3.3.4. Furthermore, define the* short-circuit capacity matrix

$$Q_{\text{sc}} \triangleq [E_L^{\text{ZI}}](B_{\text{red}} + [b_{\text{shunt}}])[E_L^{\text{ZI}}] \in \mathbb{R}^{n\times n}\,. \tag{3.43}$$

Then to first order, the solution of the reduced power flow equation (3.29) *with ZIP loads*

(3.42) *is given by*

$$E_L^{\mathrm{ZIP}} = [E_L^{\mathrm{ZI}}] \left(\mathbb{1}_n - Q_{\mathrm{sc}}^{-1} Q_L \right) . \tag{3.44}$$

Moreover, if

$$\| Q_{\mathrm{sc}}^{-1} Q_L \|_\infty < 1/2 \, , \tag{3.45}$$

then $E_L^{\mathrm{ZIP}} \in \mathbb{R}^n_{>0}$ *and the corresponding equilibrium point* $(E_L^{\mathrm{ZIP}}, E_I^{\mathrm{ZIP}})$ *of* (3.21) *is locally exponentially stable.*

Much like the technical conditions (i) and (ii) in Corollary 3.3.4, the condition (3.45) restricts the size of the constant power component in the ZIP model (3.42); it must be sufficiently small compared to the short-circuit capacity matrix.

Proof. Theorem 3.3.5 .With the ZIP load model (3.42), the reduced power flow equation (3.41) is modified to

$$Q_L = f(E_L) = -[E_L](B_{\mathrm{red}} + [b_{\mathrm{shunt}}])(E_L - E_L^{\mathrm{ZI}}) \, .$$

Expanding $f(E_L)$ around $E_L = E_L^{\mathrm{ZI}}$ to first order, we obtain

$$\begin{aligned} Q_L = f(E_L) &\simeq f(E_L^{\mathrm{ZI}}) + \frac{\partial f(E_L)}{\partial E_L}\Big|_{E_L = E_L^{\mathrm{ZI}}} (E_L - E_L^{\mathrm{ZI}}) \\ &= 0 - J_{\mathrm{red}}|_{E_L = E_L^{\mathrm{ZI}}} \cdot (E_L - E_L^{\mathrm{ZI}}) \\ &= [E_L^{\mathrm{ZI}}](B_{\mathrm{red}} + [b_{\mathrm{shunt}}])(E_L - E_L^{\mathrm{ZI}}) \, , \end{aligned}$$

which after a matrix inversion yields (3.44). To study stability, we again apply Theorem 3.3.3 and examine the Jacobian matrix of the reduced power flow, $J_{\mathrm{red}} = -\frac{\partial f(E_L)}{\partial E_L}$, which

when evaluated at E_L^{ZIP} yields

$$J_{\mathrm{red}} = [E_L^{\mathrm{ZIP}}](B_{\mathrm{red}} + [b_{\mathrm{shunt}}]) - [E_L^{\mathrm{ZI}}]^{-1}[Q_L]\,.$$

Since J_{red} is Hurwitz if and only if $-J_{\mathrm{red}}$ is an M-matrix, and since M-matrices are D-stable, we may left-multiply by $[E_L^{\mathrm{ZIP}}]^{-1}$ and J_{red} will be Hurwitz if and only if the symmetric (negative) M-matrix matrix

$$[E_L^{\mathrm{ZIP}}]^{-1} J_{\mathrm{red}} = (B_{\mathrm{red}} + [b_{\mathrm{shunt}}]) - [E_L^{\mathrm{ZIP}}]^{-1}[E_L^{\mathrm{ZI}}]^{-1}[Q_L]$$

is negative definite. Applying D-stability twice, we may left and right multiply by $[E_L^{\mathrm{ZI}}]$ and equivalently study the symmetric matrix

$$[E_L^{\mathrm{ZI}}][E_L^{\mathrm{ZIP}}]^{-1} J_{\mathrm{red}}[E_L^{\mathrm{ZI}}] = Q_{\mathrm{sc}} - [E_L^{\mathrm{ZIP}}]^{-1}[E_L^{\mathrm{ZI}}][Q_L]\,,$$

where we have identified the first term with the short-circuit matrix (3.43). Left-multiplying by Q_{sc}^{-1} and applying the Inertia Theorem, J_{red} will be Hurwitz if and only if

$$[E_L^{\mathrm{ZIP}}]^{-1}[E_L^{\mathrm{ZI}}]Q_{\mathrm{sc}}^{-1}[Q_L] - I_n\,,$$

is Hurwitz. A sufficient condition for this is that

$$\|[E_L^{\mathrm{ZIP}}]^{-1}[E_L^{\mathrm{ZI}}]Q_{\mathrm{sc}}^{-1}[Q_L]\|_\infty < 1\,. \tag{3.46}$$

However, left-multiplying (3.44) by $[E_L^{\mathrm{ZIP}}]^{-1}$, we have

$$[E_L^{\mathrm{ZIP}}]^{-1}[E_L^{\mathrm{ZI}}]Q_{\mathrm{sc}}^{-1}[Q_L] = [E_L^{\mathrm{ZIP}}]^{-1}[E_L^{\mathrm{ZI}}] - \mathbb{1}_n\,.$$

Thus, the sufficient condition (3.46) is equivalent to $\|[E_L^{\mathrm{ZIP}}]^{-1}[E_L^{\mathrm{ZI}}] - \mathbb{1}_n\|_\infty < 1$, which from examination of (3.44) holds if and only if the stated condition (3.45) holds, completing the proof. □

While the ZIP load model can accurately capture the steady-state behavior of most aggregated loads, when considering dynamic stability of a power system it is often important to check results obtained for static load models against those obtained using basic dynamic load models. A common dynamic load model is the *dynamic shunt* (DS) model $T_i\dot{b}_{\mathrm{shunt},i} = Q_i - E_i^2 b_{\mathrm{shunt},i}$, or in vector notation

$$T\dot{b}_{\mathrm{shunt}} = Q_L - [E_L]^2 b_{\mathrm{shunt}}\,. \tag{3.47}$$

where $T = \mathrm{diag}(T_1, \ldots, T_n)$ is a matrix of positive time-constants. The DS model specifies that the shunt susceptance $b_{\mathrm{shunt},i}$ is adjusted dynamically to achieve a constant power consumption Q_i; this is a common low-fidelity dynamic model for thermostatically controlled loads, induction motors, and aggregate loads behind tap-changing transformers. We restrict our attention to inductive loads $Q_i < 0$, as these are the most common in practice. The next result shows that the

Theorem 3.3.6. (Stability for "DS" Loads). *Consider the reduced power flow equation* (3.29) *with the dynamic shunt load model* (3.47). *Then to first order, the solution*

E_L^{DS} of the reduced power flow equation (3.29) *with DS loads* (3.47) *is given by*

$$E_L^{\mathrm{DS}} = [E_L^*]\left(\mathbb{1}_n - Q_{\mathrm{sc}}^{-1} Q_L\right) , \tag{3.48a}$$

$$b_{\mathrm{shunt}}^{\mathrm{DS}} = [E_L^{\mathrm{DS}}]^{-2} Q_L \, , \tag{3.48b}$$

where $Q_{\mathrm{sc}} = [E_L^*] B_{\mathrm{red}} [E_L^*]$. *Moreover, if*

$$\|Q_{\mathrm{sc}}^{-1} Q_L\|_\infty < 1/2 \tag{3.49}$$

then the corresponding equilibrium point $(E_L^{\mathrm{DS}}, E_I^{\mathrm{DS}}, b_{\mathrm{shunt}}^{\mathrm{DS}})$ *of* (3.21) *is locally exponentially stable.*

Proof. Without loss of generality, we assume that $Q_i \neq 0$ for all $i \in \mathcal{L}$, since if $Q_i = 0$ the unique steady-state of (3.47) is $b_{\mathrm{shunt},i} = 0$ and the equation can be removed. In steady-state, the DS model (3.47) is equivalent to a constant power load model, and hence the steady-state load voltages E_L^{DS} are given approximately by E_L^{ZIP} as in Theorem 3.3.5, but with ZI components $b_{\mathrm{shunt}} = \mathbb{0}_n$ and $I_{\mathrm{shunt}} = \mathbb{0}_n$, yielding the stated result. To show stability, we can no reason from Theorem 3.3.3 and jump directly to the reduced power flow equation, since this result was derived in the absence of load dynamics. Surprisingly however, a long calculation shows that applying the proof methodology of Theorem 3.3.3 to the extended dynamics (3.21)–(3.47) yields the same result: to test for stability, we need only study the Jacobian of the reduced power flow equation (3.29). A calculation analogous to that in Theorem 3.3.5 then yields the stated stability condition. □

3.3.2 Quadratic Droop Control in Parallel Microgrids

The reduced power flow equation (3.29) is particularly simple for the common class of *parallel microgrids*, which consist of a single load fed by multiple inverters in parallel

(Figure 1.1a). In this section we let nodes $\mathcal{I} = \{1, \dots, m\}$ correspond to the inverter nodes, and let node $\mathcal{V}_L = \{0\}$ be the common connection point for a total of N nodes. In this case, the susceptance matrix has the simple form

$$B = \begin{pmatrix} \sum_{i=1}^{m} b_{i0} & -b_{10} & \cdots & -b_{m0} \\ -b_{10} & b_{10} & \cdots & 0 \\ \vdots & \vdots & \ddots & \vdots \\ -b_{m0} & 0 & \cdots & b_{m0} \end{pmatrix},$$

where $b_{i0} < 0$ is the susceptance between inverter $i \in \mathcal{I}$ and the common distribution bus. For simplicity in this section we restrict ourselves to the constant power load model (2.20); all results extend to the ZIP model (2.18) with little additional effort. In this case, the algebraic power flow equation (3.20) takes the form

$$h(E) \triangleq Q_0 + \sum\nolimits_{j=1}^{m} b_{j0} E_0 (E_0 - E_j) = 0\,. \tag{3.50}$$

Before studying the equilibria of the closed-loop system, we examine closely the global structure of our constraint set $\mathcal{M} \triangleq \{E \in \mathbb{R}^{m+1} \,:\, h(E) = 0\}$.

Lemma 3.3.1. (Topology of Constraint Set for Parallel Microgrid). *Consider the power balance equation* (3.50) *for a parallel microgrid, and define the* total susceptance $b_{\text{tot}} < 0$ *and the* singular normal vector $a \in \mathbb{R}^{m+1}$ *by*

$$b_{\text{tot}} \triangleq \sum\nolimits_{i=1}^{m} b_{i0}\,, \quad a \triangleq \left(-1\,,\, \frac{b_{10}}{2b_{\text{tot}}}\,,\, \dots\,,\, \frac{b_{m0}}{2b_{\text{tot}}}\right)^T,$$

with associated hyperplane

$$\mathcal{H} \triangleq \left\{E \in \mathbb{R}^{m+1} \,|\, a^T E = 0\right\}. \tag{3.51}$$

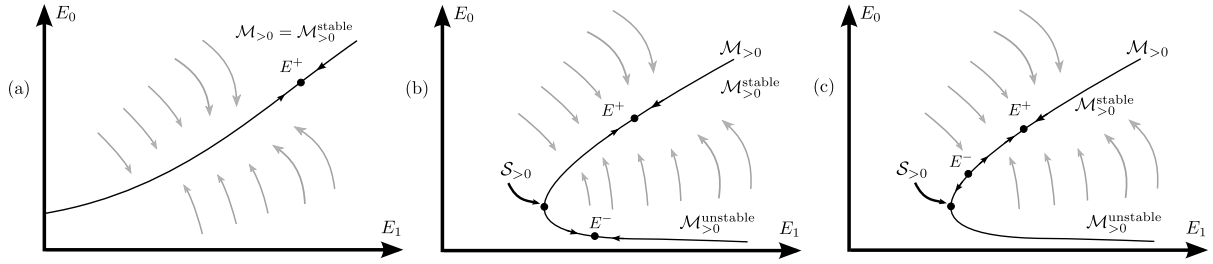

Figure 3.3: Equilibrium locations for (a) capacitive loading $Q_0 > 0$, (b) inductive loading $Q_0 \in]Q_{\text{sing}}, 0[$, and (c) highly inductive loading $Q_0 \in]Q_{\text{crit}}, Q_{\text{sing}}[$. Gray arrows represent the behavior of the associated singularly perturbed system (3.52) with parasitic term $\varepsilon \dot{E}_0$.

The following statements hold:

(i) **Singular Surface:** *The singular surface $\mathcal{S}$ of the load power balance* (3.50) *is given by $\mathcal{S} = \mathcal{M} \cap \mathcal{H}$;*

(ii) **Topology of State Space $\boldsymbol{\mathcal{M}_{>0}}$:**

(a) If $Q_0 \geq 0$, there exists a unique stable component $\mathcal{M}^{\text{stable}}$ of $\mathcal{M}$ such that $\mathcal{M}_{>0} = \mathcal{M}^{\text{stable}}_{>0}$ is nonempty and simply connected;

(b) If $Q_0 < 0$, there exist unique stable and unstable components $\mathcal{M}^{\text{stable}}$ (resp. $\mathcal{M}^{\text{unstable}}$) of $\mathcal{M}$ such that $\mathcal{M}_{>0} = \mathcal{M}^{\text{stable}}_{>0} \cup \mathcal{M}^{\text{unstable}}_{>0} \cup \mathcal{S}_{>0}$, where all sets in the union are nonempty and simply connected.

Lemma 3.3.1 is illustrated in Figure 3.3.

Remark 3.3.7. (Physically Measurable States). *It is argued in [100] that $\mathcal{M}^{\text{stable}}_{>0}$ is the only physically observable portion of the state space, in that if one performed measurements on the physical system in steady state, one would only ever obtain measurements on or near $\mathcal{M}^{\text{stable}}_{>0}$. The restriction to $\mathcal{M}_{>0}$ is clear from Remark 2.2.1. To understand the additional restriction to the stable component, consider instead of the load balance*

(3.50) *an associated* singularly perturbed *system*

$$\varepsilon \dot{E}_0 = h(E)\,, \tag{3.52}$$

where $\varepsilon > 0$. *The additional term* $\varepsilon \dot{E}_0$ *could arise due to parasitics neglected during modeling of the system. Now, note that any small disturbance or noise in the system will push the state* E *off the constraint set* $\mathcal{M}_{>0}$, *such that the "boundary layer" dynamics* (3.52) *will determine whether the state will be attracted or repelled from* $\mathcal{M}_{>0}$. *From Lemma 3.3.1,* $\mathcal{M}_{>0}^{\text{stable}}$ *is exactly the attracting portion of* $\mathcal{M}_{>0}$, *while initial conditions arbitrarily close to* $\mathcal{M}_{>0}^{\text{unstable}}$ *— if it exists — will be repelled; see Figure 3.3. Thus, if we performed a measurement on our system in steady state, we would expect to* never *observe voltages near* $\mathcal{M}_{>0}^{\text{unstable}}$. *Based on physical grounds, we therefore restrict our attention to* $\mathcal{M}_{>0}^{\text{stable}}$. □

In the following, local exponential stability of an equilibrium $E^+ \in \mathcal{M}_{>0}^{\text{stable}}$ refers to the behavior of nearby initial conditions also belonging to $\mathcal{M}_{>0}^{\text{stable}}$, see [89].

Theorem 3.3.8. (Existence of High-Voltage Equilibrium for Parallel Microgrids). *Consider the closed-loop system* (3.21) *for a parallel microgrid resulting from the quadratic droop controller* (3.19). *Define the critical voltage vector* $E_{\text{crit}} \in \mathbb{R}_{>0}^{m+1}$ *and the critical load* $Q_{\text{crit}} < 0$ *by*

$$E_{\text{crit}} \triangleq \begin{pmatrix} \frac{E_L^*}{2}\,;\, W_2 \begin{pmatrix} E_L^*/2 \\ E_I^* \end{pmatrix} \end{pmatrix}\,, \tag{3.53a}$$

$$Q_{\text{crit}} \triangleq \frac{1}{4} B_{\text{red}} (E_L^*)^2\,. \tag{3.53b}$$

The following two statements are equivalent:

(i) **Stable High Voltage Equilibrium:** *The closed-loop* (3.21) *possesses exactly one locally exponentially stable equilibrium* $E^+ \in \mathcal{M}_{>0}^{\text{stable}}$ *satisfying* $E^+ \gg E_{\text{crit}}$*;*

(ii) **Load Feasibility:** *The load is not overly inductive,*

$$Q_0 > Q_{\text{crit}}. \tag{3.54}$$

If the above statements are satisfied, E^+ *is given by*

$$E_0^+ = \frac{E_L^*}{2}\left(1 + \sqrt{1 - \frac{Q_0}{Q_{\text{crit}}}}\right), \tag{3.55a}$$

$$E_i^+ = -\frac{K_i E_i^* + b_{i0} E_0^+}{K_i + b_{i0}}, \qquad i \in \mathcal{I}. \tag{3.55b}$$

Remark 3.3.9. (Interpretation of Feasibility Condition). *Theorem 3.3.8 gives the necessary and sufficient condition for the existence of a "high" voltage equilibrium. That is, each component of the equilibrium is larger than the corresponding component of the strictly positive vector* E_{crit} *in* (3.53a)*. One can verify that* (3.25) *and* (3.27) *reduce to the scalar values*

$$B_{\text{red}} = \sum\nolimits_{j=1}^{m} \left(\frac{b_{j0} K_j}{b_{j0} + K_j}\right) < 0, \tag{3.56}$$

$$E_L^* = \frac{1}{B_{\text{red}}} \sum\nolimits_{j=1}^{m} \left(\frac{b_{j0} K_j}{b_{j0} + K_j}\right) E_j^* > 0, \tag{3.57}$$

and thus the RPFE (3.29) *reduces to a single quadratic equation. The parametric condition* (3.54) *is exactly the classic power flow feasibility result for the modified two-node network of Figure 3.4 [76, Chapter 2].*

Perhaps surprisingly, Theorem 3.3.8 shows that the voltage stability of parallel networks does not simply decouple line-by-line into m *voltage stability problems. The critical*

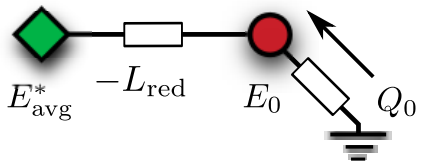

Figure 3.4: Single-line equivalent circuit for feasibility condition (3.54).

load (3.53b) *takes into account the network topology, admittances, and droop controller gains, while the ratio* Q_0/Q_{crit} *serves as an exact security metric for network monitoring. The condition* (3.54) *is asymmetric with respect to inductive* ($Q_0 < 0$) *and capacitive* ($Q_0 > 0$) *loads. This is due to the assumed inductive nature of the network, and would be reversed for a capacitive network. Moreover, note that when* $Q_0 = Q_{\text{crit}}$*, it holds that* $E^+ = E^- = E_{\text{crit}}$ *and both fixed points coalesce before disappearing in a saddle-node bifurcation [86].* □

Theorem 3.3.8 establishes the existence and local stability of a high voltage equilibrium for the closed-loop differential-algebraic system (3.21). From the explicit form of the equilibrium E^+ in (3.55), the reader may suspect that we have ignored an additional equilibrium. Indeed, under a restricted condition on the load, a "low" voltage equilibrium $E^- \in \mathcal{M}^{\text{stable}}_{>0}$ exists as well. Recall that a hyperbolic equilibrium E^- is said to be of *type-k* if k of its eigenvalues have positive real parts [100].

Theorem 3.3.10. (Unstable Low Voltage Equilibrium for Inductive Loads). *Define the singular load value as*

$$Q_{\text{sing}} \triangleq \frac{4B_{\text{red}}/b_{\text{tot}}}{(1 + B_{\text{red}}/b_{\text{tot}})^2}\, Q_{\text{crit}} \in]Q_{\text{crit}}, 0[\,. \tag{3.58}$$

The following two statements are equivalent:

(i) **Unstable Low Voltage Equilibrium:** *The closed-loop* (3.21) *possesses exactly*

one hyperbolic type-1 unstable equilibrium $E^- \in \mathcal{M}_{>0}^{\text{stable}}$ *satisfying* $E^- \ll E_{\text{crit}}$*;*

(ii) **Load Restriction :** $Q_0 \in]Q_{\text{crit}}, Q_{\text{sing}}[$.

If the above statements are satisfied, E^- *is given by*

$$E_0^- = \frac{E_{\text{avg}}^*}{2}\left(1 - \sqrt{1 - \frac{Q_0}{Q_{\text{crit}}}}\right), \tag{3.59a}$$

$$E_i^- = -\frac{K_i E_i^* + b_{i0} E_0^-}{K_i + b_{i0}}, \qquad i \in \mathcal{I}. \tag{3.59b}$$

Remark 3.3.11. (Load Restrictions). *The load restriction (ii) ensures that* $E^- \in \mathcal{M}_{>0}^{\text{stable}}$*, c.f. Remark 3.3.7. As in Theorem 3.3.8, no equilibrium* E^- *exists for* $Q_0 < Q_{\text{crit}}$*. When* $Q_0 = Q_{\text{crit}}$*,* $E^+ = E^- = E_{\text{crit}}$*. That is, the stable and unstable equilibria coalesce at value* $E_{\text{crit}} \in \mathcal{M}_{>0}^{\text{stable}}$*, then vanish in a saddle-node bifurcation leading to voltage collapse [90, 86]. When* $Q_0 = Q_{\text{sing}}$ *it holds that* $E^- \in \mathcal{S}_{>0}$*, and the stability properties of* E^- *change via a singularity-induced bifurcation [80]. Indeed, when* $Q_0 \in]Q_{\text{sing}}, 0[$ *one can show that* $E^- \in \mathcal{M}_{>0}^{\text{unstable}}$*. In this regime,* E^- *is in fact locally exponentially stable, but is unstable in the ambient space for the associated parasitic dynamics, see Figure 3.3 and Remark 3.3.7. For* $Q_0 \geq 0$*,* E^- *has negative elements and is therefore not in the state space* $\mathcal{M}_{>0}$*.* □

Proof. A quick calculation using (3.56) and (3.57) shows that that $Q_{\text{sing}}/Q_{\text{crit}} = 4\alpha(1-\alpha)$, where $\alpha \triangleq B_{\text{red}}/(B_{\text{red}} + b_{\text{tot}}) \in]0, 1/2[$. Since $\alpha \mapsto 4\alpha(1-\alpha) \in]0, 1[$ for $\alpha \in]0, 1/2[$, it holds that $Q_{\text{sing}} \in]Q_{\text{crit}}, 0[$.

(ii)⇒(i): For $Q_0 \in]Q_{\text{sing}}, Q_{\text{crit}}[$, one may proceed as in the proof of Theorem 3.3.8 to derive (3.59) and show that $E^- \in \mathcal{M}_{>0}^{\text{stable}}$ and that $E^- \ll E_{\text{crit}}$. It remains to show that E^- is hyperbolic and type-1. One may quickly calculate from (3.59) that when

$Q_0 = Q_{\text{sing}}$,

$$E_0^- = E_{0,\text{sing}} \triangleq \frac{B_{\text{red}}}{(B_{\text{red}} + b_{\text{tot}})} E_L^* \in]0, E_{\text{L}}^*/2[\,.$$

It is therefore clear that for Q_0 satisfying (ii), $E_0^- \in]E_{0,\text{sing}}, E_{\text{avg}}^*/2[$. By proceeding as in the proof of Theorem 3.3.8, one may arrive at a generalized eigenvalue problem $M(E^-)v = \lambda[E^-]^{-1}\tau v$. Here, the matrix $M(E^-)$ takes the form

$$M(E^-) = \begin{pmatrix} \alpha(\gamma) & B_{LI} \\ B_{IL} & B_{II} + K_I \end{pmatrix},$$

where $\gamma = E_0^- - E_{0,\text{sing}} > 0$, and $\alpha(\gamma)$ is defined by

$$\alpha(\gamma) \triangleq \frac{\gamma(B_{\text{red}} + b_{\text{tot}})^2}{E_L^* B_{\text{red}} + \gamma(B_{\text{red}} + b_{\text{tot}})}\,.$$

Due to condition (ii), $\gamma \in]0, E_{\text{avg}}^*/2 - E_{0,\text{sing}}[$, and hence $\alpha(\gamma) \in]0, B_{\text{red}} - b_{\text{tot}}[$. Moreover, note that $\alpha(\gamma)$ is a strictly positive and monotonically increasing function of γ for $\gamma \in]0, E_{\text{avg}}^*/2 - E_{0,\text{sing}}[$. As before in Theorem 3.3.8, we calculate the reduced matrix

$$M_{\text{red}}(E^-) = B_{II} + K_I - B_{IL}B_{LI}/\alpha(\gamma)\,, \tag{3.60}$$

and study the reduced generalized eigenvalue problem $M_{\text{red}}(E^-)u = \lambda[E_I^-]^{-1}\tau_I u$. From (3.60), it's clear that for sufficiently small $\alpha(\gamma)$ (and hence, for sufficiently small γ), the second term becomes sufficiently large such that $M_{\text{red}}(E^-)$ becomes indefinite. Let us examine the other extreme, where $\gamma \to E_{\text{avg}}^*/2 - E_{0,\text{sing}}$. First, note that the following facts hold:

1. $B_{IL}B_{LI}$ is a rank-one positive semidefinite matrix with non-zero eigenvalue $\sum_{j=1}^m b_{j0}^2$;

2. $\lim_{\gamma \to E_{\text{avg}}^*/2 - E_{0,\text{sing}}} \alpha(\gamma) = B_{\text{red}} - b_{\text{tot}}$.

One may verify by explicit calculation that in the limit as $\gamma \to E^*_{\text{avg}}/2 - E_{0,\text{sing}}$, $M_{\text{red}}(E^-)$ has an eigenvalue at zero corresponding to the eigenvector $(B_{II} + K_I)^{-1}B_{IL}$. Since the addition of a rank one matrix can change the rank of $B_{II} + B_I$ by no more than one, we further conclude that zero is a simple eigenvalue. Since $\alpha(\gamma)$ is a strictly positive and monotonically increasing function of γ for $\gamma \in]0, E^*_{\text{avg}}/2 - E_{0,\text{sing}}[$, and the eigenvalues of a matrix are continuous functions of the matrix entries, we conclude that $M_{\text{red}}(E^-)$ is indefinite for all values of $\gamma \in]0, E^*_{\text{avg}}/2 - E_{0,\text{sing}}[$ — and hence all values of Q_0 satisfying (ii) — with $m - 1$ positive eigenvalues and one negative eigenvalue. This shows that E^- is a hyperbolic type-1 unstable fixed point and completes (i)⇒(ii). The converse implication follows, since if (ii) is not satisfied, $E^- \notin \mathcal{M}^{\text{stable}}_{>0}$. □

Taken together, Lemma 3.3.1 along with Theorems 3.3.8 and 3.3.10 give a clear picture of the dynamics on the state space; depending on the problem parameters, there are always either zero, one, or two equilibria in $\mathbb{R}^{m+1}_{>0}$ (Figure 3.3).

3.3.3 Revisiting Conventional Voltage Droop Control

As we have seen, the analysis of a parallel microgrid controlled by the quadratic droop controller (3.19) is considerably simpler than the analogous but seemingly intractable problem for the conventional droop controller (3.18).

We can in fact leverage the results of Sections 3.3.1 and 3.3.2 to provide a partial analysis of the conventional droop controller (3.18). The following result — the proof of which follows by comparing (3.18) and (3.19) — relates the equilibria of the two closed-loop systems for a special choice of controller gains.

Lemma 3.3.2. (Equilibria of Conventional Droop Controller). *Consider the respective closed-loop systems resulting from the conventional droop controller* (3.18) *and*

the quadratic droop controller (3.19) *for an arbitrary network topology. The following two statements are equivalent:*

(i) **Quadratic System:** $E \in \mathcal{M}_{>0}$ *is an equilibrium of the quadratic droop-controlled system with controller gains* $K_i < 0$, $i \in \mathcal{I}$;

(ii) **Conventional System:** $E \in \mathcal{M}_{>0}$ *is an equilibrium of the conventionally droop-controlled system with controller gains* $C_i = -K_i E_i$ *where* $K_i < 0$, $i \in \mathcal{I}$.

Theorem 3.3.12. (Stability of Conventional Droop Controller). *Consider the closed-loop differential-algebraic system*

$$0 = Q_0 + \sum\nolimits_{j=1}^{m} b_{j0} E_0 (E_0 - E_j)\,, \tag{3.61a}$$

$$\tau_i \dot{E}_i = -C_i (E_i - E_i^*) - Q_{\mathrm{e},i}(E)\,, \qquad i \in \mathcal{I}\,, \tag{3.61b}$$

resulting from the conventional droop controller (3.18) *in a parallel microgrid. Assume that the stability condition* (3.54) *for quadratic droop control holds, and that the controller gains are chosen as in Lemma 3.3.2. If*

$$\max_{i,j \in \{1,\dots,m\}} \frac{E_i^*}{E_j^*} < 2\,, \tag{3.62}$$

then E^+*, as given by* (3.55)*, is locally exponentially stable for the voltage droop controlled system* (3.61).

Proof. That E^+ is an equilibrium of both the quadratic droop closed-loop system (3.21) and the conventional droop closed-loop system (3.61) follows from Lemma 3.3.2.

To show stability, one may proceed as in the proof of Theorem 3.3.8 and arrive at a

generalized eigenvalue problem $\widetilde{M}(E^+)v = -\lambda[E^+]^{-1}\tau v$, where

$$\widetilde{M}(E^+) = M(E^+) + \begin{pmatrix} \mathbb{0} & \mathbb{0} \\ \mathbb{0} & K_I\left([E_I]^{-1}[E_I^*] - I_m\right) \end{pmatrix},$$

with the components of E_I being given by (3.55b). Again appealing to [64, Theorem 1], we study the Schur complement with respect to the bottom right block, which after a simple but tedious calculation is found to be given by

$$S = \sum_{j=1}^{m} \frac{K_j b_{j0}}{K_j + b_{j0}} \left(2 - \frac{E_L^*}{E_0^+} + \frac{E_j^* - E_0^+}{\frac{K_j(K_j+2b_{j0})}{b_{j0}^2} E_j^* + E_0^+} \right).$$

Motivated by (3.55a), define $\beta \triangleq E_0^+ - E_{\text{avg}}^*/2 > 0$. Notice that condition (3.62) implies that $2E_{i,\min}^* > E_{i,\max}^*$, and Proposition A.2.1 (ii) implies that $E_{i,\max}^* \geq E_L^*$. Hence, (3.62) implies that $E_i^* > E_L^*/2$ for each $i \in \{1, \ldots, m\}$. Hence, one may verify that the term in parenthesis is positive for all $\beta \geq 0$. By the same reasoning as in the proof of Theorem 3.3.8, we conclude that the $m \times m$ reduced matrix associated with $\widetilde{M}$ is negative definite for any E_0^+ as given by (3.55a)-(3.55b). It follows that E^+ is locally exponential stable for the conventional droop controlled system (3.61). □

The mild extra condition (3.62) in Theorem 3.3.12 requires that the inverter voltage set points are sufficiently similar, and in practice is always satisfied.

Chapter 4

Distributed Secondary Control of Inverter-Based Power Grids

4.1 Introduction

In Chapter 3 we provided detailed analyses of primary controllers for microgrids. One consequence of these results is that primary droop controllers lead to steady-state frequency and voltage deviations of the inverter variables from their nominally rated values. The next level in the microgrid control hierarchy, termed secondary control, is tasked with removing these deviations. Since secondary control techniques for frequency and voltage have somewhat different motivations and implementation issues, we review them separately.

Frequency Regulation: Many techniques have been suggested to restore the network frequency, ranging on the spectrum from centralized to decentralized [59], and each with its own advantages and disadvantages. One centralized technique is to mimic Automatic Generation Control from bulk power systems. This is implemented using area control errors on slow time-scales, a centralized integral controller, and one-to-all communication

[53]. However, this centralized approach conflicts with the microgrid paradigm of distributed generation and autonomous management. A decentralized technique is to use a slower integral control *locally* at each inverter [85]. This implicitly assumes that the measured local frequency is equal to the steady-state network frequency, and therefore relies on a *separation of time-scales* between the fast, synchronization-enforcing primary droop controller and the slower, secondary integral controller [85, 49]. Except in special cases, this approach destroys the power sharing properties established by primary control [5], and is too slow to dynamically regulate the grid frequency during rapid load changes.

In [14, 15] control strategies were proposed in which DG units communicate their frequencies, voltages and reactive power injections to one another in order to perform secondary control and share active and reactive power. The methods have two drawbacks: first, all inverters must communicate with all other inverters, requiring a dense communication architecture. Second, the controller gains must be finely tuned in order to maintain active power sharing; see [21] for a detailed analysis.

Voltage Regulation In high-voltage networks, the sharing among generators of reactive power demand is usually not a major concern due to capacitive compensation of both loads and transmission lines; voltages at generators are therefore regulated to fixed values by the excitation system [53]. Voltage regulation has subsequently been adopted as the standard for voltage secondary control in microgrids [85, 40]. However, in small-scale microgrid applications, the low ratings of DG units, small electrical distances between units, and the lack of static compensation requires an accurate sharing of reactive power demand among DGs to prevent overloading. In Section 4.3 we highlight how voltage regulation and reactive power sharing are conflicting objectives.

Due to the line impedance effect, the voltage droop controller (3.1b) is unable to share reactive power demand among even identical inverters operating in parallel [59]. In [34],

an alternative primary droop controller was proposed for reactive power sharing among parallel inverters with the same rated voltages. The method requires each unit to have a measurement of the common load voltage, limiting its applicability in complex microgrid scenarios. Similarly, the centralized secondary control architecture proposed in [12] for reactive power sharing requires each unit to communicate with a central controller. The distributed voltage controller proposed in [14, 15] require all DGs to communicate with all others directly. Moreover, since the controller regulates DG voltages to their nominal values, it is be unable to share reactive power between heterogeneous units connected through varying line impedances. See [12, 14] and the references therein for more.

4.1.1 Contributions and Organization

In this section we present a general and fully distributed framework for secondary frequency and voltage control in islanded microgrids. Our designs overcome the limitations of existing strategies by combining decentralized proportional droop control and integral control with distributed averaging algorithms. We therefore refer to our proposed controllers as **DAPI** (Distributed Averaging Proportional Integral) controllers. These controllers use decentralized control actions and sparse communication among neighboring DG units to achieve precise frequency regulation, active power sharing, and a tunable trade-off between voltage regulation and reactive power sharing. The distributed architecture eliminates the need for a central supervisory control: additional DGs are integrated through a low-bandwidth communication link to an existing DG, with the communication topology being a tunable design variable. The DAPI controllers are model-free, in the sense that they require no *a priori* knowledge of the microgrid topology, line impedances or load demands.

There are four main technical contributions in this chapter. First, in Section 4.2 we introduce the frequency DAPI controller frequency stabilization and active power

sharing. Through the use of a distributed-averaging algorithm, the proposed controller dynamically regulates the network frequency to a nominal value, while preserving the proportional power sharing properties of the frequency-droop controller. We show that this controller is locally stabilizing, without relying on the classic assumption of a time-scale separation between the primary (droop) and secondary (integral) control loops.

Second, in Section 4.3 we highlight and clearly demonstrate a fundamental limitation of voltage control: precise voltage regulation and precise reactive power sharing are conflicting objectives. The presentation frames and motivates our subsequent controller designs.

Third, in Section 4.4 we introduce the voltage DAPI controller. This distributed voltage controller accounts for the conflict between voltage regulation and reactive power sharing by allowing for a tunable compromise between the two objectives. We build intuition for our design by detailing several tuning strategies. Taken together, the two DAPI controllers form a distributed duo for plug-and-play microgrid control.

Fourth, in Section 4.4 we present a small-signal voltage stability analysis of the microgrid under DAPI control, derive sufficient conditions on the controller gains and microgrid parameters for closed-loop stability, and study the transient performance of the system under changes in the controller gains.

Fifth and finally, in Section 4.5 we present extensive experimental results validating our DAPI designs. The experimental microgrid consists of four heterogeneous DGs in a non-parallel configuration, with high R/X connections and distributed load. We validate our designs, and move beyond our theoretical results by demonstrating controller performance under communication link failures and plug-and-play operation.

4.2 Distributed Secondary Control of Frequency/Active Power

As is evident from the expression for ω_{sync} in Theorem 3.2.1, the frequency-droop controller typically leads to a deviation of the steady-state operating frequency from the nominal value ω^*. Intuitively, this is not surprising: the droop controller is essentially a proportional controller, and proportional control of a first order system leads to steady-state deviations.

Again in light of Theorem 3.2.1, it is clear that modifying the nominal active power injection P_i^* via the transformation $P_i^* \longrightarrow P_i^* - \omega_{\text{sync}} D_i$ (for $i \in \mathcal{I}$) in the controller (3.3) will yield zero steady state frequency deviation (c.f. the auxiliary system (3.9) with $\widetilde{\omega}_{\text{sync}} = 0$). Unfortunately, the information to calculate ω_{sync} is not available locally at each inverter. As originally proposed in [85], after the frequency of each inverter has converged to ω_{sync}, a slower, "secondary" control loop can be used locally at each inverter. Each local secondary controller slowly modifies the nominal power injection P_i^* until the network frequency deviation is zero. This procedure implicitly assumes that the measured frequency value $\dot{\theta}_i(t)$ is a good approximation of ω_{sync}, and relies on a separation of time-scales between the fast, synchronization-enforcing primary droop controller and the slower secondary integral controller. This methodology is employed in [85, 72, 49]. For large droop coefficients D_i, this approach can be particularly slow (Theorem 3.2.1 (b)), with this slow response leading to an inability of the controller to dynamically regulate the network frequency in the presence of a time-varying load. Moreover, these decentralized integral controllers destroy the power sharing properties established by the primary droop controller. In what follows, we pursue an alternative scheme for frequency restoration which does not implicitly rely on a separation of time-scales as in [85, 72, 49]. Assuming the existence of a communication network among the inverters, we expand on the conventional frequency-droop design (3.1a) and propose the

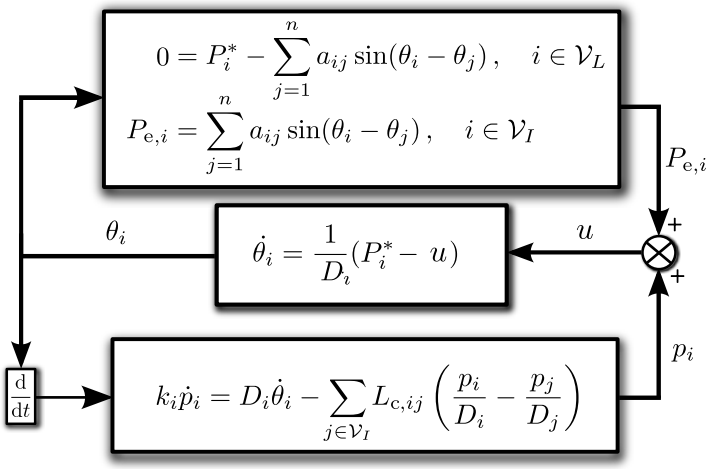

Figure 4.1: Block diagram of DAPI frequency control. The upper control loop is the droop controller (3.2).

distributed-averaging proportional-integral (DAPI) controller

$$D_i \dot{\theta}_i = P_i^* - p_i - P_{e,i}, \quad i \in \mathcal{I}, \tag{4.1}$$

$$k_i \dot{p}_i = D_i \dot{\theta}_i + \sum_{j \in \mathcal{I}} L_{c,ij} \left(\frac{p_i}{D_i} - \frac{p_j}{D_j} \right), \ i \in \mathcal{I}, \tag{4.2}$$

where $p_i \in \mathbb{R}$ is an auxiliary power variable and $k_i > 0$ is a gain, for each $i \in \mathcal{I}$.[3] The matrix $L_c \in \mathbb{R}^{m \times m}$ is the Laplacian matrix corresponding to a weighted, undirected and connected *communication graph* $G_c(\mathcal{V}_I, \mathcal{E}_c, A_c)$ between the inverters, see Figure 4.6. The DAPI controller (4.1)–(4.2) is depicted in Figure 4.1, and will be shown to have the following two key properties. First of all, the controller is able to quickly regulate the network frequency under large and rapid variations in load. Secondly, the controller accomplishes this regulation while *preserving* the power sharing properties of the primary frequency-droop controller (3.2).

The closed-loop dynamics resulting from the DAPI controller (4.1)–(4.2) are given by

[3]The presented results extend to discrete time and asynchronous communication, see [48].

$$0 = P_i^* - \sum\nolimits_{j=1}^{n} a_{ij} \sin(\theta_i - \theta_j)\,, \quad i \in \mathcal{L}\,, \tag{4.3}$$

$$D_i \dot{\theta}_i = P_i^* - p_i - \sum\nolimits_{j=1}^{n} a_{ij} \sin(\theta_i - \theta_j)\,, \; i \in \mathcal{I}\,, \tag{4.4}$$

$$\begin{aligned} k_i \dot{p}_i = P_i^* - p_i - \sum\nolimits_{j=1}^{n} a_{ij} \sin(\theta_i - \theta_j) \\ + \sum\nolimits_{j \in \mathcal{I}} L_{\mathrm{c},ij} \left(\frac{p_i}{D_i} - \frac{p_j}{D_j} \right), \quad i \in \mathcal{I}\,. \end{aligned} \tag{4.5}$$

The following result establishes local stability of the desired equilibrium of (4.3)–(4.5) as well as the power sharing properties of the DAPI controller.

Theorem 4.2.1. (Stability of DAPI-Controlled Network). *Consider an acyclic network of droop-controlled inverters and loads in which the inverters can communicate through the weighted graph G_c, as described by the closed-loop system* (4.3)–(4.5) *with parameters $P_i^* \in [0, \overline{P}_i], D_i > 0$ and $k_i > 0$ for $i \in \mathcal{I}$, and connected communication Laplacian $L_{\mathrm{c}} \in \mathbb{R}^{m \times m}$. The following two statements are equivalent:*

(i) **Stability of Droop Controller:** *The droop control stability condition* (3.7) *holds;*

(ii) **Stability of DAPI Controller:** *There exists an arc length $\gamma \in [0, \pi/2[$ such that the system* (4.4)–(4.5) *possess a locally exponentially stable and unique equilibrium $\left(\theta^*, p^*\right) \in \Delta_G(\gamma) \times \mathbb{R}^m$.*

If the equivalent statements (i) and (ii) hold true, then the unique equilibrium is given as in Theorem 3.2.1 (ii), along with $p_i^* = D_i \omega_{\mathrm{avg}}$ for $i \in \mathcal{I}$. Moreover, if the droop coefficients are selected proportionally, then the DAPI controller preserves the proportional power sharing property of the primary droop controller.

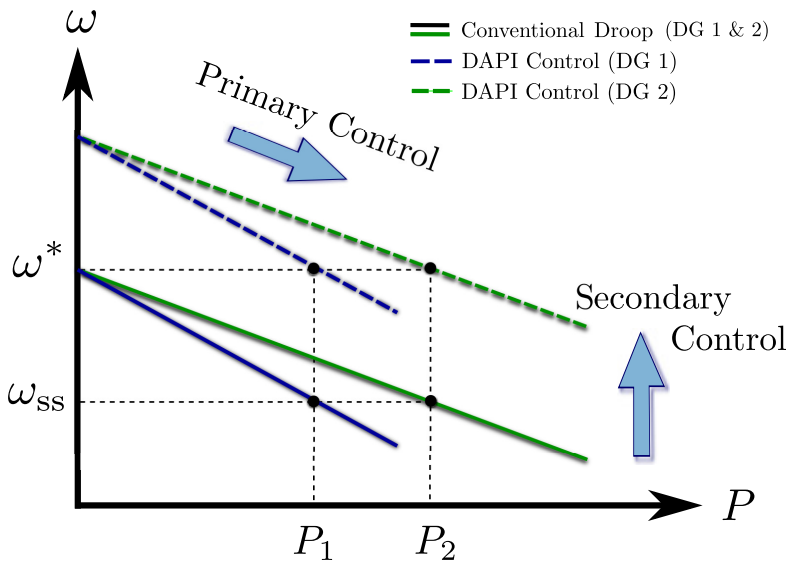

Figure 4.2: Graphical interpretation of DAPI control shows droop characteristics with (dashed lines) and without (solid lines) secondary control action. One can interpret the DAPI secondary control action as a uniform shifting of all droop characteristics by an amount $\omega^* - \omega_{\rm ss}$.

Note that Theorem 4.2.1 asserts the exponential stability of an *equilibrium* of the closed-loop (4.3)–(4.5), and hence, a synchronization frequency $\omega_{\rm sync}$ of zero. The network therefore synchronizes to the nominal frequency ω^*. A graphical interpretation of the DAPI control action is shown in Figure 4.2, where droop curves for two different inverters are *uniformly* shifted upwards by an amount equal to $\omega_{\rm ss} = \omega_{\rm sync}$.

Proof. Consider the closed-loop (4.3)–(4.5) arising from the DAPI controller (4.1)–(4.2). We formulate our problem in the error coordinates $\widetilde{p}_i(t) \triangleq p_i(t) - D_i\omega_{\rm avg}$, and write (4.3)–(4.5) in vector notation as

$$\mathcal{D}\begin{bmatrix}\mathbb{0}_n\\ \dot{\theta}_I\end{bmatrix} = \widetilde{P} - P_{\rm e} - \begin{bmatrix}\mathbb{0}_n\\ \widetilde{p}\end{bmatrix}, \tag{4.6}$$

$$K\dot{\widetilde{p}} = \widetilde{P}_I - P_{{\rm e},I} - (I_m + L_{\rm c}D_I^{-1})\widetilde{p}, \tag{4.7}$$

where we have defined $\mathcal{A} \triangleq \mathrm{diag}(\{a_{ij}\}_{\{i,j\}\in\mathcal{E}})$, $P_{\mathrm{e}} \triangleq B\mathcal{A}\mathbf{sin}(B^T\theta) = (P_{\mathrm{e},L}, P_{\mathrm{e},I})$, $\mathcal{D} \triangleq \mathrm{blkdiag}(I_n, D_I)$, $K \triangleq \mathrm{diag}(\{k_i\}_{i\in\mathcal{I}})$ and partitioned the vector of power injections by load and inverter nodes as $\widetilde{P} = (\widetilde{P}_L, \widetilde{P}_I)^T$. Equilibria of (4.6)–(4.7) satisfy

$$\mathbb{0}_{n+2m} = \underbrace{\begin{bmatrix} I_n & \mathbb{0} & \mathbb{0} \\ \mathbb{0} & D_I^{-1} & I_m \\ \mathbb{0} & I_m & D_I + L_{\mathrm{c}} \end{bmatrix}}_{Q_1} \underbrace{\begin{bmatrix} I_n & \mathbb{0} & \mathbb{0} \\ \mathbb{0} & I_m & \mathbb{0} \\ \mathbb{0} & \mathbb{0} & D_I^{-1} \end{bmatrix}}_{Q_2} \underbrace{\begin{bmatrix} \widetilde{P} - P_{\mathrm{e}} \\ -\widetilde{p} \end{bmatrix}}_{x}. \tag{4.8}$$

The positive semidefinite matrix Q_1 has one dimensional kernel spanned by $(\mathbb{0}_n, D_I\mathbb{1}_m, -\mathbb{1}_m)$, while Q_2 is positive definite. Note however that since $\widetilde{P} - P_{\mathrm{e}} \in \mathbb{1}_{n+m}^{\perp}$, and $Q_2 x = (\widetilde{P} - P_{\mathrm{e}}, -D_I^{-1}\widetilde{p})$, it holds that $Q_2 x \notin \mathrm{Ker}(Q_1)$. Thus, (4.8) holds if and only if $x = \mathbb{0}_{n+m}$; that is, $\widetilde{p} = \widetilde{p}^* = \mathbb{0}_m$ and $\widetilde{P} - P_{\mathrm{e}} = \mathbb{0}_{n+m}$. Equivalently, from Theorem 3.2.1, the latter equation is solvable for a unique (modulo rotational symmetry) value $\theta^* \in \Delta_G(\gamma)$ if and only if the parametric condition (3.7) holds.

To establish the local exponential stability of the equilibrium $(\theta^*, \widetilde{p}^*)$, we linearize the DAE (4.6)–(4.7) about the regular fixed point $(\theta^*, \widetilde{p}^*)$ and eliminate the resulting algebraic equations, as in the proof of Theorem 3.2.1. The Jacobian $J(\theta^*, \widetilde{p}^*)$ of the reduced system of ordinary differential equations can then be factored as $J(\theta^*, \widetilde{p}^*) = -Z^{-1}X$, where $Z = \mathrm{blkdiag}(I_m, K)$ and

$$X = \underbrace{\begin{bmatrix} D_I^{-1} & I_m \\ I_m & L_{\mathrm{c}} + D_I \end{bmatrix}}_{=X_1=X_1^T} \underbrace{\begin{bmatrix} L_{\mathrm{red}}(\theta^*) & \mathbf{0} \\ \mathbf{0} & D_I^{-1} \end{bmatrix}}_{=X_2=X_2^T}.$$

Thus, the problem of local exponential stability of $(\theta^*, \widetilde{p}^*)$ reduces to the generalized eigenvalue problem $-X_1X_2v = \lambda Z v$, where $\lambda \in \mathbb{R}$ is an eigenvalue and $v \in \mathbb{R}^{2m}$ is

the associated eigenvector. We will proceed via a continuity-type argument. Consider momentarily a perturbed version of X_1, denoted by X_1^ϵ, obtained by adding the matrix ϵI_m to the lower-right block of X_1, where $\epsilon \geq 0$. Then for every $\epsilon > 0$, X_1^ϵ is positive definite. Defining $y \triangleq Zv$, we can write the generalized eigenvalue problem $X_1^\epsilon X_2 v = -\lambda Z v$ as $X_2 Z^{-1} y = -\lambda (X_1^\epsilon)^{-1} y$. The matrices on both left and right of this generalized eigenvalue problem are now symmetric, with $X_2 Z^{-1} = \text{blkdiag}(L_{\text{red}}, D_I^{-1} K^{-1})$ having a simple eigenvalue at zero corresponding to rotational symmetry. By applying the Courant-Fischer Theorem to this transformed problem, we conclude (for $\epsilon > 0$ and modulo rotational symmetry) that all eigenvalues are real and negative.

Now, consider again the unperturbed case with $\epsilon = 0$. Notice that the matrix X_2 is positive semidefinite with kernel spanned by $(\mathbb{1}_m, \mathbb{0}_m)$ corresponding to rotational symmetry, while X_1 is positive semidefinite with kernel spanned by $(-D_I \mathbb{1}_m, \mathbb{1}_m)$. Since $\text{Image}(L_{\text{red}}(\theta^*)) = \mathbb{1}_m^\perp$, $\text{Image}(X_2) \cap \text{Ker}(X_1) = \emptyset$, that is, $X_2 v$ is never in the kernel of X_1. Thus we conclude that $\text{Ker}(X_1 X_2) = \text{Ker}(X_2)$. Now we return to the original eigenvalue problem in the form $X_1 X_2 v = -\lambda Z v$. Since the eigenvalues of a matrix are continuous functions of the matrix entries, and $\text{Ker}(X_1 X_2) = \text{Ker}(X_2)$, we conclude that the number of negative eigenvalues does not change as $\epsilon \to 0^+$, and the eigenvalues therefore remain real and negative. Hence, the equilibrium $(\theta^*, \widetilde{p}^*)$ of the DAE (4.6)–(4.7) is (again, modulo rotational symmetry) locally exponentially stable.

To show the final statement, note from the modified primary controller (4.1) that the steady state power injection at inverter $i \in \mathcal{I}$ is given by $P_{\text{e},i} = P_i^* - p_i(t = \infty) = P_i^* - \omega_{\text{avg}} D_i$, which is exactly the steady state power injection when only the primary droop controller (3.2) is used. The result then follows from Theorem (3.2.6). This completes the proof of Theorem 4.2.1. □

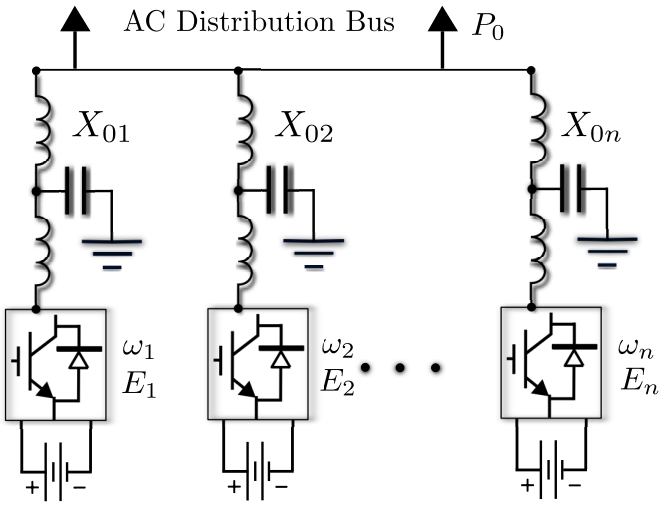

Figure 4.3: Schematic of DGs operating in a parallel microgrid.

4.3 Fundamental Limitations of Voltage Control

In this section we illustrate the fundamental conflict between two secondary control goals: voltage regulation and reactive power sharing. For simplicity of exposition, we focus on a parallel microgrid consisting of two identical DGs connected to a common distribution bus (Figure 4.3). The reactances of the two lines connecting the DGs to the common bus are different; in particular, $X_{01} > X_{02}$.

Figure 4.4 depicts the E-Q droop characteristics before and after a standard, voltage-regulating secondary control action. Without secondary control, the inverters operate at voltages E_1 and E_2 with reactive power injections Q_1 and Q_2 (solid black line). Since $Q_1 \neq Q_2$, reactive power is not shared; this is the "line impedance effect". Application of voltage-regulating secondary control ensures that both DG voltage magnitudes are restored to the common rating E^* (dotted blue and green lines are the post-secondary control droop characteristics). Note however that the inverter power injections change to $Q_1' < Q_1$ and $Q_2' > Q_2$. The application of standard secondary control therefore *worsens* the already poor sharing of reactive power between the DGs.

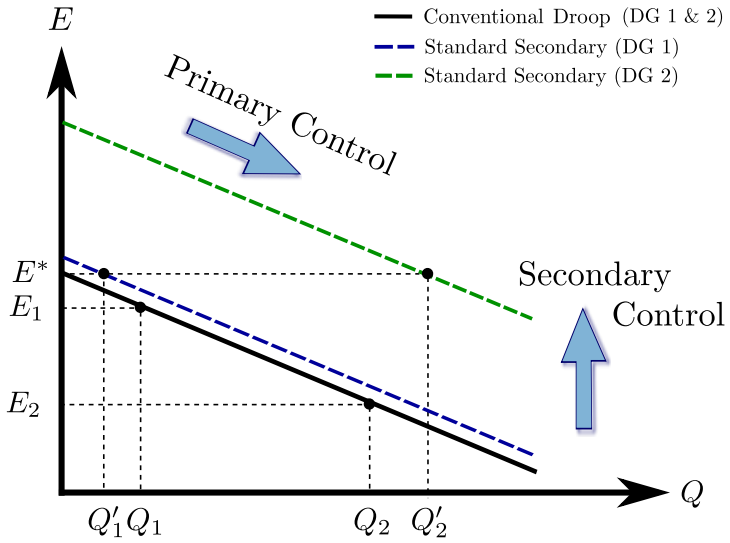

Figure 4.4: E-Q droop and standard secondary control for two parallel inverters with identical ratings, operating through reactive lines with $X_{01} > X_{02}$.

For the same problem setup, Figure 4.5 depicts the E-Q droop characteristics before and after a power sharing enforcing secondary control action is taken.[1] While the identical inverters now proportionally share the reactive power by both injecting Q'', the resulting voltage values E_1'' and E_2'' are more dissimilar than they were with only primary control.

Table 4.1: Relationships between voltage magnitudes and reactive power injections for different control actions.

Control Method	Voltage Magnitudes	Reactive Powers
Primary Control	$E_2 < E_1 < E^*$	$Q_1 < Q_2$
Standard Sec. ($'$)	$E_2' = E_1' = E^*$	$Q_1' < Q_1 < Q_2 < Q_2'$
Power Sharing ($''$)	No Relationship	$Q_1'' = Q_2'' = Q''$

Table 4.1 collects the relationships between voltage magnitudes and reactive power injections for the different control actions described above. We observe that — except

[1] This control action is not uniquely determined; there are many shiftings of the droop characteristics which lead to power sharing (Section 4.4).

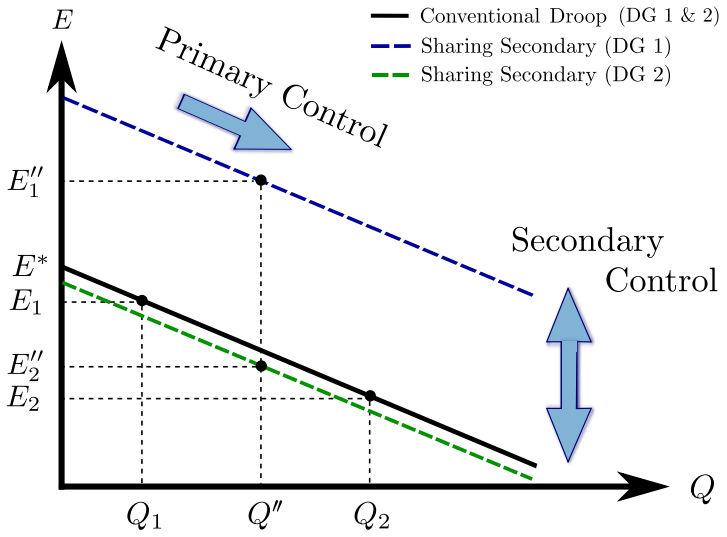

Figure 4.5: E-Q droop and power sharing secondary control for two parallel inverters with identical ratings, operating through reactive lines with $X_{01} > X_{02}$.

under special circumstances — precise voltage regulation leads to large errors in reactive power sharing, as shown in Figure 4.4. Conversely, the objective of reactive power sharing does not uniquely determine the DG bus voltages, and when implemented improperly can result in poor voltage profiles as shown in Figure 4.5. The accuracy of reactive power sharing that can be achieved therefore depends on both the upper and lower limits for the DG voltage magnitudes, and on the homogeneity of the line reactances. We conclude that an ideal secondary voltage controller should allow for a *tunable compromise* between voltage regulation and reactive power sharing.

4.4 Distributed Secondary Control of Voltage/Reactive Power

Note: In this section B is *not* the bus susceptance matrix, but instead denotes an adjacency matrix for a communication graph among the DGs performing secondary voltage control.

As noted in Section 3.3, the E-Q droop controller (3.1b) is unable to share reactive

power between DGs. Moreover, in Section 4.3 we described the conflict between voltage regulation and reactive power sharing. With these problems in mind, we propose the second DAPI controller

$$E_i = E^* - n_i Q_{\mathrm{e},i} + e_i\,, \qquad i \in \mathcal{I}\,, \tag{4.9a}$$

$$\kappa_i \frac{\mathrm{d}e_i}{\mathrm{d}t} = -\beta_i (E_i - E^*) - \sum_{j\in\mathcal{I}} b_{ij} \left(\frac{Q_{\mathrm{e},i}}{Q_i^*} - \frac{Q_j}{Q_j^*} \right)\,, \qquad i \in \mathcal{I}\,, \tag{4.9b}$$

where $e_i \in \mathbb{R}$ is the secondary control variable, $Q_i^* > 0$ is the ith DGs reactive power rating, and $\beta_i, \kappa_i > 0$ are gains. The matrix $B \in \mathbb{R}^{m\times m}$ with elements $b_{ij} > 0$ is the adjacency matrix of a communication network between the DGs. The secondary controller (4.9b) achieves a tunable compromise between voltage regulation and reactive power sharing. We consider four cases:

Case 1 ($\boldsymbol{\beta = 0}$, $\boldsymbol{B \neq 0}$): In this case the first term in (4.9b) is disappears, leaving only the second term. Steady-state requires the derivative on the left-hand side of (4.9b) to be zero, which occurs if and only if $Q_{\mathrm{e},i}/Q_i^* = Q_{\mathrm{e},j}/Q_j^*$ for all inverters. Thus, the steady-state is a power sharing configuration. The secondary control variables e_i converge to values which shift the individual droop curves as necessary to establish proportional power sharing, see Figure 4.5. However, as discussed in Section 4.3, under such a control action DG voltages can drift quite far from their nominal values.

Case 2 ($\boldsymbol{\beta \neq 0}$, $\boldsymbol{B = 0}$): In this case the second term in (4.9b) disappears, and the controller reduces to the standard decentralized voltage-regulating secondary control discussed in Section 4.3. Reactive power is shared poorly (Figure 4.4).

Case 3 ($\boldsymbol{\beta \neq 0}$, $\boldsymbol{B \neq 0}$): In this regime (4.9a)–(4.9b) achieves a compromise between reactive power sharing and voltage regulation based on the relative sizes of the gains β_i and b_{ij}.

Case 4 (Smart Tuning): As a specialization of Case 3, consider having a specific

DG i implement the controller (4.9b) with $\beta_i \neq 0$ and $b_{ij} = 0$, while the all other DGs $j \neq i$ implement (4.9b) with $\beta_j = 0$ and $b_{jk} \neq 0$.[2] That is, DG i regulates its voltage to the nominal value, and the voltages at DGs $j \neq i$ are then controlled to share power in a manner consistent with the voltage regulation of DG i (cf. Section 4.3). This tuning sets up a "leader-follower" [48] relationship among the DGs, where the voltages at DGs $j \neq i$ will form a cluster around the voltage value of $E_i = E^*$ of DG i.

The above cases are tested experimentally in Section 4.5.1.

Remark 4.4.1. (Remarks on DAPI Control). *The communication layers between DG units described the adjacency matrices A and B are* design variables of the DAPI controllers*. This customizable architecture allows for design flexibility. For example, to add redundancy against communication channels being permanently disconnected, supplementary communication can be introduced. Note that the communication architecture need not mirror the electrical topology of the network (Figure 4.8), and that the controllers do not rely on high-gain techniques such as feedback linearization [19]. A detailed schematic of the DAPI control architecture is shown in Figure 4.6.*

The time-constants k_i and κ_i in (4.15b) *and* (4.9b) *allow for a precise tuning of the secondary control speed. A conventional choice is to make k_i and κ_i sufficiently large, enforcing a time-scale separation between primary and secondary control. This however is not* required *– our experimental results suggest that primary and secondary control can be performed on similar time scales without stability issues or performance degradation. Table 4.2 provides a simple qualitative reference for the effects of the control parameters in* (4.15) *and* (4.9)*.*

Stability & Performance of DAPI Voltage Control: While the secondary frequency controller (4.15b) will never destabilize the primary controller (4.15a), the sec-

[2]This directed communication tuning requires that DG i sends information to at least one neighbor.

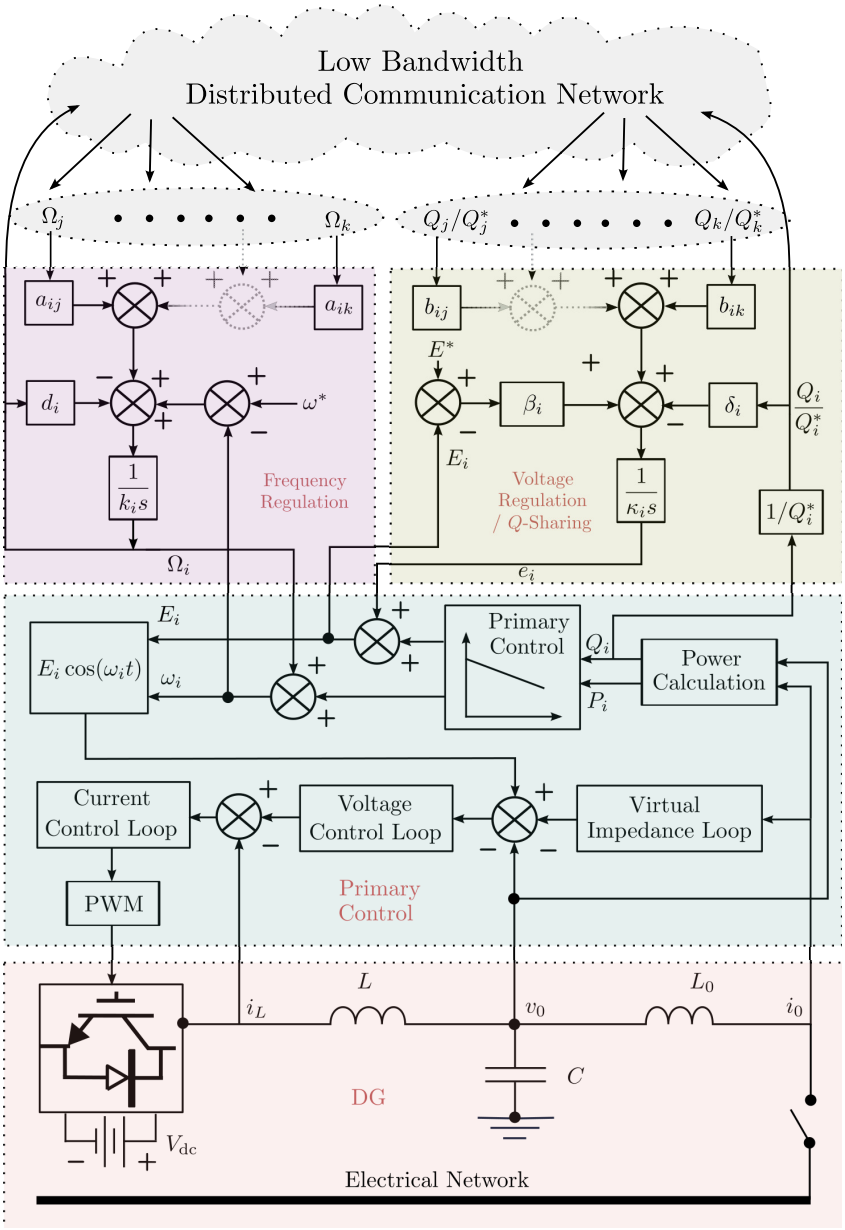

Figure 4.6: Low-level block diagram of the proposed DAPI control architecture for a single DG. For simplicity we have have abbreviated $d_i = \sum_{j=1}^{n} a_{ij}$ and $\delta_i = \sum_{j=1}^{n} b_{ij}$.

ondary voltage controller (4.9b) can potentially destabilize (4.9a). This possibility exists due to the previously discussed conflict between reactive power sharing and voltage regulation. A full nonlinear stability analysis of the voltage/reactive power DAPI controller

Table 4.2: Qualitative effects of controller gains

Gain	Qualitative Change Upon Increase
k_i	Slows frequency regulation at DG i
κ_i	Slows voltage regulation / Q-sharing at DG i
a_{ij}	Faster P-sharing between DGs i and j
b_{ij}	Improved steady-state Q-sharing between DGs i and j
β_i	Improved steady-state voltage regulation at DG i

(4.9a)–(4.9b) is extremely challenging and beyond the scope of this article; a partial analysis for a simpler controller can be found in [13]. In Section 4.4 we present a small-signal stability analysis of (4.9a)–(4.9b), along with sufficient conditions which ensure stable operation. In Section 4.4 we explore the effect of the controller gains in (4.15),(4.9) on the transient performance of the closed-loop system.

Small-Signal Stability of Voltage DAPI Control: To avoid unnecessary technical complications, we model any delay in adjusting the output voltage in (4.9a) with a simple low-pass filter, yielding the dynamic system $\mathrm{d}E_i/\mathrm{d}t = -(E_i - E_i^*) - n_i Q_i + e_i$, and assume loads are impedances collocated with DGs. Both of these assumptions can be relaxed at the expense of more complicated formulae. Under the standard decoupling assumption in which reactive power is related strongly to differences in voltage magnitudes [53], the reactive power injection (2.8b) at the ith DG takes the form

$$Q_i = -E_i^2 Y_{\mathrm{load},ii} + E_i \sum\nolimits_{j=1}^{n} Y_{\mathrm{bus},ij}(E_i - E_j)\,, \tag{4.10}$$

where Y_{load} is diagonal matrix of load susceptances and $Y_{\text{bus}} = Y_{\text{bus}}^T$ is the microgrid's bus admittance matrix [53]. In vector notation, the system equations (4.9),(4.10) are[3]

$$\dot{E} = -(E - E^*) - NQ + e\,, \tag{4.11a}$$

$$\kappa\dot{e} = -\beta(E - E^*) - L_c[Q^*]^{-1}Q\,, \tag{4.11b}$$

$$Q = [E]YE\,, \tag{4.11c}$$

where E, E^* and e are the vectors of voltage magnitudes, voltage set points, and secondary control variables, N, β and κ are diagonal matrices of controller gains, Q and Q^* are the vectors of DG reactive power injections and reactive power ratings, $L_{\text{c}} = \text{diag}(\sum_{j=1}^{n} b_{ij}) - B$ is the Laplacian matrix [57] corresponding to the communication network among the DGs, and $Y = -(Y_{\text{bus}} + Y_{\text{load}})$. When implementing the controller (4.9) in practice, the voltages E_i will remain near their nominal values E^*. We can exploit this to obtain a linear dynamic system by making the approximation that $[E] \simeq [E^*]$ in (4.11c); details on this approximation technique can be found in [9]. After making this approximation and inserting (4.11c) into (4.11b), the nonlinear system (4.11a)–(4.11b) becomes the linear system

$$\dot{x} = Wx + u\,, \tag{4.12}$$

where $x = (E, e)$, $u = (E^*, \kappa^{-1}\beta E^*)$, and

$$W = \begin{pmatrix} -W_1 & I_n \\ -W_2 & 0_n \end{pmatrix} = \begin{pmatrix} -(I_n + N[E^*]Y) & I_n \\ -\kappa^{-1}(\beta + L_c[Q^*]^{-1}[E^*]Y) & 0_n \end{pmatrix},$$

where I_n (resp. 0_n) is the $n \times n$ identity matrix (resp. zero matrix). For future use, we note that all eigenvalues of $-W_1$ are real and negative since W_1 is similar to a sym-

[3]Here $[z]$ denotes the diagonal matrix with the vector z along the diagonal.

metric M-matrix, as can be verified by using the similarity transform TW_1T^{-1} where $T = N_I^{-1/2}[E_I^*]^{-1/2}$. We now derive sufficient conditions under which the linearized system (4.12) is exponentially stable. Specifically, we will assume that the characteristic polynomial $\det(sI_{2n} - W) = 0$ of (4.12) has a root in the closed right-half complex plane, and derive conditions under which this assumption is contradicted. These conditions will therefore ensure all characteristic roots are in the left-half complex plane, and thus ensure stability. Since $-W_1$ has negative eigenvalues, it follows that $\det(sI_n + W_1) \neq 0$, and using the Schur complement determinant formulae for block matrices we may simplify the characteristic polynomial as

$$\det(sI_{2n} - W) = \det(s^2 I_n + sW_1 + W_2) = 0\,. \tag{4.13}$$

Since the determinant is zero, the matrix $s^2 I_n + sW_1 + W_2$ must be singular, and therefore the polynomial (4.13) has a solution if and only if $x^T(s^2 I_n + sW_1 + W_2)x = 0$ for some real vector x of unit length. The latter is simply a scalar quadratic equation of the form $s^2 + \alpha_1 s + \alpha_2 = 0$, where $\alpha_1 = x^T W_1 x$ and $\alpha_2 = x^T W_2 x$. If it is true that

$$\lambda_{\min}(W_1 + W_1^T) > 0\,, \tag{4.14a}$$

$$\lambda_{\min}(W_2 + W_2^T) > 0\,, \tag{4.14b}$$

where $\lambda_{\min}(\cdot)$ is the smallest eigenvalue of the matrix argument, then $\alpha_1, \alpha_2 > 0$ and all solutions of $s^2 + \alpha_1 s + \alpha_2 = 0$ satisfy $\mathrm{Re}(s) < 0$ by the Routh-Hurwitz criterion. This contradicts our assumption that the characteristic polynomial has a closed right-half plane root, and hence under the conditions (4.14) the linearized system is exponentially stable.

Let us now physically interpret the stability conditions (4.14). The first condition

(4.14a) restricts the DGs from being too dissimilar. For example, if all DGs have the same droop gains n_i and voltage set points E^*, then W_1 is a scalar values times Y and (4.14a) is always true. For dissimilar DGs, the intuition for (4.14a) is that given equal voltage set points, DGs with high ratings should be connected to the microgrid through stiff lines of high admittance. To understand the second condition (4.14b), we first consider the case of pure voltage regulation (Case 2 in Section 4.4) where $\beta_i \neq 0$ and $L_{\mathrm{c}} = 0_n$. Then $W_2 = \kappa^{-1}\beta > 0$ is diagonal and (4.14b) is satisfied. The voltage regulation gains β_i always act to stabilize the system. Since eigenvalues are continuous functions of matrix parameters, the system is also stable for non-zero but sufficiently small power sharing gains b_{ij}. In the more general case where the power sharing gains b_{ij} are also non-zero, the condition (4.14b) properly accounts for the complicated interplay between the microgrid's electrical stiffness matrix Y and the averaging control action L_{c} in the product $L_c[Q^*]^{-1}[E^*]Y$. Intuitively, (4.14b) will be satisfied when all line impedances are sufficiently uniform and all DGs are sufficiently similar, since in this case reactive power sharing is not in strong conflict with the line impedance effect (cf. Section 4.3). The stability conditions (4.14) are both satisfied in all experiments presented in Section 4.5.

Transient Performance of DAPI Control The impact of the controller gains k_i, a_{ij}, κ_i, β_i and b_{ij} on the steady-state equilibrium was discussed in detail in Sections 4.2–4.4 and summarized in Table 4.2. We now examine the impact of these controller gains on the system's *transient performance*. To do this, we consider a case study with four DGs (Figure 4.8), with the system parameters of Table 4.3. The communication network among the DGs is a ring, and the controller gains a_{ij} and b_{ij} are given by (4.17); a_{ij} are constants, while b_{ij} are parameterized by a single constant b. For all DGs $i = 1, \ldots, 4$, the other control parameters k_i, κ_i and β_i are taken as uniform constants k, κ and β, respectively. The nominal values for these gains are $k = 1.7\,\mathrm{s}$, $\kappa = 1\,\mathrm{s}$, $\beta = 1.2$, and

$b = 180\,\mathrm{V}$ (the same as in Study 1c of Section 4.5).

We increment the gains independently in intervals around their nominal values, and for each iteration we (i) numerically determine the system operating point from (2.7),(4.15),(4.9), (ii) linearize the closed-loop system around the operating point, and (iii) plot the eigenvalues of the linearization. These eigenvalue traces are displayed in Figure 4.7, where black crosses denote the eigenvalues for the nominal controller gains and arrows indicate the direction of increasing gain.

Eigenvalues on the real axis are strongly associated with the frequency dynamics (4.15a)–(4.15b), while complex conjugate eigenvalues are associated with the voltage dynamics (4.9a)–(4.9b). These conjugate eigenvalues lead to an underdamped voltage response: physically, this is a manifestation of the line impedance effect, which the controller (4.9a)–(4.9b) must overcome to establish reactive power sharing. As the frequency time-constant k is increased (blue), real eigenvalues move towards the origin leading to slow, smooth frequency/active power response. Conversely, decreasing k leads to fast (but still overdamped) frequency regulation. Increasing a_{ij} has an effect nearly identical to decreasing k, and we have therefore omitted the trace and held a_{ij} constant. Increasing the voltage time-constant κ (red) causes the underdamped conjugate eigenvalues to collapse onto the real axis, leading to an overdamped voltage/reactive power response for sufficiently slow secondary control. Increasing either feedback gain b or β (green and gold) results in an increasingly underdamped voltage/reactive power response.

Taken together, Table 4.2, the stability conditions (4.14), and the eigenvalue traces of Figure 4.7 provide a solid foundation for understanding the DAPI controllers (4.15)–(4.9). Our experimental results demonstrate that despite the simplifying assumptions in the preceding analysis, the DAPI controllers (4.15)–(4.9) can be tuned for both stability and high performance.

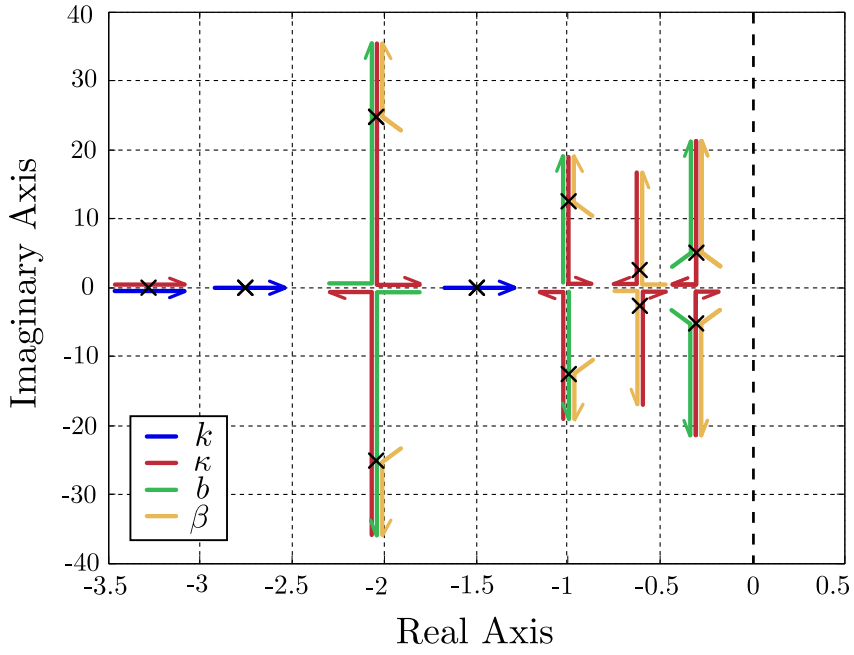

Figure 4.7: Eigenvalue traces of closed-loop system (2.7),(4.15),(4.9) as controller gains are varied. Arrows indicate the direction increasing gain. The absence of a trace indicates that the parameter under consideration has negligible effect on the respective eigenvalue. System parameters are taken from Study 1c of Section 4.5. Black crosses indicate eigenvalue locations for the nominal gains used in Study 1c. Several fast eigenvalues are omitted for clarity.

4.5 Experimental Validation of DAPI Control

This section presents experimental results validating the DAPI controllers presented in Sections 4.2 and 4.4. All experiments were performed at the Intelligent Microgrid Laboratory (Aalborg University, Denmark). Recall that the controllers are

$$\omega_i = \omega^* - m_i P_i + \Omega_i \,, \qquad i \in \mathcal{I} \,, \tag{4.15a}$$

$$k_i \frac{\mathrm{d}\Omega_i}{\mathrm{d}t} = -(\omega_i - \omega^*) - \sum_{j \in \mathcal{I}}^{n} a_{ij} \left(\Omega_i - \Omega_j\right) \,, \qquad i \in \mathcal{I} \,, \tag{4.15b}$$

where Ω_i is the secondary control variable and k_i is a positive gain. The first equation (4.15a) is the standard droop controller with the additional secondary control input Ω_i.

$$E_i = E^* - n_i Q_i + e_i\,, \qquad i \in \mathcal{I}\,, \tag{4.16a}$$

$$\kappa_i \frac{\mathrm{d}e_i}{\mathrm{d}t} = -\beta_i (E_i - E^*) - \sum_{j=1}^{n} b_{ij} \left(\frac{Q_i}{Q_i^*} - \frac{Q_j}{Q_j^*} \right), \qquad i \in \mathcal{I}\,, \tag{4.16b}$$

where e_i is the secondary control variable, Q_i^* is the ith DGs reactive power rating, and β_i, κ_i are positive gains. The $n \times n$ matrix B with elements $b_{ij} > 0$ is the adjacency matrix of a communication network between the DGs.

A schematic of the experimental setup is shown in Figure 4.8, consisting of four DGs interconnected through impedances. Loads are present locally at units 1 and 4, and units 1 and 4 are rated for twice as much power as units 1 and 3 (Table 4.3). The DAPI controllers (4.15a)–(4.9b) were implemented in Simulink®, with measurements recorded via a dSPACE® 1006. See [40, 35] for details on the inner voltage, current and impedance control loops.

This section is organized into four studies, beginning with a characterization of controller performance, and then examining robustness under communication link failure, heterogeneous controller gains, and plug-and-play operation. The communication structure is shown in Figure 4.8, with the adjacency matrices $A = [a_{ij}]$ in (4.15b) and $B = [b_{ij}]$ in (4.9b) being

$$A = \begin{pmatrix} 0 & 1 & 0 & 1 \\ 1 & 0 & 1 & 0 \\ 0 & 1 & 0 & 1 \\ 1 & 0 & 1 & 0 \end{pmatrix}, \quad B = b \cdot \begin{pmatrix} 0 & 1 & 0 & 1 \\ 1 & 0 & 1 & 0 \\ 0 & 1 & 0 & 1 \\ 1 & 0 & 1 & 0 \end{pmatrix}, \tag{4.17}$$

where $b \geq 0$ varies depending on the study under consideration. All other parameters are as reported in Table 4.3. All plots are color-coded in correspondence with Figure 4.8:

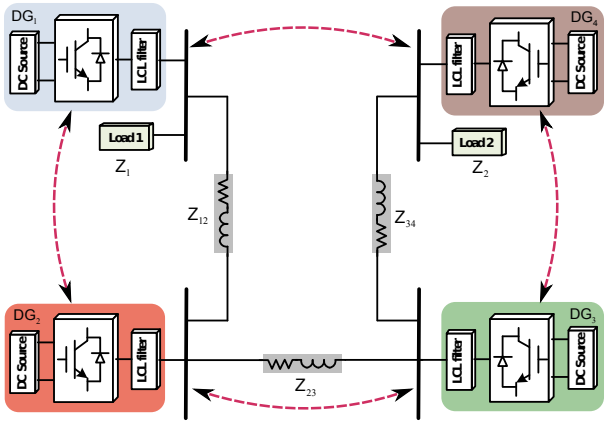

Figure 4.8: Schematic of the experimental microgrid setup, consisting of four DGs interconnected through heterogeneous impedances. Loads are collocated at DGs one and four. Red dotted lines denote communication links.

DG 1 (blue), DG 2 (red), DG 3 (green), and DG 4 (brown).

4.5.1 Study 1: Controller Performance

Studies in this section illustrate the performance of the DAPI controllers (4.15a)–(4.16b) under various controller tunings. In all four sub-studies 1a–1d, only primary droop controllers (4.15a) and (4.16a) are running up to $t = 7\,\mathrm{s}$, at which time the secondary controllers (4.15b) and (4.16b) are activated. The local load at DG unit 4 is detached at $t = 22\,\mathrm{s}$, then reattached at $t = 36\,\mathrm{s}$.

First considering the frequency dynamics in the top portion of Figure 4.9, the frequency deviation experienced under primary droop control is quickly eliminated by the DAPI controller (4.15a)–(4.15b), and frequency regulation is maintained throughout load changes with minimal transients. Active power is accurately shared amongs the heterogeneous DGs throughout the entire runtime. This robust frequency and active power behavior is identical in all other sub-studies, and thus we omit the plots due to space considerations. The remainder of studies 1a and 1b in Figures 4.9 and 4.10 highlight the conclusions drawn in Section 4.3 regarding the limitations of voltage secondary control.

Table 4.3: Electrical and control parameters.

Parameter	Symbol	Value
Electrical Setup		
Nominal Frequency	$\omega^*/2\pi$	$50\,\mathrm{Hz}$
DC Voltage	V_{dc}	$650\,\mathrm{V}$
Nominal Voltages	E^*	$325.3\,\mathrm{V}$ ($230\,\mathrm{V}$ rms)
Filter Capacitance	C	$25\,\mu\mathrm{F}$
Filter Inductance	L_f	$1.8\,\mathrm{mH}$
Output Impedance	L_0	$1.8\,\mathrm{mH}$
Line Impedance (1,2)	Z_{12}	$R = 0.8\,\Omega,\ L = 3.6\,\mathrm{mH}$
Line Impedance (2,3)	Z_{23}	$R = 0.4\,\Omega,\ L = 1.8\,\mathrm{mH}$
Line Impedance (3,4)	Z_{34}	$R = 0.7\,\Omega,\ L = 1.9\,\mathrm{mH}$

Control Parameters			
Parameter	Symbol	DGs 1&4	DGs 2&3
Rated Active Power	P_i^*	1400 W	700 W
Rated Reactive Power	Q_i^*	800 VAr	400 VAr
$P-\omega$ Droop Coeff.	m_i	$2.5\cdot10^{-3}\ \frac{\mathrm{rad}}{\mathrm{W\cdot s}}$	$5\cdot10^{-3}\ \frac{\mathrm{rad}}{\mathrm{W\cdot s}}$
$Q-E$ Droop Coeff.	n_i	$1.5\cdot10^{-3}\ \frac{\mathrm{V}}{\mathrm{VAr}}$	$3\cdot10^{-3}\ \frac{\mathrm{V}}{\mathrm{VAr}}$
Int. Frequency Gain	k_i	$1.7\,\mathrm{s}$	$1.7\,\mathrm{s}$
Int. Voltage Gain	κ_i	$1\,\mathrm{s}$	$1\,\mathrm{s}$

Tuning for pure reactive power sharing: Figure 4.9 shows results for the voltage DAPI controller (4.16a)–(4.16b) tuned for power sharing ($\beta_i = 0$, $b = 50\,\mathrm{V}$), with no attempt at voltage regulation, as in Case 1 of Section 4.4. While reactive power is shared accurately, voltage magnitudes deviate from their nominal values $E^* = 325.3\,\mathrm{V}$ (cf. Figure 4.5).

Tuning for pure voltage regulation: Conversely, Figure 4.10 reports results for the same controller tuned to regulate voltage levels without reactive power sharing ($\beta_i = 2.2$, $b = 0\,\mathrm{V}$), as in Case 2 of Section 4.4. While voltage levels are tightly regulated, reactive power sharing among the units is poor (cf. Figure 4.4). As explained in Section 4.3, the poor performance in Figure 4.10 is a general property of *all* voltage controllers strategies

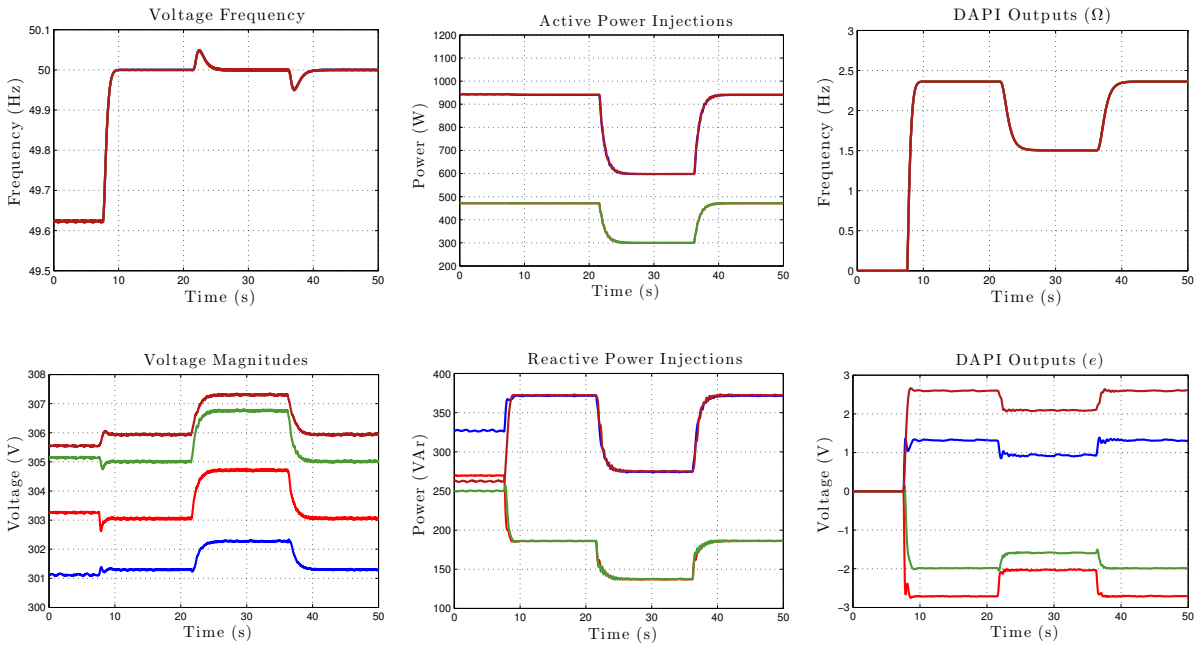

Figure 4.9: Study 1a – reactive power sharing without voltage regulation, with control parameters $b = 50\,\mathrm{V}$, $\beta_1 = \beta_2 = \beta_3 = \beta_4 = 0$. In correspondence with Figure 4.5 of Section 4.3, the quality of voltage regulation is quite poor.

that exactly regulate DG voltage levels.

Compromised tuning: Figure 4.11 displays the results for Study 1c, in which the DAPI controllers (4.15a)–(4.9b) are implemented with $b = 180\,\mathrm{V}$ and uniform controller gains $\beta_i = 1.2$, as in Case 3 of Section 4.4. Considering the voltage dynamics, the voltage DAPI controller (4.16a)–(4.16b) achieves a *compromise* between voltage regulation and reactive power sharing. Voltage magnitudes are roughly clustered around $E^* = 325.3\,\mathrm{V}$, while reactive power is approximately shared.

Smart tuning: Figure 4.12 displays the results for Study 1d, in which the DAPI controllers (4.15a)–(4.9b) are implemented with $b = 100\,\mathrm{V}$ and $\beta_2 = 4$, $\beta_1 = \beta_3 = \beta_4 = 0$, in accordance with the discussion of Case 4 in Section 4.4. In comparison with the voltage dynamics of Study 1c, the voltage regulation in Figure 4.12 shows a slight improvement,

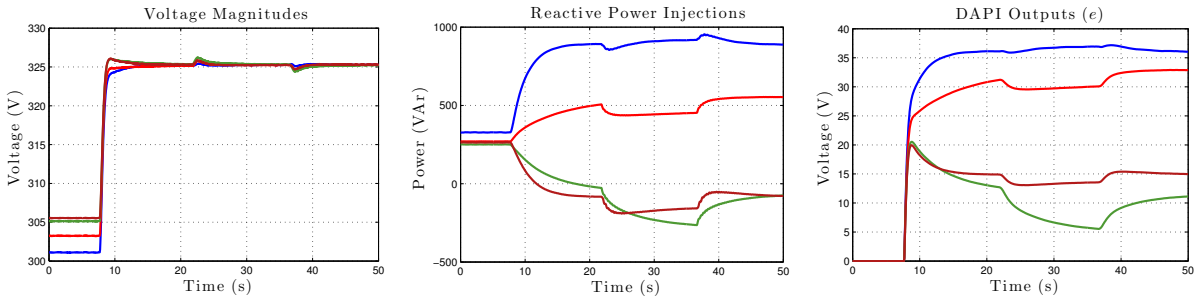

Figure 4.10: Study 1b – voltage regulation without reactive power sharing, with parameters $b = 0\,\mathrm{V}$, $\beta_1 = \beta_2 = \beta_3 = \beta_4 = 2.2$. In correspondence with Figure 4.4 of Section 4.3, the quality of reactive power sharing is quite poor.

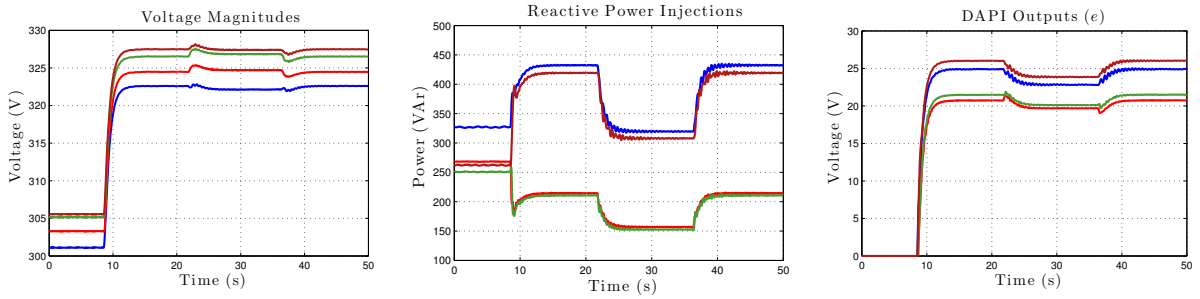

Figure 4.11: Study 1c – a compromise between voltage regulation and reactive power sharing, with control parameters $\beta_1 = \beta_2 = \beta_3 = \beta_4 = 1.2$, $b = 180\,\mathrm{V}$.

while the reactive power sharing is noticeably improved, maintaining accurate sharing through load changes and during transients. Note that this performance improvement has been achieved while *reducing* the controller gain b which enforces reactive power sharing. Due to this reduction in controller gain, the ringing in the reactive power signal during transients is noticeably improved from Study 1c to Study 1d, in agreement with the stability and root locus analyses of Section 4.4.

4.5.2 Study 2: Communication Link Failure

In this study the communication link (Figure 4.8) between DG units 3 and 4 fails at $t = 2\,\mathrm{s}$. At $t = 7\,\mathrm{s}$ the local load at unit 4 is detached, and is reattached at $t = 18\,\mathrm{s}$.

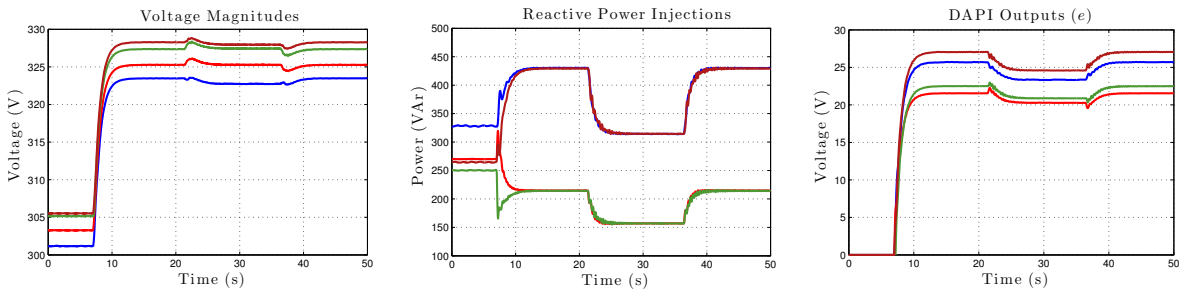

Figure 4.12: Study 1d – accurate reactive power sharing and good voltage regulation, with control parameters $\beta_1 = \beta_3 = \beta_4 = 0$, $\beta_2 = 4$ and $b = 100\,\mathrm{V}$.

Control parameters are the same as in Study 1d. As the results in Figure 4.13 show, the DAPI controllers (4.15a)–(4.9b) maintain the high performance from Study 1d despite the absence of the communication link between DG units 3 and 4 (cf. Remark 4.4.1).

4.5.3 Study 3: Non-Uniform Controller Gains

We examine the behavior of the frequency DAPI controller (4.15a)–(4.15b) under inhomogeneous controller gains. Control parameters are the same as in Study 1d, except for variations in the integral gains $k_1 = 1.5\,\mathrm{s}$, $k_2 = 1\,\mathrm{s}$, $k_3 = 2\,\mathrm{s}$ and $k_4 = 0.5\,\mathrm{s}$. The results are displayed in Figure 4.14. Note that the inhomogeneous controller gains leads to varying transient responses for the DGs, but the steady-state behavior and stability of the system is unchanged. This illustrates the utility of the gains k_i and κ_i in tuning the transient response of the DAPI-controlled microgrid.

4.5.4 Study 4: Plug-and-Play Functionality

The plug-and-play functionality of the controllers was tested by disconnecting unit 3 at $t = 10\,\mathrm{s}$, and reconnecting it at $t = 30\,\mathrm{s}$. A synchronization process was used in the downtime to synchronize unit 3 with the remaining microgrid before reconnection. Control parameters are the same as in Study 1d, and the results are displayed in Figure

4.15. As in previous experiments, the DAPI controllers (4.15a)–(4.9b) maintain accurate power sharing and frequency and voltage regulation before, during, and after the plug-and-play procedure, with minimal transients. The bus voltages and bus frequencies remain well regulated despite the disconnection of DG 3.

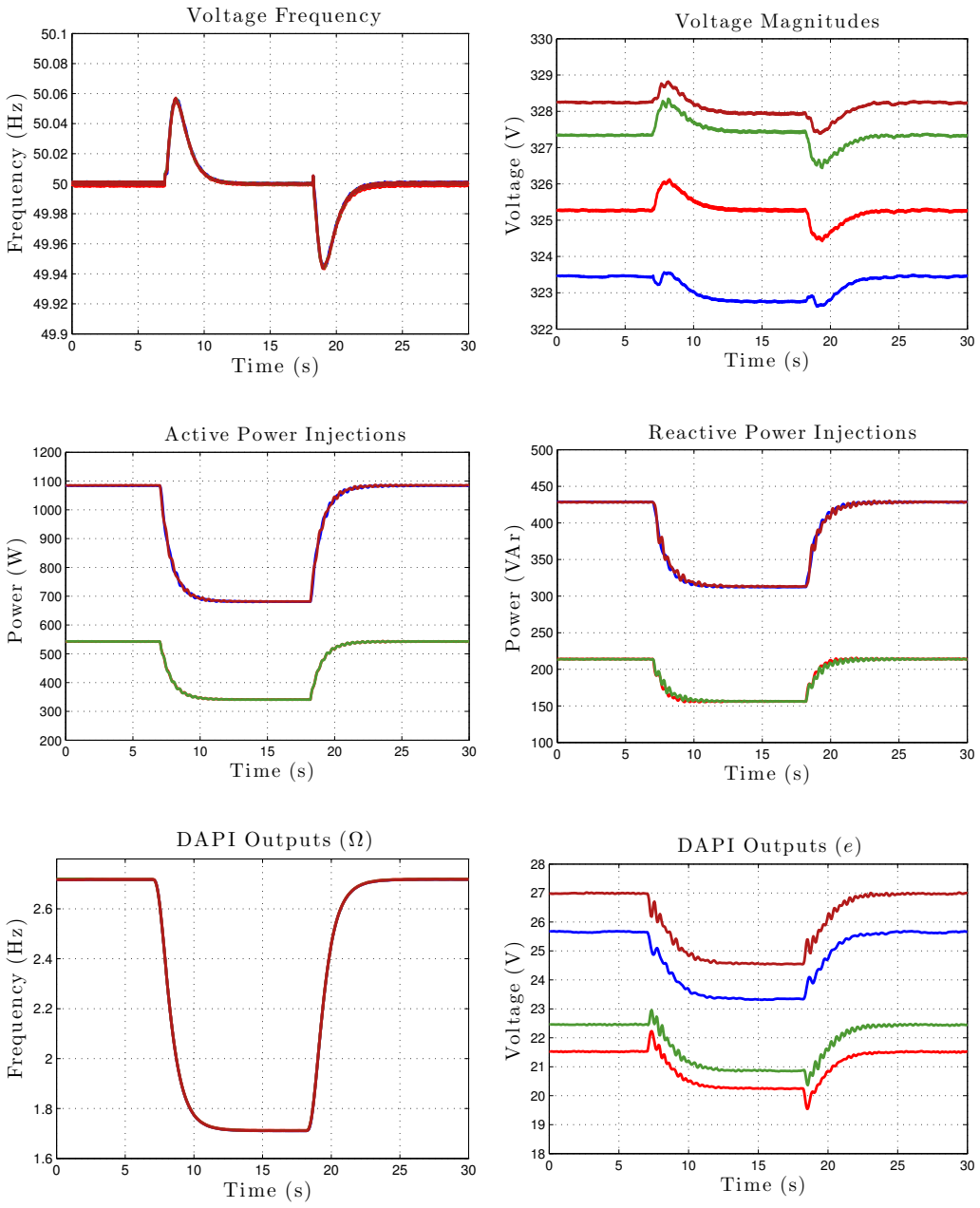

Figure 4.13: Study 2 – DAPI performance under communication link failure. Control parameters are the same as in Study 1d.

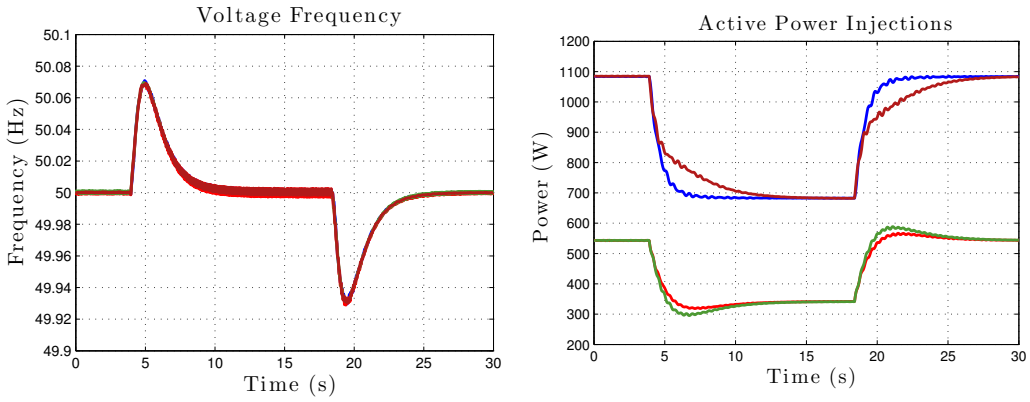

Figure 4.14: Study 3 – DAPI performance with heterogeneous controller gains. Control parameters are the same as in Study 1d.

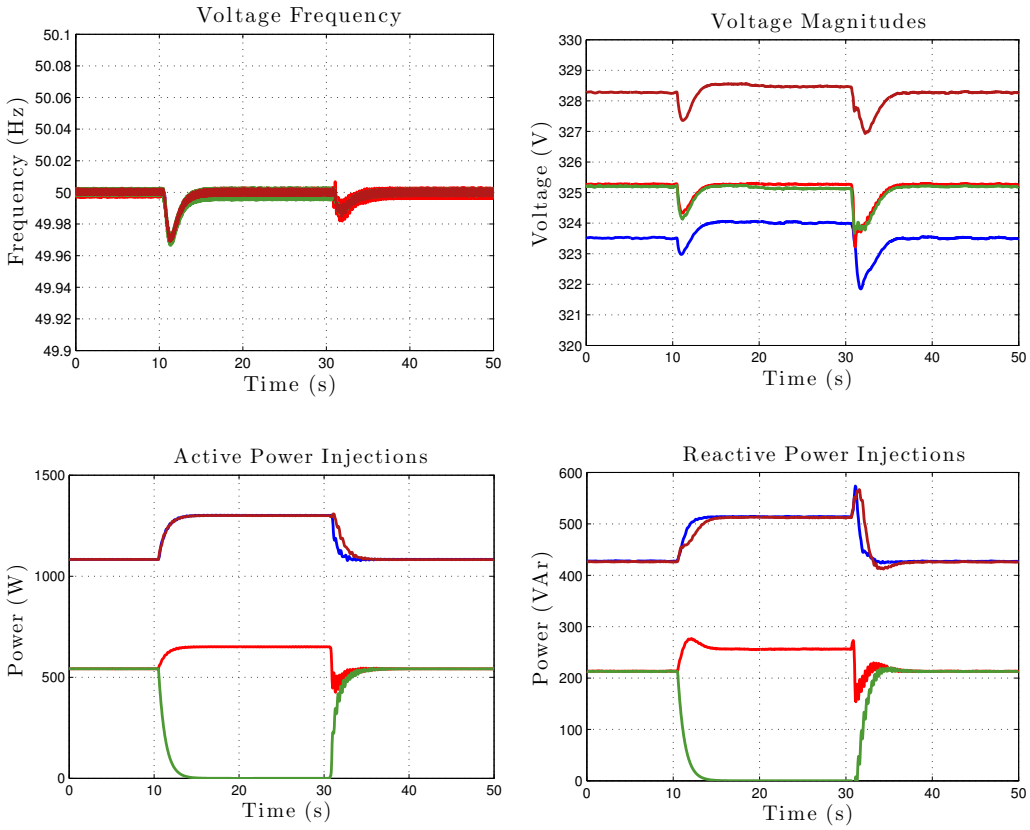

Figure 4.15: Study 4 – DAPI performance under plug-and-play operation. Control parameters are the same as in Study 1d.

Chapter 5

Conclusions

5.1 Summary

In this thesis has consisted of two main parts. In Chapter 3 we have provided a detailed theoretical analysis of primary control in inverter-based power grids. Our results combine analysis techniques from systems and control theory, coupled oscillators, algebraic graph theory, and multi-agent systems in order to accurately quantify the limits of classical primary controllers through necessary and sufficient nonlinear conditions for local stability. For voltage control, we found it convenient to redesign the reactive power droop controller by adding a quadratic nonlinearity. Unlike the conventional droop controller, our proposed quadratic design is physically well motivated, and can be interpreted within "control by interconnection" paradigm. This leads to an elegant circuit-theoretic description of the closed-loop, and to an exact analysis of the network equilibria and their stability properties.

In Chapter 4 we introduced a general distributed control methodology for secondary control in islanded microgrids. By leveraging distributed averaging algorithms from multi-agent systems, the DAPI controllers achieve frequency regulation while sharing

active power proportionally, and can be tuned to achieve either voltage regulation, reactive power sharing, or a compromise between the two. A small-signal stability analysis has been presented for the voltage DAPI controller along with a performance study, and the controllers have been validated through extensive experimental testing.

5.2 Tangential Contributions

In this section we briefly summarize some side-projects which are tangentially related to the contents of this thesis.

Resistive Networks with CPD's: In a standard distribution network scenario, the utility provides a stiff reference voltage at the point of common coupling, while the remaining load nodes in the network tend to take on roughly the same voltage value within a few percent, modulo differences needed for current flows. In [3] we examined what would happen in the absence of such a utility connection; given that certain powers are supplied and demanded, what does the network voltage profile look like in the absence of a stiff reference point? Somewhat surprisingly, we found that the distribution network and the power demands of sources and sinks combine to determine an intrinsic voltage level for the network, independent of a stiff reference from a utility.

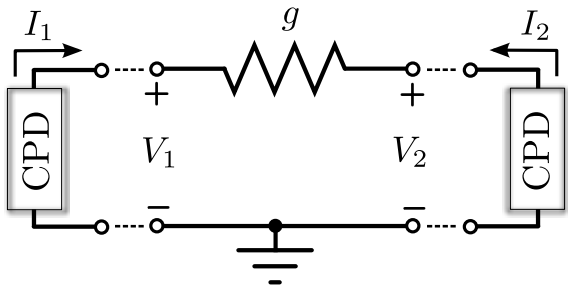

Figure 5.1: A resistive two-port terminated with two constant power devices.

Tertiary Control in Microgrids: A tertiary operation and control layer has the objective to minimize an *economic dispatch problem*, that is, an appropriate quadratic cost of the accumulated generation [78]:

$$\underset{\theta\in\mathbb{T}^n,\, u\in\mathbb{R}^{n_I}}{\text{minimize}} \quad f(u) = \sum\nolimits_{i\in\mathcal{V}_I} \frac{1}{2}\alpha_i u_i^2 \tag{5.1a}$$

$$\text{subject to} \qquad P_i^* + u_i = P_{\mathrm{e},i}(\theta) \qquad \forall\, i \in \mathcal{I}\,, \tag{5.1b}$$

$$P_i^* = P_{\mathrm{e},i}(\theta) \qquad \forall\ i \in \mathcal{L}\,, \tag{5.1c}$$

$$|\theta_i - \theta_j| \le \gamma_{ij}^{(\mathrm{AC})} \qquad \forall\, \{i,j\} \in \mathcal{E}\,, \tag{5.1d}$$

$$P_{\mathrm{e},i}(\theta) \in [0, \overline{P}_i] \qquad \forall\, i \in \mathcal{I}\,, \tag{5.1e}$$

Here, $\alpha_i > 0$ is the cost coefficient for source $i \in \mathcal{V}_I$. The decision variables are the angles θ and secondary control inputs u. The non-convex equality constraints (5.1b)-(5.1c) are the nonlinear steady-state secondary control equations, the *security constraint* (5.1d) limits the power flow on each branch $\{i,j\} \in \mathcal{E}$ with $\gamma_{ij}^{(\mathrm{AC})} \in [0, \pi/2[$, and (5.1e) is a *generation constraint*. In [8, 2] we showed that the set of minimizers of the nonlinear and non-convex AC economic dispatch optimization problem are in one-to-one correspondence with the minimizers of a convex DC dispatch problem. Our next result shows a surprising symbiotic relationship between primary/secondary control and tertiary. We show that the minimum of the AC economic dispatch can be achieved by a decentralized droop control design. Whereas similar conditions are known for related transmission system problems [18, 6, 11, 17, 32, 33, 10, 7] (in a simplified linear and convex setting with lossless DC power flows), we also establish a converse result: every droop controller results in a steady-state which is the minimizer of some AC economic dispatch. We deduce, among others, that the optimal droop coefficients are inversely proportional to the marginal generation costs, and the conventional power sharing objectives is a particular case.

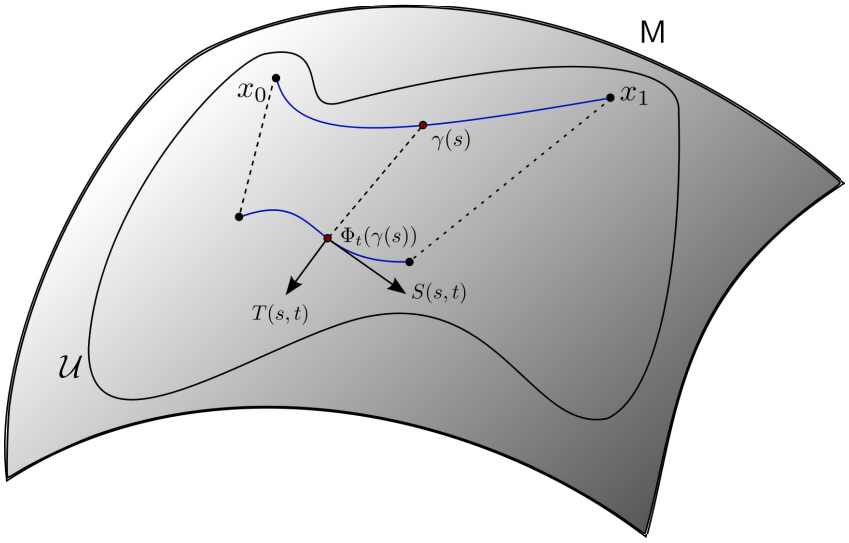

Figure 5.2: Contraction implies that system trajectories converge towards one another – the distance between arbitrary trajectories decreases.

Contraction Theory on Riemannian Manifolds: Problems of synchronization in power networks are essentially questions regarding the convergence of system trajectories towards one another. However, rather than evolving on $\mathbb{R}^n$, frequency dynamics of power networks evolve on the compact manifold $\mathbb{T}^n$, rendering many standard nonlinear stability results applicable only locally. In an attempt to overcome these limitations, we explored the literature on incremental stability and contraction theory, formulated the main stability results and conditions in [16] in the intrinsic, geometric framework of differential geometry. Ultimately we found that the results could not be easily applied to problems in power networks due to issues of determining invariant sets, but the idea of rigorously applying contraction theory to power network dynamics continues to attract serious interest.

5.3 Future Research Directions

While this thesis is among the first to present a set of cohesive analysis and synthesis results for microgrid control, many interesting and important problems remain entirely unresolved. In this final section we present a few interesting (if difficult, or speculative) directions for future research.

Decentralized Droop Control in Heterogeneous Networks: The droop controllers analyzed in this work are designed for use in networks with inductive characteristics. In Remarks 2.2.2 we commented on how under uniform R/X ratios, a rotation in the space of power injections can transform lossy power flow into lossless power flow, allowing the application of analysis and control techniques such as the droop controllers considered herein. This approach is rather elegant, in that the transformed system "looks like" a lossless system. While reasonable in highly engineered settings, in plug-and-play situations in real-life networks, this validation approach suffers two drawbacks: (1) real distribution networks are often built in an ad-hoc manner, with various types of distribution lines installed at different points in time, and (2) objectives such as active and reactive power sharing are difficult to analyze due to the rotation of power coordinates.

An open and extremely important problem is to design a provably stable decentralized or distributed control strategy for microgrids with heterogeneous R/X ratios. The controller should be simple, intuitive, and yield performance guarantees comparable the ones provided herein. While we are skeptical that this problem is feasible in a decentralized framework, its solution seems attainable if one allows for a distributed control framework with communication.

Another issue not addressed in this work is a nonlinear analysis of reactive power sharing, as an analysis of the voltage-droop controller (3.1b) is difficult to perform. Large-

signal stability of the voltage controller (4.9a)-(4.9b) remains an open analysis problem. Moreover, the secondary control goals of voltage regulation and reactive power sharing ignore an important factor for microgrid stability: the voltage levels at loads which are not collocated with DGs. An open problem is to design a controller guaranteeing that voltage levels at non-collocated load buses remain within tolerances while maintaining a high level of performance.

Dynamic Architectures for Distributed Power Grid Control: Localized response properties of power grids [95, 93, 92] imply that large-scale centralized control architectures are inefficient, in that given an area in need of control action, all relevant state information is already local to that area, and control actions must also be taken at least relatively locally. This localized response is a result of the nonlinear diffusive behavior of power networks; under normal operation, state variables are insensitive to disturbances that are electrically distant.

It follows that optimal control architectures for power grids should be sensitivity-limited, with local control options being exhausted before electrically distant controls are implemented. Moreover, recognizing that power grids are dynamic networks, control areas should not be static, but should evolve dynamically with the condition of the system.

Appendix A

Technical Lemmas

A.1 Useful Results

Lemma A.1.1. (Sherman-Morrison Formula, [99]). *Let $A, B \in \mathbb{R}^{n\times n}$ and let A be nonsingular. If $A + B$ is nonsingular, then*

$$(A + B)^{-1} = A^{-1} - A^{-1}(I_n + BA^{-1})^{-1}BA^{-1}\,.$$

A.2 Chapter 3

Proposition A.2.1. (Properties of Reduced Quantities). *The following statements hold:*

(i) $-B_{\text{red}}$ *is an* M*-matrix;*

(ii) W_1 *and* W_2 *are row-stochastic;*

(iii) $E_L^* > \mathbb{0}_n$ *component-wise.*

Proof. **(*i*) :** The first fact follows from the closure of the set of symmetric positive definite M-matrices under the Schur complement, as $-B_{\text{red}}$ is the Schur complement of $-(B +$

blkdiag$(\mathbb{0}, K_I)$) with respect to the $-(B_{II} + K_I)$ block [22, Lemma 2.1], [62].

(ii) **:** We begin with W_2. Since $B_{II}+K_I$ is a principal sunblock of (B+blkdiag$(\mathbb{0}, K_I)$), the negative of which is an M-matrix, it is invertible and has an inverse with nonpositive elements. Moreover, both $-B_{IL}$ and K_{IL} are nonpositive, and it follows that W_2 is nonnegative. We expand the inverse using the Sherman Morrison Formula (Lemma A.1.1) to obtain

$$\begin{aligned} W_2 &= (K_I + B_{II})^{-1} \begin{bmatrix} -B_{IL} & K_I \end{bmatrix} \\ &= \left(B_{II}^{-1} - B_{II}^{-1}(I_m + K_I B_{II}^{-1})^{-1} K_I B_{II}^{-1}\right) \begin{bmatrix} -B_{IL} & K_I \end{bmatrix} \\ &= (I_m - B_{II}^{-1}(I_m + K_I B_{II}^{-1})^{-1} K_I) \begin{bmatrix} -B_{II}^{-1} B_{IL} & B_{II}^{-1} K_I \end{bmatrix} . \end{aligned}$$

Left-multiplying by $\mathbb{1}_{n+m}$ and turning the crank, we calculate that

$$\begin{aligned} W_2 \mathbb{1}_{n+m} &= (I_m - B_{II}^{-1}(I_m + K_I B_{II}^{-1})^{-1} K_I) \left(\mathbb{1}_m + B_{II}^{-1} K_I \mathbb{1}_m\right) \\ &= \mathbb{1}_m + B_{II}^{-1} K_I \mathbb{1}_m - B_{II}^{-1}(I_m + K_I B_{II}^{-1})^{-1} K_I (\mathbb{1}_m + B_{II}^{-1} K_I \mathbb{1}_m) \\ &= \mathbb{1}_m + B_{II}^{-1} K_I \mathbb{1}_m - B_{II}^{-1}(I_m + K_I B_{II}^{-1})^{-1} K_I (I_m + B_{II}^{-1} K_I) \mathbb{1}_m \\ &= \mathbb{1}_m + B_{II}^{-1} K_I \mathbb{1}_m - B_{II}^{-1}(I_m + K_I B_{II}^{-1})^{-1} (I_m + K_I B_{II}^{-1}) K_I \mathbb{1}_m \\ &= \mathbb{1}_m + B_{II}^{-1} K_I \mathbb{1}_m - B_{II}^{-1} K_I \mathbb{1}_m \\ &= \mathbb{1}_m , \end{aligned}$$

where we have used the fact that $-B_{II}^{-1} B_{IL}$ is row-stochastic. We proceed similarly for $W_1 = -B_{\text{red}}^{-1} B_{LI} \left(K_I + B_{II}\right)^{-1} K_I$. Since $-B_{\text{red}}$ is an M-matrix, $-B_{\text{red}}^{-1}$ has nonnegative elements. Likewise, $(K_I + B_{II})^{-1}$ has nonpositive elements, K_I has strictly negative elements, and B_{LI} has nonnegative elements. It follows that W_1 is nonnegative. Multiplying

by $\mathbb{1}_n$ and turning the crank, we calculate that

$$\begin{aligned}
W_1\mathbb{1}_m &= -B_{\text{red}}^{-1}B_{LI}\left((K_I+B_{II})^{-1}K_I\mathbb{1}_m - (K_I+B_{II})^{-1}B_{IL}\mathbb{1}_n + (K_I+B_{II})^{-1}B_{IL}\mathbb{1}_n\right)\\
&= -B_{\text{red}}^{-1}B_{LI}W_2\mathbb{1}_{n+m} - B_{\text{red}}^{-1}B_{LI}(K_I+B_{II})^{-1}B_{IL}\mathbb{1}_n\\
&= -B_{\text{red}}^{-1}B_{LI}\mathbb{1}_m - B_{\text{red}}^{-1}\underbrace{B_{LI}(K_I+B_{II})^{-1}B_{IL}}_{B_{LL}-B_{\text{red}}}\mathbb{1}_n\\
&= \mathbb{1}_n - B_{\text{red}}^{-1}\left(B_{LL}\mathbb{1}_n + B_{LI}\mathbb{1}_m\right)\\
&= \mathbb{1}_n - B_{\text{red}}^{-1}\mathbb{0}_n\\
&= \mathbb{1}_n.
\end{aligned}$$

where we have used the definition of B_{red} and the fact that L has zero row sum. Item (iii) then follows from (ii) since $E_L^* = W_1E_I^*$ and E_I^* has strictly positive entries. □

Lemma 3.3.1

Proof. **(i):** Differentiating the load equation (3.50) with respect to E_0 and dividing by b_{tot} gives the hyperplane $\mathcal{H}$, which when restricted to $\mathcal{M}$ as in (3.51) gives the singular surface.

(ii): Combining the expression for the hyperplane in (3.51) and the load balance (3.50) by solving each for $-\sum_{j=1}^{N-1} b_{j0}E_j$ and equating them, we calculate that $E_0 = \pm\sqrt{Q_0/b_{\text{tot}}}$. Since $b_{\text{tot}} < 0$ by definition, it follows that for $Q_0 \geq 0$ there are no singular points in the strictly positive orthant $\mathbb{R}^{N+1}_{>0}$. For $Q_0 < 0$, E_0 must take on the unique positive value $\bar{E}_0 = \sqrt{Q_0/b_{\text{tot}}}$. Substituting $\bar{E}_0$ back into the load balance (3.50), we find explicitly that $\mathcal{S}\cap\mathbb{R}^{N+1}_{>0} = \{E \in \mathcal{M}\cap\mathbb{R}^{n+1}_{>0} \ : \ E_0 = \bar{E}_0 \text{ and } \bar{E}_0 = \frac{1}{2b_{\text{tot}}}\sum_{j=1}^{N-1} b_{j0}E_j\}$. Let

S^{s} (resp. S^{u}) be the set of points $E \in \mathbb{R}^{N+1}_{>0}$ where $\frac{\partial h}{\partial E} < 0$ (resp. $\frac{\partial h}{\partial E} > 0$). That is,

$$S^{\mathrm{s}} \triangleq \left\{ E \in \mathbb{R}^{N+1}_{>0} \,\middle|\, E_0 > \frac{1}{2b_{\mathrm{tot}}} \sum\nolimits_{j=1}^{N-1} b_{j0} E_j \right\},$$
$$S^{\mathrm{u}} \triangleq \left\{ E \in \mathbb{R}^{N+1}_{>0} \,\middle|\, E_0 < \frac{1}{2b_{\mathrm{tot}}} \sum\nolimits_{j=1}^{N-1} b_{j0} E_j \right\}.$$

Clearly S^+ and S^- are separated by the unrestriced version of the hyperplane in (3.51). Define

$$\mathcal{M}^{\mathrm{stable}}_{>0} \triangleq \{E \in \mathcal{M} \cap \mathbb{R}^{n+1}_{>0} \ : \ E_0 > \bar{E}_0\},$$
$$\mathcal{M}^{\mathrm{unstable}}_{>0} \triangleq \{E \in \mathcal{M} \cap \mathbb{R}^{n+1}_{>0} \ : \ E_0 < \bar{E}_0\}.$$

We will show that $\mathcal{M}^{\mathrm{stable}}_{>0} \subset S^{\mathrm{s}}$, and hence conclude that $\mathcal{M}^{\mathrm{stable}}_{>0}$ is a stable component (Figure A.1). Take $E \in \mathcal{M}^{\mathrm{stable}}_{>0}$. Then from (3.50), E satisfies

$$\frac{1}{2b_{\mathrm{tot}}} \sum\nolimits_{j=1}^{N-1} b_{j0} E_j = \frac{1}{2}\left(E_0 + \frac{\bar{E}_0^2}{E_0}\right), \tag{A.3}$$

where we have rewritten Q_0 in terms of $\bar{E}_0$. One quickly verifies that the right-hand side of (A.3) is less than E_0 for $E_0 > \bar{E}_0$, and thus for every $E \in \mathcal{M}^{\mathrm{stable}}_{>0}$. It follows that $\mathcal{M}^{\mathrm{stable}}_{>0} \subset S^{\mathrm{s}}$, and an analogous argument shows that $\mathcal{M}^{\mathrm{unstable}}_{>0} \subset S^{\mathrm{u}}$. It follows that $\mathcal{M}^{\mathrm{stable}}_{>0}$ and $\mathcal{M}^{\mathrm{unstable}}_{>0}$ are disjoint, completing the proof. □

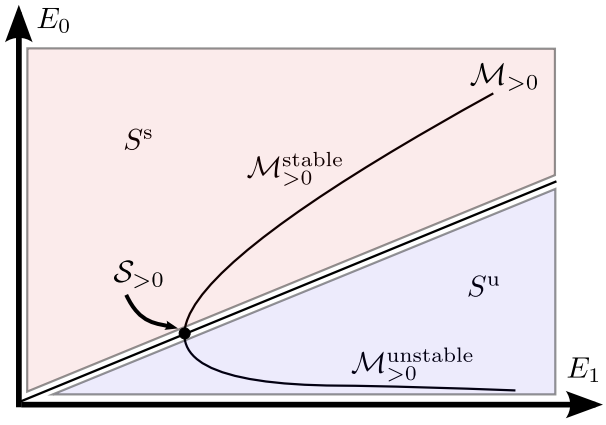

Figure A.1: Constraint manifold and associated constructions for one inverter and one inductive load $Q_0 < 0$.

Bibliography

[1] S. Bolognani and S. Zampieri. "On the Existence and Linear Approximation of the Power Flow Solution in Power Distribution Networks". In: *IEEE Transactions on Power Systems* (2015). to appear.

[2] F. Dörfler, J. W. Simpson-Porco, and F. Bullo. "Breaking the Hierarchy: Distributed Control & Economic Optimality in Microgrids". In: *IEEE Transactions on Control of Network Systems* (2015). To appear.

[3] J. W. Simpson-Porco, F. Dörfler, and F. Bullo. "On Resistive Networks of Constant Power Devices". In: *IEEE Transactions on Circuits and Systems II: Express Briefs* 62.8 (2015), pp. 811–815.

[4] J. W. Simpson-Porco et al. "Secondary Frequency and Voltage Control of Islanded Microgrids via Distributed Averaging". In: *IEEE Transactions on Industrial Electronics* (2015). To appear.

[5] M. Andreasson et al. "Distributed Control of Networked Dynamical Systems: Static Feedback, Integral Action and Consensus". In: *IEEE Transactions on Automatic Control* 59.7 (2014), pp. 1750–1764.

[6] M. Andreasson et al. "Distributed PI-control with applications to power systems frequency control". In: *American Control Conference*. Portland, OR, USA, June 2014, pp. 3183–3188.

[7] M. Bürger, C. De Persis, and S. Trip. "An internal model approach to (optimal) frequency regulation in power grids". In: *arXiv preprint arXiv:1403.7019* (2014).

[8] F. Dörfler, J. W. Simpson-Porco, and F. Bullo. "Plug-and-play control and optimization in microgrids". In: *IEEE Conf. on Decision and Control*. Los Angeles, CA, USA, Dec. 2014, pp. 211–216.

[9] B. Gentile et al. "On reactive power flow and voltage stability in microgrids". In: *American Control Conference*. Portland, OR, USA, June 2014, pp. 759–764.

[10] Na Li et al. "Connecting Automatic Generation Control and Economic Dispatch from an Optimization View". In: *American Control Conference*. Portland, OR, USA, June 2014, pp. 735–740.

[11] E. Mallada and S. H. Low. "Distributed Frequency-Preserving Optimal Load Control". In: *IFAC World Congress*. Cape Town, South Africa, Aug. 2014, pp. 5411–5418.

[12] A. Micallef et al. "Reactive Power Sharing and Voltage Harmonic Distortion Compensation of Droop Controlled Single Phase Islanded Microgrids". In: *IEEE Transactions on Smart Grid* 5.3 (2014), pp. 1149–1158.

[13] J. Schiffer et al. "A consensus-based distributed voltage control for reactive power sharing in microgrids". In: *European Control Conference*. Strasbourg, France, June 2014, pp. 1299–1305.

[14] Q. Shafiee, J. M. Guerrero, and J. C. Vasquez. "Distributed Secondary Control for Islanded Microgrids - A Novel Approach". In: *IEEE Transactions on Power Electronics* 29.2 (2014), pp. 1018–1031.

[15] Q. Shafiee et al. “Robust Networked Control Scheme for Distributed Secondary Control of Islanded Microgrids”. In: *IEEE Transactions on Industrial Electronics* 61.10 (2014), pp. 5363–5374.

[16] J. W. Simpson-Porco and F. Bullo. “Contraction Theory on Riemannian Manifolds”. In: *Systems & Control Letters* 65 (2014), pp. 74–80.

[17] Seungil You and Lijun Chen. “Reverse and Forward Engineering of Frequency Control in Power Networks”. In: *IEEE Conf. on Decision and Control*. Los Angeles, CA, USA, Dec. 2014, pp. 191–198.

[18] Martin Andreasson et al. “Distributed vs. Centralized Power Systems Frequency Control under Unknown Load Changes”. In: *European Control Conference*. Zürich, Switzerland, July 2013, pp. 3524–3529.

[19] A. Bidram et al. “Distributed Cooperative Secondary Control of Microgrids Using Feedback Linearization”. In: *IEEE Transactions on Power Systems* 28.3 (2013), pp. 3462–3470.

[20] S. Bolognani and S. Zampieri. “A distributed control strategy for reactive power compensation in smart microgrids”. In: *IEEE Transactions on Automatic Control* 58.11 (2013), pp. 2818–2833.

[21] H. Bouattour et al. “Further results on distributed secondary control in microgrids”. In: *IEEE Conf. on Decision and Control*. Florence, Italy, Dec. 2013, pp. 1514–1519.

[22] F. Dörfler and F. Bullo. “Kron Reduction of Graphs with Applications to Electrical Networks”. In: *IEEE Transactions on Circuits and Systems I: Regular Papers* 60.1 (2013), pp. 150–163.

[23] F. Dörfler, M. Chertkov, and F. Bullo. "Synchronization in Complex Oscillator Networks and Smart Grids". In: *Proceedings of the National Academy of Sciences* 110.6 (2013), pp. 2005–2010.

[24] B. Gentile. "Approximate Solution to the Reactive Power Flow and its Application to Voltage Stability in Microgrids". MA thesis. Università di Padova, Italy, Oct. 2013.

[25] J. M. Guerrero et al. "Advanced Control Architectures for Intelligent Microgrids – Part I: Decentralized and Hierarchical Control". In: *IEEE Transactions on Industrial Electronics* 60.4 (2013), pp. 1254–1262.

[26] J. M. Guerrero et al. "Advanced Control Architectures for Intelligent Microgrids – Part II: Power Quality, Energy Storage, and AC/DC Microgrids". In: *IEEE Transactions on Industrial Electronics* 60.4 (2013), pp. 1263–1270.

[27] H.S.V.S. Kumar Nunna and S. Doolla. "Multiagent-Based Distributed-Energy-Resource Management for Intelligent Microgrids". In: *IEEE Transactions on Industrial Electronics* 60.4 (2013), pp. 1678–1687.

[28] J. W. Simpson-Porco, F. Dörfler, and F. Bullo. "Synchronization and Power Sharing for Droop-Controlled Inverters in Islanded Microgrids". In: *Automatica* 49.9 (2013), pp. 2603–2611.

[29] J. W. Simpson-Porco, F. Dörfler, and F. Bullo. "Voltage stabilization in microgrids via quadratic droop control". In: *IEEE Conf. on Decision and Control*. Florence, Italy, Dec. 2013, pp. 7582–7589.

[30] J. W. Simpson-Porco et al. "Stability, power sharing, & distributed secondary control in droop-controlled microgrids". In: *IEEE Int. Conf. on Smart Grid Communications*. Vancouver, BC, Canada, Oct. 2013, pp. 672–677.

[31] Z. Wang, M. Xia, and M. D. Lemmon. "Voltage Stability of Weak Power Distribution Networks with Inverter Connected Sources". In: *American Control Conference*. Washington DC, USA, June 2013, pp. 6592–6597.

[32] Xuan Zhang and Antonis Papachristodoulou. "A real-time control framework for smart power networks with star topology". In: *American Control Conference*. Washington, DC, USA, 2013, pp. 5062–5067.

[33] Changhong Zhao et al. "Power system dynamics as primal-dual algorithm for optimal load control". In: *arXiv preprint arXiv:1305.0585* (2013).

[34] Q.-C. Zhong. "Robust Droop Controller for Accurate Proportional Load Sharing Among Inverters Operated in Parallel". In: *IEEE Transactions on Industrial Electronics* 60.4 (2013), pp. 1281–1290.

[35] Q.-C. Zhong and T. Hornik. *Control of Power Inverters in Renewable Energy and Smart Grid Integration*. Wiley-IEEE Press, 2013. ISBN: 0470667095.

[36] M. Savaghebi et al. "Secondary Control for Voltage Quality Enhancement in Microgrids". In: *IEEE Transactions on Smart Grid* 3.4 (2012), pp. 1893–1902.

[37] J. W. Simpson-Porco, F. Dörfler, and F. Bullo. "Droop-controlled inverters are Kuramoto oscillators". In: *IFAC Workshop on Distributed Estimation and Control in Networked Systems*. Santa Barbara, CA, USA, Sept. 2012, pp. 264–269.

[38] Smart Grid Investment Grant Program. *Application of automated controls for voltage and reactive power management - initial results*. Tech. rep. U.S. Department of Energy, Dec. 2012.

[39] F. Dörfler and F. Bullo. "On the Critical Coupling for Kuramoto Oscillators". In: *SIAM Journal on Applied Dynamical Systems* 10.3 (2011), pp. 1070–1099.

[40] J. M. Guerrero et al. "Hierarchical Control of Droop-Controlled AC and DC Microgrids–A General Approach Toward Standardization". In: *IEEE Transactions on Industrial Electronics* 58.1 (2011), pp. 158–172.

[41] H. Xin et al. "A Self Organizing Strategy for Power Flow Control of Photovoltaic Generators in a Distribution Network". In: *IEEE Transactions on Power Electronics* 26.3 (2011), pp. 1462–1473.

[42] W. Yao et al. "Design and analysis of the droop control method for parallel inverters considering the impact of the complex impedance on the power sharing". In: *IEEE Transactions on Industrial Electronics* 58.2 (2011), pp. 576–588.

[43] F. Garin and L. Schenato. "A Survey on Distributed Estimation and Control Applications Using Linear Consensus Algorithms". In: *Networked Control Systems*. Ed. by A. Bemporad, M. Heemels, and M. Johansson. LNCIS. Springer, 2010, pp. 75–107.

[44] M. Mesbahi and M. Egerstedt. *Graph Theoretic Methods in Multiagent Networks*. Princeton University Press, 2010.

[45] A. Mohd et al. "Review of control techniques for inverters parallel operation". In: *Electric Power Systems Research* 80.12 (2010), pp. 1477–1487.

[46] A. J. van der Schaft. "Characterization and partial synthesis of the behavior of resistive circuits at their terminals". In: *Systems & Control Letters* 59.7 (2010), pp. 423–428.

[47] D. S. Bernstein. *Matrix Mathematics*. 2nd ed. Princeton University Press, 2009.

[48] F. Bullo, J. Cortés, and S. Martínez. *Distributed Control of Robotic Networks*. Princeton University Press, 2009. ISBN: 978-0-691-14195-4.

[49] J. M. Guerrero et al. “Control Strategy for Flexible Microgrid Based on Parallel Line-Interactive UPS Systems”. In: *IEEE Transactions on Industrial Electronics* 56.3 (2009), pp. 726–736.

[50] Y. U. Li and C.-N. Kao. “An accurate power control strategy for power-electronics-interfaced distributed generation units operating in a low-voltage multibus microgrid”. In: *IEEE Transactions on Power Electronics* 24.12 (2009), pp. 2977–2988.

[51] A. Arenas et al. “Synchronization in complex networks”. In: *Physics Reports* 469.3 (2008), pp. 93–153.

[52] E. C. Furtado, L. A. Aguirre, and L. A. B. Tôrres. “UPS Parallel Balanced Operation Without Explicit Estimation of Reactive Power – A Simpler Scheme”. In: *IEEE Transactions on Circuits and Systems II: Express Briefs* 55.10 (2008), pp. 1061–1065.

[53] J. Machowski, J. W. Bialek, and J. R. Bumby. *Power System Dynamics*. 2nd ed. John Wiley & Sons, 2008. ISBN: 0-470-72588-0.

[54] R. Majumder et al. “Power system stability and load sharing in distributed generation”. In: *Power System Technology and IEEE Power India Conference*. New Delhi, India, Oct. 2008, pp. 1–6.

[55] Y. Mohamed and E. F. El-Saadany. “Adaptive decentralized droop controller to preserve power sharing stability of paralleled inverters in distributed generation microgrids”. In: *IEEE Transactions on Power Electronics* 23.6 (2008), pp. 2806–2816.

[56] M. N. Marwali, J.-W. Jung, and A. Keyhani. “Stability Analysis of Load Sharing Control for Distributed Generation Systems”. In: *IEEE Transactions on Energy Conversion* 22.3 (2007), pp. 737–745.

[57] R. Olfati-Saber, J. A. Fax, and R. M. Murray. "Consensus and cooperation in networked multi-agent systems". In: *Proceedings of the IEEE* 95.1 (2007), pp. 215–233.

[58] W. Ren, R. W. Beard, and E. M. Atkins. "Information consensus in multivehicle cooperative control: Collective group behavior through local interaction". In: *IEEE Control Systems Magazine* 27.2 (2007), pp. 71–82.

[59] J. A. P. Lopes, C. L. Moreira, and A. G. Madureira. "Defining control strategies for microgrids islanded operation". In: *IEEE Transactions on Power Systems* 21.2 (2006), pp. 916–924.

[60] J. M. Guerrero et al. "Output Impedance Design of Parallel-Connected UPS Inverters With Wireless Load-Sharing Control". In: *IEEE Transactions on Industrial Electronics* 52.4 (2005), pp. 1126–1135.

[61] Z. Lin, B. Francis, and M. Maggiore. "Necessary and sufficient graphical conditions for formation control of unicycles". In: *IEEE Transactions on Automatic Control* 50.1 (2005), pp. 121–127.

[62] F. Zhang. *The Schur Complement and Its Applications*. Springer, 2005.

[63] M. Dai et al. "Power flow control of a single distributed generation unit with nonlinear local load". In: *IEEE Power Systems Conference and Exposition*. New York, USA, Oct. 2004, pp. 398–403.

[64] R. Riaza. "A matrix pencil approach to the local stability analysis of non-linear circuits". In: *Int. Journal of Circuit Theory and Applications* 32.6 (2004), pp. 23–46.

[65] S. Barsali et al. “Control techniques of dispersed generators to improve the continuity of electricity supply”. In: *IEEE Power Engineering Society Winter Meeting*. New York, NY, USA, Jan. 2002, pp. 789–794.

[66] E. A. A. Coelho, P. C. Cortizo, and P. F. D. Garcia. “Small-signal stability for parallel-connected inverters in stand-alone AC supply systems”. In: *IEEE Transactions on Industry Applications* 38.2 (2002), pp. 533–542.

[67] R. H. Lasseter. “MicroGrids”. In: *IEEE Power Engineering Society Winter Meeting*. Vol. 1. 2002, pp. 305–308. DOI: 10.1109/PESW.2002.985003.

[68] R. Ortega et al. “Interconnection and damping assignment passivity-based control of port-controlled Hamiltonian systems”. In: *Automatica* 38.4 (2002), pp. 585–96.

[69] C. D. Godsil and G. F. Royle. *Algebraic Graph Theory*. Vol. 207. Graduate Texts in Mathematics. Springer, 2001. ISBN: 0387952411.

[70] C. D. Meyer. *Matrix Analysis and Applied Linear Algebra*. SIAM, 2001. ISBN: 0898714540.

[71] H. Goldstein, C. Poole, and J. Safko. *Classical Mechanics*. 3rd ed. Addison-Wesley, 2000.

[72] R. Lasseter and P. Piagi. “Providing premium power through distributed resources”. In: *Annual Hawaii Int. Conference on System Sciences*. Maui, HI, USA, Jan. 2000, pp. 4042–4051.

[73] S. H. Strogatz. “From Kuramoto to Crawford: Exploring the onset of synchronization in populations of coupled oscillators”. In: *Physica D: Nonlinear Phenomena* 143.1 (2000), pp. 1–20.

[74] B. C. Lesieutre, P. W. Sauer, and M. A. Pai. "Existence of solutions for the network/load equations in power systems". In: *IEEE Transactions on Circuits and Systems I: Fundamental Theory and Applications* 46.8 (1999), pp. 1003–1011.

[75] P. W. Sauer and M. A. Pai. *Power System Dynamics and Stability*. Prentice Hall, 1998.

[76] T. Van Cutsem and C. Vournas. *Voltage Stability of Electric Power Systems*. Springer, 1998.

[77] A. Tuladhar et al. "Parallel operation of single phase inverter modules with no control interconnections". In: *Applied Power Electronics Conference and Exposition*. Atlanta, GA, USA, Feb. 1997, pp. 94–100.

[78] A. J. Wood and B. F. Wollenberg. *Power Generation, Operation, and Control*. 2nd ed. John Wiley & Sons, 1996. ISBN: 0471586994.

[79] H.-D. Chiang and C. C. Chu. "Theoretical foundation of the BCU method for direct stability analysis of network-reduction power system models with small transfer conductances". In: *IEEE Transactions on Circuits and Systems I: Fundamental Theory and Applications* 42.5 (1995), pp. 252–265.

[80] V. Venkatasubramanian, H. Schattler, and J. Zaborsky. "Dynamics of large constrained nonlinear systems-a taxonomy theory". In: *Proceedings of the IEEE* 83.11 (1995), pp. 1530–1561.

[81] A. Berman and R. J. Plemmons. *Nonnegative Matrices in the Mathematical Sciences*. SIAM, 1994.

[82] N. Biggs. *Algebraic Graph Theory*. 2nd ed. Cambridge University Press, 1994. ISBN: 0521458978.

[83] P. Kundur. *Power System Stability and Control*. McGraw-Hill, 1994. ISBN: 007035958X.

[84] C. W. Taylor. *Power System Voltage Stability*. McGraw-Hill, 1994. ISBN: 0-07-063184-0.

[85] M. C. Chandorkar, D. M. Divan, and R. Adapa. "Control of parallel connected inverters in standalone AC supply systems". In: *IEEE Transactions on Industry Applications* 29.1 (1993), pp. 136–143.

[86] I. Dobson. "Observations on the geometry of saddle node bifurcation and voltage collapse in electrical power systems". In: *IEEE Transactions on Circuits and Systems I: Fundamental Theory and Applications* 39.3 (1992), pp. 240–243.

[87] M. Ilić. "Network theoretic conditions for existence and uniqueness of steady state solutions to electric power circuits". In: *IEEE International Symposium on Circuits and Systems*. San Diego, CA, USA, May 1992, pp. 2821–2828.

[88] H.D. Chiang and M.E. Baran. "On the existence and uniqueness of load flow solution for radial distribution power networks". In: *IEEE Transactions on Circuits and Systems* 37.3 (1990), pp. 410–416.

[89] D. J. Hill and I. M. Y. Mareels. "Stability theory for differential/algebraic systems with application to power systems". In: *IEEE Transactions on Circuits and Systems* 37.11 (1990), pp. 1416–1423. ISSN: 0098-4094.

[90] I. Dobson and H. D. Chiang. "Towards a theory of voltage collapse in electric power systems". In: *Systems & Control Letters* 13.3 (1989), pp. 253–262.

[91] L. O. Chua, C. A. Desoer, and E. S. Kuh. *Linear and Nonlinear Circuits*. McGraw-Hill, 1987. ISBN: 0070108986.

[92] Marija Ilić-Spong, James S. Thorp, and Mark W. Spong. "Localized Response Performance of the Decoupled $Q-V$ Network". In: *IEEE Transactions on Circuits and Systems* 33.3 (1986), pp. 316–322.

[93] J. Thorp, D. Schulz, and M. Ilić-Spong. "Reactive Power-voltage problem: conditions for the existence of solution and localized disturbance propagation". In: *International Journal of Electrical Power & Energy Systems* 8.2 (1986), pp. 66–74.

[94] R. A. Horn and C. R. Johnson. *Matrix Analysis*. Cambridge University Press, 1985. ISBN: 0521386322.

[95] Marija Ilic-Spong, M. Spong, and Robert Fischl. "The no-gain theorem and localized response for the decoupled $P - \theta$ power network with active power losses included". In: *IEEE Transactions on Circuits and Systems* 32.2 (1985), pp. 170–177.

[96] R. Kaye and F.F. Wu. "Analysis of linearized decoupled power flow approximations for steady-state security assessment". In: *IEEE Transactions on Circuits and Systems* 31.7 (1984), pp. 623–636.

[97] F. Wu and S. Kumagai. "Steady-state security regions of power systems". In: *IEEE Transactions on Circuits and Systems* 29.11 (1982), pp. 703–711.

[98] A. R. Bergen and D. J. Hill. "A structure preserving model for power system stability analysis". In: *IEEE Transactions on Power Apparatus and Systems* 100.1 (1981), pp. 25–35.

[99] H. V. Henderson and S. R. Searle. "On deriving the inverse of a sum of matrices". In: *SIAM Review* 23.1 (1981), pp. 53–60.

[100] S. Sastry and C. Desoer. "Jump behavior of circuits and systems". In: *IEEE Transactions on Circuits and Systems* 28.12 (1981), pp. 1109–1124.

[101] C. Meyer and M. Stadelmaier. "Singular M-matrices and inverse positivity". In: *Linear Algebra and its Applications* 22 (1978), pp. 139–156.